NOTICE: When government or other drawings, specifications or other data are used for any purpose other than in connection with a definitely related government procurement operation, the U. S. Government thereby incurs no responsibility, nor any obligation whatsoever; and the fact that the Government may have formulated, furnished, or in any way supplied the said drawings, specifications, or other data is not to be regarded by implication or otherwise as in any manner licensing the holder or any other person or corporation, or conveying any rights or permission to manufacture, use or sell any patented invention that may in any way be related thereto.

411433

411433

THE BLUNT-BODY PROBLEM IN HYPERSONIC FLOW AT LOW REYNOLDS NUMBER

By: H.K. Cheng

Contract No. Nonr 2653(00)
CAL Report No. AF-1285-A-10
June 1963

CORNELL AERONAUTICAL LABORATORY, INC.
OF CORNELL UNIVERSITY, BUFFALO 21, N. Y.

N-63-4-2

CORNELL AERONAUTICAL LABORATORY, INC.
BUFFALO 21, NEW YORK

CAL REPORT NO. AF-1285-A-10

THE BLUNT-BODY PROBLEM IN HYPERSONIC FLOW AT LOW REYNOLDS NUMBER

CONTRACT NO. Nonr 2653(00)

JUNE 1963

AUTHOR: Hsien K. Cheng
Hsien K. Cheng

APPROVED BY: A. Hertzberg
A. Hertzberg, Head
Aerodynamic Research Dep't.

DDC
AUG 3 1963

FOREWORD

This report was originally prepared under the sponsorship of the U. S. Navy through the Office of Naval Research (Mechanics Branch), Contract No. 2653(00), and was presented at the IAS 31st Annual Meeting, New York, New York, January 21-23, 1963.

As pointed out in the text, a part of the study with the wedge and cone problems was carried out for the U. S. Air Force through the Office of Scientific Research, under Contract AF 49(638)-952.

Since the completion of the original version of the report, which has been distributed as IAS paper No. 63-92, errata as well as points of ambiguity have been called to the writer's attention; this version has been revised to incorporate the desirable changes.

THE BLUNT-BODY PROBLEM IN HYPERSONIC FLOW AT LOW REYNOLDS NUMBER

H. K. CHENG
Cornell Aeronautical Laboratory, Inc., Buffalo, New York

ABSTRACT

Existing theoretical analyses and experimental results of the stagnation region in hypersonic flow at low Reynolds number are discussed. The approach based on the thin-shock-layer approximation is extended to study flow fields beyond the stagnation region as well as in the shock-transition zone.

The basic flow model consists of two adjoining thin layers: a shock-transition zone and a shock layer. The system of partial differential equations governing the high-density shock layer reduces to the parabolic type. The system governing the shock-transition zone reduces to ordinary differential equations similar to those of the one-dimensional shock wave. They give rise to a set of conservation relations across the shock, which account for the transport processes immediately behind the shock but do not involve details of shock-wave structure. With the modified Rankine-Hugoniot relations, the flow field in the shock layer can be determined independently of the shock-transition zone. An essential feature of this formulation is that, when applied in conjunction with nonslip surface conditions, it always yields the appropriate surface heat-transfer rate and skin friction (for unit accommodation coefficients) in the free-molecule limit. Comparison with more exact solutions of Levinsky and Yoshihara, and of Van Dyke, reveals the adequacy of the present theory in both the merged-layer regime and the inviscid limit.

A finite-difference method is developed for solving the shock-layer equations. As examples of flow around simple blunt or nonslender shapes, the problems of the paraboloid, hyperboloid, as well as the wedge and cone have been analyzed for a perfect gas with constant specific heats. Generally, solutions for low Reynolds number reveal substantial changes in total enthalpy and tangential velocity across the shock, analogous to surface slip effects. The solutions provide smooth transitions from the boundary-layer theory to the free-molecule limit. The velocity and temperature gradients near the inner edge of the shock layer increase with distance from the stagnation point or the apex, indicative of boundary-layer development. Results obtained for paraboloids and hyperboloids indicate the existence of a remarkably wide range of Reynolds number (corresponding to the boundary-layer through the incipient-merged-layer regime) in which the distributions of heat-transfer rate and skin friction on a smooth blunt body remain essentially unchanged.

Also studied is nonequilibrium dissociation with species diffusion in shock layers under influence of strong surface cooling. Solutions for the stagnation region based on a single dissociation-recombination kinetic model show a substantial concentration jump across the shock, and extensive influence of surface cooling at low Reynolds number. The role of pressure diffusion in a viscous shock layer is also discussed.

LIST OF SYMBOLS

a	nose radius
b	a parameter which appears in the equation of the surface $z^2 = \lambda + \frac{b}{4}\lambda^2$, and is zero for a paraboloid and is positive for a hyperboloid
c_f	$\equiv \mu \frac{\partial u}{\partial y} \Big/ \frac{1}{2}\rho_\infty U_\infty^2$, coefficient of skin friction
c_H	$\equiv k \frac{\partial T}{\partial y} \Big/ \rho_\infty U_\infty (H_\infty - H_w)$, coefficient of heat transfer
c_p, c_v, γ	specific heat at constant pressure, volume, and the ratio $\frac{c_p}{c_v}$, rsp.
D_{12}	coefficient of binary diffusion
f	$\equiv K\Psi \Big/ \rho_\infty U_\infty \bar{z} (\pi \bar{z})^{\frac{1}{2}} \sqrt{2\bar{u}_*}$, the nondimensionalized stream function with $\partial f/\partial \eta = \bar{u}/\bar{u}_*$ defined as the velocity field
H	$\equiv \frac{1}{2}(u^2 + v^2) + h$, total specific enthalpy
h	specific enthalpy
k, k_T	$\equiv \frac{2}{3} Pr \Big/ \left[\sqrt{1 + \frac{4}{K^2}} - 1\right]$, and the thermal diffusion ratio defined in pp. 519 of Ref. 80 (Hirschfelder, Curtiss and Bird), rsp.
k_r'	recombination rate constant
K^2, K_o^2	$\equiv \varepsilon \frac{\rho_\infty U_\infty a}{\mu_o}\left(\frac{T_*}{T_o} \cdot \frac{\mu_o}{\mu_*}\right)$ and $\varepsilon \frac{\rho_\infty U_\infty a}{\mu_o}$, respectively
K_T	$\equiv \frac{m_1 + m_2}{m_2 - m_1} \frac{k_T}{\alpha(1-\alpha)}$, where m_1 and m_2 are the mass of the gas particles of species 1 and species 2, respectively
K_p	the equilibrium constant
Le	$\equiv \rho D_{12} \bar{c}_p / k$, Lewis number (where $\bar{c}_p$ denotes mean value of c_p for the mixture).
M_∞	the free stream Mach number
N	$\equiv \frac{\mu}{\mu_*} \cdot \frac{T_*}{T}$
Pr	$\equiv c_p \mu / k$, Prandtl number
p, ρ, T	pressure, density and temperature, respectively
$\bar{p}$	$\equiv p / \rho_\infty U_\infty^2 \sin^2\beta$, dimensionless pressure

q, q_{BL}	rate of energy transported to the body surface (per unit time area), and the rate of heat transfer to surface according to the boundary-layer solution, respectively
Q	heat of formation per unit mass of atom
R_s, r	radius of curvature of the shock and $(y+a)$, respectively
R_1, R_2	$\equiv \frac{\mathcal{R}}{M_1}$, $\frac{\mathcal{R}}{M_2}$, respectively, gas constants for atoms and molecules
Re_b, Re_F	$\equiv \rho_\infty U_\infty a/\mu_0$ and $\rho_t \sqrt{H_\infty}\, a/\mu_t$, respectively
$\bar{T}$	$\equiv T/T_0$, dimensionless temperature
T_*	reference temperature used in the determination of the constant of proportionality in the linear representation $\mu = \frac{\mu_*}{T_*} T$
U_∞	free-stream velocity
u, v	velocity components in the x and y directions, respectively
$\bar{u}$, $\bar{v}$	$\equiv \frac{u}{U_\infty \cos\beta}$ and $\frac{-v}{U_\infty \sin\beta}$, respectively
V'	the diffusion velocity of the atomic species
w	rate of production of atomic species (in mass) per unit volume
W	$\equiv \frac{\bar{u}^2}{2}$
x, y	the curvilinear coordinates of which x is the distance along the body, y is the distance normal to the body surface or the surface or the shock interface (see discussion in Eqs. (5.1) and (5.2))
x'	the distance measured along the axis of symmetry
$\bar{x}$	$\equiv \varepsilon \frac{\rho_\infty U_\infty x}{\mu_0} \left(\frac{\mu_0}{\mu_*} \cdot \frac{T_*}{T_0}\right) \sec\beta$
Z	the distance of the surface from the axis of symmetry
α	the atomic concentration in mass fraction
β, Λ	shock angle and yaw angle, respectively
γ_w	recombination efficiency of atoms at the wall

Δ, δ_s — the lateral extents of the shock layer and of the shock-transition zones, respectively

ϵ — $\equiv \frac{\gamma-1}{\gamma+1}$

ε — $\equiv \frac{\gamma-1}{2\gamma}$

ζ, λ — $\equiv \sqrt{\psi/\rho_\infty U_\infty z(\pi z)^\nu}$ and $2\frac{x'}{a}$, respectively

η, ξ — $\equiv \left(\frac{9-\nu}{3}\varepsilon\right)^{1/4}\sqrt{1+\nu}\,K\int_0^y \frac{\rho\, dy}{\rho_\infty a}$ and $\frac{x}{a}$, respectively, the transformed coordinates employed in the analysis for the higher Reynolds number regime

$\bar{\eta}$ — $\equiv \frac{3}{4}\rho_\infty U_\infty \sin\beta \int_{y_2}^{y} \frac{dy}{\mu}$, the transformed coordinate

θ — dimensionless temperature defined in Eq. (8.13)

Θ — $\equiv \frac{H - H_w}{H_\infty - H_w}$ dimensionless enthalpy

κ — thermal conductivity

κ_c — $\equiv \frac{d\beta}{dx}$, longitudinal curvature of the surface

μ — viscosity

ν — a parameter which is zero in the plane case, and is unity in the axisymmetry case

ρ_D — a constant defined by Eq. (8.8)

σ — $\equiv a \sin\beta \cos\beta / z$

$\bar{\sigma}$ — $\equiv \rho_\infty / \varepsilon_\infty \rho_D$

τ_w — surface skin friction

χ — parameter defined in Eq. (8.11)

ψ — the stream function with $\frac{\partial \psi}{\partial x} = -(2\pi z)^\nu \rho v$ and $\frac{\partial \psi}{\partial y} = (2\pi z)^\nu \rho u$

$\bar{\psi}$ — $\equiv \psi / \rho_\infty U_\infty z (\pi z)^\nu$

Ω, Ω_* — $\equiv \frac{\rho_w}{\rho_s\left(\frac{8\varepsilon}{3}\right)^{3/4}}\sqrt{\frac{\mu_w}{\rho_w U_\infty a}}\,\frac{\left(1-\frac{8\varepsilon}{3}\right)}{\varepsilon\sqrt{2(1+\varepsilon)}}$, $\frac{\left(1-\frac{8\varepsilon}{3}\right)}{\sqrt{2}\left(\frac{8\varepsilon}{3}\right)^{3/4}K}$, respectively

ω — an exponent in the viscosity and temperature relation $\mu \propto T^\omega$

Subscripts

$W, \infty, *, s$	pertaining to the surface condition, the free-stream condition, the typical condition behind the shock, and the condition within the shock or the shock-transition zone, respectively
$0, 1, 2$	pertaining to the stagnation condition in the free stream, and to the conditions in front of, and immediately behind, the shock, respectively (except for the terms in the development of Eq. (6.8)
t	pertaining to the stagnation condition behind the bow shock in an inviscid flow

TABLE OF CONTENTS

INTRODUCTION

A number of effective methods have been developed for analyzing inviscid hypersonic flows and the associated boundary layers around blunt bodies (see, for example, Ref. 1-4). Much less has been done, however, for the corresponding problems at low Reynolds number or low density. The analysis of the low-density phenomena is nevertheless basic to the study of many problems of high-speed flight at high altitude where the thin-boundary-layer concept no longer applies. In this paper, the problem of hypersonic rarefied-gas flow will be studied within the framework of the continuum theory.

With an increasing degree of rarefaction, the continuum theory begins to break down. Consequently, a valid description of the flow field will have to be based on the kinetic theory to account for the collision processes. The transition from the continuum to the free-molecule limits from the viewpoint of flight application was considered some time ago by Tsien.[5] Tsien classified the problems of rarefied-gas flow into four regimes: the continuum, the slip-flow, the transitional, and the free-molecule regimes. It was proposed at that time that departure from the classical continuum model in the slip-flow regime may be accounted for by including in the governing equations the higher-order (Burnett) terms in a formal development for the solution to the Boltzmann equation.[6] However, the growing body of evidence from both experimental and theoretical studies has since shown disagreement with these higher-order equations, and, in most instances has indicated that the relatively simpler Navier-Strokes equations, with appropriate boundary conditions to account for the slip effects (and transport coefficients evaluated according to the Chapman-Enskog theory), are superior.[7,8] A continuum-

flow model based on the Navier-Stokes equations thus promises a domain of applicability far more extensive than previously conceived. This view [9-12] is shared by the writer, and the present study attempts to extend the continuum-flow theory, as far as is permissible, into the range of rarefied gas dynamics.

It is apparent that solution to the transitional regime, as well as the final justification of the continuum analysis, will have to come from the Boltzmann equation governing the velocity-distribution function. A number of approximate methods have been developed in recent years to overcome the difficulty of solving the Boltzmann equation.[13,14,15] However, a method which is satisfactory in both accuracy and simplicity has yet to become available. Of significance in this respect is the recent study of the shock-transition zone by Liepman and co-workers,[16] in which a variant of Krook's collision model[17] is adopted.* The solution obtained shows little difference from the Navier-Stokes solution on the higher-pressure side of the shock even for a Mach number of ten. It seems to provide support to the idea that the Navier-Stokes equations are adequate for describing flow fields even when the shock wave structure becomes important.**

The problem of hypersonic flow of rarefied gas around a blunt body has been discussed previously by Probstein in Ref. 11 where an extensive

---

*With this model, the Boltzmann equation is simplified to one formally resembling a relaxation equation.

**To further augment this idea, it would be desirable to include in the shock-structure analysis of Liepman and co-workers the effects of shock curvature as well as velocity and temperature gradients behind the shock.

account of the analyses of the stagnation region in the various flow regimes is also given. Recently, the problem has been reviewed by Van Dyke,[12] emphasizing the second-order boundary-layer theory. The present report consists of two parts: In Part I, the existing analyses of the stagnation region will be discussed with emphasis on the more recent studies related to the viscous-layer and merged-layer regimes. A comparison with experimental results is included. The discussion is oriented toward the thin-shock-layer approach which is to be further developed in Part II.

In Part II, the thin-shock-layer approach to the viscous blunt-body problem is extended to study flow fields other than, or removed from, the stagnation region. The new development includes an extension of the thin-layer approximation to analyze the shock-transition zone and a finite-difference method for solving the shock-layer equations without similarity assumptions. Among the particular problems studied are viscous hypersonic flows over wedges, paraboloids, and other simple nonslender shapes, as well as nonequilibrium dissociation with species diffusion in the shock layer under the influence of strong surface cooling.

PART I. REVIEW OF EXISTING RESEARCH ON STAGNATION REGION

The manner in which flow regimes are classified is, of course, quite arbitrary, and varies from one problem to another. For a stagnation region in hypersonic flow, Probstein and Kemp[10] observe that there are six regimes between the boundary-layer and free-molecule limits. Figure 1, reproduced from Ref. 11, illustrates the extent of the various regimes in terms of flight speed and altitude. The boundaries delimiting each of these regimes were originally estimated by Probstein[11] for an ARDC 1959 model atmosphere and a cooled body of one-foot nose radius, assuming the compression ratio across the shock to be ten. These regimes, numbered below in the order of increasing degree of rarefaction, may be characterized by the following descriptions.

(1) Vorticity-Interaction Regime - The boundary layer is still thin, but the second-order effects become appreciable. They include slip and temperature jump, surface curvatures and the interaction of the boundary layer, through its finite thickness, with the outer flow. For the axisymmetric case, the most important of these effects is that resulting from the external vorticity.

(2) Viscous-Layer Regime - The viscous region becomes an appreciable fraction of the shock layer and may be too thick to permit application of the boundary-layer concept.

(3) Incipient-Merged Layer Regime - The viscous and other transport effects are no longer negligible behind the shock, and the thickness of the shock itself becomes an appreciable fraction of the shock layer. Hence the shock as

a surface of discontinuity may no longer be an adequate description.

(4) Fully-Merged Layer Regime - The shock thickness is comparable to, and perhaps even greater than, that of the shock layer. Not only is the shock layer fully viscous, but the shock-transition zone may no longer be distinguished from other parts of the flow field.

(5) Transitional Regime - The collision frequency among gas particles is not high enough to make the continuum description valid, yet not sufficiently low to make the kinetic-theory description simple.

(6) First Collision Regime - There is only a small fraction of incident particles experiencing one collision or more before reaching the body surface.

The present report mainly concerns regimes (1)-(4). The study will be made under the assumption of a continuum flow model governed by the Navier-Stokes equations. That assumption has in fact been implicit in the determination of the various boundaries in Fig. 1. For later reference, the regimes (3) and (4) together may be called the merged-layer regime.

Aside from providing a general picture of the flow field at various degrees of rarefaction, the above classification serves to indicate the appropriate flow models for analysis. Attempts to analyze the stagnation region for regimes (1)-(4) have resulted in three main approaches. One, which applies to regime (1), assumes small departure from the boundary-layer limit. This approach, which has been most extensively treated, may be identified with the higher-order boundary-layer theories. In another, applicable to regimes (2), (3), and partly to (4), one considers viscous and other transport effects throughout the shock layer, and integrates numerically a system of simplified Navier-

Stokes equations along the axis of symmetry. Encompassing both of these approaches is a third approach, favored by the present author, which utilizes the thin-shock-layer approximation familiar from the inviscid hypersonic flow theory.[18-21] The analysis based on this third approach only requires the distinction between two flow regimes, labelled I and II in Fig. 1.1. Regime I contains regimes (1) and (2) of the foregoing classification; Regime II contains (3) and the main part of (4). Current theories will be discussed under these three main approaches in Sections 1-3. The results of theories and experiments from several sources are compared in Section 4.

1. SECOND-ORDER BOUNDARY-LAYER THEORIES

The second-order corrections to the boundary-layer theory may be subdivided in various categories: the external vorticity effect, slip and temperature-jump effects; the non-vanishing surface curvature effects; and the boundary-layer displacement effect. The boundary-layer displacement affects directly the matching of the boundary layer with the outer vortical flow, and also induces pressure and velocity changes in the outer "inviscid flow". On account of their subtle nature, the subdivision concerning displacement effects has been rather arbitrary.

The relatively earlier analyses of Hayes and Probstein,[4] Rott and Lenard[22] and Kemp[23] are devoted primarily to the effect of external vorticity. More systematic treatments of the second-order effects are subsequently given by Van Dyke,[24] Lenard[25] and Maslen.[26] The analysis of Ferri, Zakkay and Ting[27] considers vorticity effect and may also be regarded as belonging to this class. There has been considerable disagreement among the various analyses

of slip and temperature-jump effects, as well as the vorticity and displacement effects. Readers are referred to Van Dyke's review[12] for the many critical discussions and comments. The following discussion will concern only certain outstanding aspects of the higher-order theories which must be considered subsequently in this paper: the external vorticity effect, the displacement effect, and the slip and the temperature-jump effects.

1.1 External Vorticity Effect

In his earlier work on the external-vorticity effect, Hayes[28] assumes that the boundary-layer displacement does not appreciably change the pressure and velocity distributions along each streamline in the outer flow. He arrives at a modified outer boundary condition for the velocity field f_η in the form

$$f_\eta^2 = 1 + 2\Omega f \qquad \eta \longrightarrow \infty \tag{1.1}$$

where Ω, termed the vorticity-interaction parameter, is the ratio of the external vorticity to some average value of vorticity in the boundary layer. This condition was applied to study the axisymmetric stagnation-point boundary layer by Hayes and Probstein.[4] In this case, Ω is given by Hayes and Probstein as

$$\Omega \equiv \frac{(\rho_w/\rho_2)\left(1-\frac{8\epsilon}{3}\right)}{\sqrt{2}\,\epsilon\left(\frac{8\epsilon}{3}\right)^{3/4}\sqrt{1+\epsilon}}\sqrt{\frac{\mu_w}{\rho_w U_\infty a}} \tag{1.2}$$

Equation (1.1) shows clearly that external vorticity effectively increases the velocity at the boundary layer's outer edge. One may note that since Eq. (1.1) does not contain η, it also allows for the streamline displacement in the matching of the inner and outer velocity fields.

The above boundary condition may be replaced simply by

$$\frac{d^2 f}{d\eta^2} \longrightarrow \Omega \qquad (\eta \longrightarrow \infty) \tag{1.3}$$

The equivalence of Eqs. (1.1) and (1.3) is guaranteed by the differential equations governing f, as noted by Kemp[23] and Moore.[29]

The method based on the local-similarity principle has been a very useful tool for analysis of heat transfer from a hypersonic boundary layer to a relatively cold body.[4, 30, 31] It is natural to anticipate an extension of the method to account for the external-vorticity effect. This is presumably the viewpoint of Ferri, Zakkay and Ting[27] who treat the vorticity interaction on the basis of a local-flat-plate similarity. This basis implies however that the velocity profile is completely unaffected by the tangential pressure gradient as well as by the external vorticity. The outer inviscid flow is assumed to have a linear velocity profile and is completely unaltered (and undeflected) by the presence of the boundary layer. The procedure of joining the inner and outer solutions appears to be a rather complicated one which involves matching the velocity and temperature fields over two separate boundaries. One of the final equations used (Eqs. (34) or (38) of Ref. 27) may nevertheless be identified in form with Hayes' boundary condition Eq. (1.1).

1.2 Displacement Effect

Except for the displacement effect implicit in the boundary condition of Eq. (1.1), Hayes and Probstein's vorticity-interaction theory assumes no displacement effect on the outer flow. This assumption is justified in the case of a thin shock layer. In order to account for the displacement effect completely, one has to solve the difficult elliptic problem (presumably by iteration), and this has been done only by Van Dyke.[12] Unfortunately, the problem is further obscured by an apparent confusion over the division of the vorticity and displacement effects. While Van Dyke's analysis[24] is

believed to be the most systematic and elegant, his subdivision of the interaction problem into the effect of "entropy gradient" (i.e. vorticity) and the effect of "displacement speed"* is not completely satisfactory. In each of these effects, according to this classification, there is a second-order effect appearing in both the outer boundary condition as well as in the governing differential equations. The second-order corrections in the differential equations actually arise from the change in the pressure at the boundary layer's outer edge, and may therefore be combined as the displacement effect on the external pressure. The combined effect turns out to be, in most cases, much smaller than if separately calculated, and, as already noted, is negligible in the thin-shock-layer approximation.

1.3 Slip and Temperature-Jump Effects

While the analyses of Rott and Lenard,[22,25] as well as Van Dyke,[24] show sizable slip effects, Maslen's analysis[26] reveals that these effects are definitely negligible for heat-transfer analysis. It may be noted that the results of these analyses depend, of course, on the specific coefficients entering the slip and temperature-jump conditions. The large temperature-jump effects reported by Rott and Lenard, and by Van Dyke are rather surprising, since these effects are known to vanish in either the limit of a vanishing wall-to-stagnation temperature ratio or the limit of a vanishingly thin shock layer.[12]

*The change in velocity at the outer edge associated with the boundary-layer displacement.

2. ANALYSIS OF VISCOUS SHOCK LAYER BASED ON SIMILARITY ASSUMPTION

When departure from the boundary-layer limit is too large for the concept to be applicable, the full Navier-Stokes or other appropriate equations must be used to describe the stagnation region. Most of the existing analyses in this class use the Rankine-Hugoniot shock relations as an outer boundary condition, and, therefore, can be applied only to the viscous-layer regime. However, in the merged-layer regimes, the Rankine-Hugoniot relations are not applicable and have to be modified. In order to make the analyses tractable, it has been found necessary to invoke the similarity assumption for the flow field in the stagnation region.* This assumption is justified for two types of models: one assumes a constant density, the other a thin shock layer.

2.1 Similar Solutions Based on Constant Density

Assuming a constant density behind a spherical or cylindrical shock which is concentric with a spherical or cylindrical body, Probstein and Kemp[10] have reduced the Navier-Stokes equations in the stagnation region to a system of ordinary differential equations. Solutions are obtained for a cold surface both in the viscous-layer and in the incipient-merged-layer regimes. The analysis in the latter regime must include the thickness-curvature effect of the shock and the modification of the Rankine-Hugoniot relations to allow for the transport effects immediately behind the shock. In Probstein and Kemp's model,[10] the shock-transition zone is treated separately from, but simultaneously with, the shock layer. In spite of the many idealizations of the flow

*The similarity assumption amounts to postulating the flow field to be in a certain form, so that a separation of the variables may be achieved in the governing differential equations. By the similarity, the problem is reduced to one involving only ordinary differential equations.

model, the analysis of Probstein and Kemp was first to reveal the many important features of the viscous-layer and incipient-merged-layer regimes. This constant-density model perhaps describes more appropriately the physical problem of an insulated body, which has been considered by Hoshizaki[32] in the viscous-layer regime. The constant-density viscous-layer model has been analyzed by Oguchi[33] to include a magnetic field. Oguchi[34] has, in fact, applied a systematic expansion in the density ratio $\frac{\gamma-1}{\gamma+1}$ to describe analytically the constant-density viscous-layer model. Although the range of validity of Oguchi's solution is limited by the viscous-layer model and by the breakdown of the formal expansion at high Reynolds number, the simplicity to be gained by the thin-shock-layer approach is quite evident from the analysis.

2.2 Similar Solution Based on Thin Shock Layer

The stagnation-point boundary layer is much easier to handle than the corresponding problem based on the full Navier-Stokes equations because the boundary-layer equations are parabolic and amenable to separation of variables for the stagnation-point problem. The Navier-Stokes equations may, however, be simplified also to the parabolic type by assuming that the shock layer (which includes the boundary layer as a part) is thin. In this way, the similarity assumption in the stagnation region can be justified without the assumption of constant density. Thus, Ho and Probstein[34] integrate numerically the simplified Navier-Stokes equations along the axis of symmetry from the body to the shock in the viscous-layer regime. The reduced equations are similar to the boundary-layer equations except that the outer boundary is now at a finite distance from the surface (where the Rankine-Hugoniot shock conditions

are to be satisfied) and that the tangential pressure gradient is not a constant. Herring[35] postulated simply that the boundary-layer equations hold between the body and the shock. His analysis of the stagnation region is then virtually the same as Ho and Probstein's, except for the fact that the tangential pressure gradient term in the momentum equation is a constant determined by its value at the shock. Chung[36] studied nonequilibrium dissociation in the viscous stagnation region. He carried out his study within the framework of the viscous-layer model of Ho and Probstein, but evaluates the tangential-pressure-gradient term as in Herring's analysis. The results of Chung's calculation will be discussed later in connection with the study of Section 7 of Part II. Also using a viscous-layer model, Goldberg and Scala[37] studied mass transfer in the hypersonic shock layer. The validity of some of their results may be questionable because of the local chemical equilibrium postulated.

The use of the Rankine-Hugoniot relations in the viscous-layer model presupposes that the shock thickness and the transport effects behind the shock are not important. Germain and Guiraud,[38] and also Chow and Ting,[39] noted, however, that, in order to claim superiority over the vorticity and other second-order boundary-layer theories, theories based on the viscous-layer model should also include the shock thickness effects. These effects, though small for a high shock compression ratio, have been analyzed as corrections in Refs. 38 and 39.

A more recent analysis of the stagnation region in the merged-layer regimes is given by Levinsky and Yoshihara.[40] They, unlike Probstein and Kemp[10] who assume a constant density for the shock layer and treat the shock-transition zone by an approximate method, applied the compressible viscous-

flow equations along the axis of symmetry from the body upstream to infinity, including the shock-transition zone. Although a great number of the higher-order terms from the Navier-Stokes equations are retained in their analysis, the reduced system of equations is self-consistent only to the leading approximation. This is apparent from the assumption of a density field having spherical symmetry. On account of this degree of approximation, the analysis cannot be applied to the entire domain of the "fully-merged-layer regime" as originally defined by Probstein and Kemp[10] (which permits a rather thick shock) without sacrifice of accuracy. The numerical solution of this analysis will be discussed later in connection with the new treatment of the shock-transition zone developed in Part II.

Most analyses described above have to make use in one way or another of the thin-shock-layer assumption. This assumption has been used only to make the similarity solution possible. Strictly speaking, these analyses are no more accurate than the leading approximation given by the inviscid shock-layer theory.[18-21] An approach making consistent use of the thin-shock-layer approximation may therefore describe the problem with equal accuracy. In fact, under this approximation, the analysis of the stagnation region embodies the analyses of both Sections 1 and 2.

3. THIN-SHOCK-LAYER THEORY

An analysis of the stagnation region based on a more consistent application of the thin-shock-layer approximation has been given in a previous paper by the author.[41] By this thin-layer approach, curvature, slip and displacement all become negligible higher-order effects. The essential features of that

analysis will be discussed below. In addition to reviewing the basic work on the axisymmetric problem, previous related analysis for yawed cylinders will also be discussed.

3.1 Two Continuum-Flow Regimes

In the thin-layer approach, there are two important parameters ε and K^2 defined as

$$\varepsilon \equiv \frac{\gamma-1}{2\gamma} \quad , \quad K^2 \equiv \varepsilon \frac{\rho_\infty U_\infty a}{\mu_o} \left(\frac{T_*}{T_o} \cdot \frac{\mu_o}{\mu_*} \right) \tag{3.1}$$

The parameter K^2, except for a factor weakly dependent on the reference temperature, is essentially the product of ε and the Reynolds number Re_b used by Probstein and Kemp.[10] For the analyses of the stagnation region in hypersonic flow, the problem falls into two regimes (see Fig. 1).

$$\left.\begin{aligned} &\text{Regime I:} \quad O(1) \leq \varepsilon K^2 < \infty \\ &\text{Regime II:} \quad O(\varepsilon) \leq \varepsilon K^2 \leq O(1) \end{aligned}\right\} \tag{3.2}$$

Note that the lower limit of Regime II includes a major portion of the fully merged-layer regime where the shock layer and the shock-transition zone are comparable in thickness.* Also, because of the overlap at $\varepsilon K^2 = O(1)$, the viscous-layer regime is covered by both Regime I and II.

3.2 The Higher Reynolds Number Regime

The problem of the stagnation region with axisymmetry is reducible in Regime I, which includes also the viscous-layer regime, i.e. $\varepsilon K^2 = O(1)$,

*In terms of ε and K^2, the domain of the incipient-merged-layer and fully-merged-layer regimes defined originally by Probstein and Kemp are, respectively, $O(\sqrt{\varepsilon}) \leq \varepsilon K^2 \leq O(1)$ and $O(\varepsilon^{3/2}) \leq \varepsilon K^2 \leq O(\sqrt{\varepsilon})$

virtually to the vorticity-interaction theory of Hayes and Probstein.[4] This is possible because under the thin-shock-layer approximation, which is subject to an error of order ε, the asymptotic solutions to the stagnation-point boundary layer also describe the inviscid (vortical) portion of the shock layer. Since the Reynolds number in this regime is still quite high, one may replace the shock boundary by $\eta \to \infty$ in the boundary-layer coordinate. A more detailed discussion of this reduction is given in Ref. 41.

The system of equations governing the axisymmetric stagnation region in Regime I is

$$\left.\begin{aligned} &f''' + ff'' = \tfrac{1}{2}\left[f'^{2} - \frac{T_w}{T_o} - \left(1 - \frac{T_w}{T_o}\right)\theta\right] \\ &\theta'' + Pr f \theta' = 0 \\ &f(0) = f'(0) = \theta(0) = 0 \\ &\theta(\infty) = 1 \;;\quad f'(\infty) = \Omega_* \end{aligned}\right\} \tag{3.3}$$

where the parameter

$$\Omega_* \equiv \frac{1 - \frac{8\varepsilon}{3}}{\sqrt{2}\left(\frac{8\varepsilon}{3}\right)^{3/4} K} \tag{3.4}$$

is basically the same as Ω of Hayes and Probstein (if the reference temperature T_* is equal to the wall temperature T_w, Ω_* can be reduced essentially to Ω). One recalls that, in arriving at Eq. (3.3) or its equivalent, Hayes and Probstein assume Ω small and have to invoke the principle that the flow properties along the outer streamlines are not affected by the boundary-layer displacement. Under the present thin-shock-layer approximation, this principle is fully justified, and the current controversy regarding the vorticity-displacement effect is by-passed. In the present formulation, the magnitude of Ω_* is not necessarily small, in fact, in the

viscous-layer regime, $\Omega_* = O(\varepsilon^{-1/4})$. In the case of plane flows, the external vorticity vanishes at the surface and has relatively small influence on the boundary layer. The treatment of the viscous-layer regime based on Eq. (3.3), in addition to having removed the need for simultaneously determining the shock stand-off distance with other unknowns, has the merit of combining the specific-heat ratio γ and the Reynolds number into the parameter Ω_*.

3.3 The Lower Reynolds Number Regime

Although the slip and temperature-jump at the surface may eventually become larger at lower Reynolds number, they cannot exceed the order $\gamma\sqrt{\varepsilon \frac{T_w}{T_o}}\, c_H$, i.e. $\gamma\sqrt{\varepsilon \frac{T_w}{T_o}}$, so long as the thin-shock-layer approximation applies.[42,43] For a cold body, these effects may therefore be neglected, or separately treated. On the other hand, the transport processes immediately behind the curved bow shock give rise to substantial changes in the tangential velocity component and total enthalpy across the shock. These effects resemble the slip temperature jump phenomena. Probstein in Refs. 10 and 11 emphasizes the importance of the shock-thickening effects in the merged-layer regimes. The study under the thin-shock-layer approximation[41,42] reveals, however, that the contribution of the finite shock thickness is only secondary and may be neglected as compared to the more important "slip effects" at the shock. (This will be further confirmed by the development in Section 5.3) In fact, this is borne out by Probstein and Kemp's[10] analysis of the shock-transition zone (although it was not clearly brought out in that work).* Thus, even in the merged-layer regime the Rankine-Hugoniot relations need only be modified

*The slip-like transport effects at the shock have recently been studied by Pan and Probstein in the leading-edge region of a sharp flat plate.[43]

to account for the transport effects behind the shock, treating it as a surface of discontinuity. Contributing to this result are two factors: first, the shock thickness in the regimes considered is still thin in comparison with the shock's radius of curvature, and second, the average density within the shock-transition zone is actually much closer to the low free-stream density than that in the thin-shock layer behind it.

For the axisymmetric stagnation region and a linear viscosity-temperature relation, an analytical development is possible in this regime. In terms of the variable $\zeta = \sqrt{\psi/\rho_\infty U_\infty \pi z^2}$, related to the stream function, the leading terms in the development for the tangential velocity component and the enthalpy function are simply

$$\bar{u} \equiv \frac{u}{U_\infty \cos\beta} = K^2\left[\sqrt{1+\frac{4}{K^2}}-1\right]\zeta/2$$
$$\Theta \equiv \frac{H-H_w}{H_\infty - H_w} = \Gamma_{\frac{1}{3}}(k\zeta^3)\Big/\left[\Gamma_{\frac{1}{3}}(k)+k^{-2/3}e^{-k}\right] \qquad (3.5)$$

where $\Gamma_{\frac{1}{3}}(t)$ is the incomplete gamma function of order 1/3 in the argument t, and the parameter k is equal to $2Pr/3\left[\sqrt{1+\frac{4}{K^2}}-1\right]$. The second terms in the development, which are proportional to ε, have been determined and given in Ref. 41.* Except for a constant of proportionality, the velocity ratio $\bar{u}$ of Eq. (3.7) is identified in form with the corresponding solution of inviscid Newtonian shock-layer theory for $\varepsilon \to 0$.[19,20]

---

*Because of the dependence on K, the magnitudes of the correction terms are actually not given by $O(\varepsilon)$ but are considerably larger near the body (See Ref. 42). By a systematic expansion in terms of $\frac{\gamma-1}{\gamma+1}$, Shidlovsky[44] has recently obtained an analytic development similar to that described above.

3.4 Stagnation Region of a Cylinder at Yaw

The same thin-layer model has been applied to analyze the stagnation region of a cylinder at yaw.[42]

In the case of an unyawed cylinder, the heat-transfer rate determined from the analysis (for $\varepsilon = 0.10$, $T_w/T_0 \to 0$) shows little departure from the rate based on the boundary-layer theory for K^2 as small as 1.0 even though the velocity and enthalpy profiles obtained would suggest considerable difference from the boundary-layer theory. Apparently, the (higher-order) vorticity effect and the slip-like effects behind the shock tend to compensate each other.

The analysis for the yawed cylinder is essentially similar, and is particularly simple for unit Prandtl number. The essential parameter governing the yawed cylinder is

$$K^2 \sec \Lambda$$

where Λ is the yaw angle. The analysis carried out for unit Prandtl number shows insensitivity of the enthalpy profile to yaw at both high and low Reynolds numbers. This result suggests a yaw independence principle. Accordingly, the heat-transfer rates for all yaw angles can be correlated as

$$\frac{C_H}{\cos \Lambda} \quad \text{vs} \quad K^2 \sec \Lambda$$

For $\mu \propto T^{\omega}$, and taking into account the dependence of the reference temperature on the yaw angle, the parameter $K^2 \sec \Lambda$ may be replaced by

$$(K^2)_{\Lambda=0} (\sec \Lambda)^{2\omega - 1}$$

This rule of correlation is consistent with the previous results obtained by Reshotko et al[82,83] for the boundary-layer limit. The results of Ref. 42

show that the correlation is reasonably accurate even for yaw angles as large as 60°.

4. COMPARISON OF RESULTS FOR STAGNATION-POINT HEAT TRANSFER

The heat-transfer rate is a quantity of engineering interest, and can also be measured in experiments conducted in low-density tunnels. Some controversy appears to have arisen in recent years concerning the predicted and measured values of this quantity at the stagnation point of a sphere. In the following, the heat-transfer rates predicted by the various theories will first be examined.

4.1 Theoretical Results

The theoretical results may be discussed in two ranges corresponding to high and to low Reynolds numbers.

High Reynolds-Number - It is advantageous to consider first the results obtained from the thin-shock-theory, which is not restricted to the small vorticity effect. The result based on numerical integration of Eq. (3.3) for $Pr = 0.71$, gives (best fit in the range of $0 \leq \Omega_* \leq 1, 0 < \frac{T_w}{T_o} < 0.40$)

$$\frac{q - q_{BL}}{q_{BL}} = 0.50\,\Omega_* - 0.11\,\Omega_*^2 \qquad (4.1)$$

where q is the surface heat-transfer rate and the subscript BL signifies the boundary-layer limit.

With the exception of the theoretical results of Ferri and co-workers,[27] there is a reasonable consistency between Eq. (4.1) and the vorticity effects predicted by others based on the second-order boundary layer theory. Van Dyke in Ref. 24, assumes $Pr = 0.71$, $T_w/T_o = 0.20$, and $\gamma = 1.40$. In

the form of Eq. (3.5), his results* (excluding the temperature-jump effect) give the value 0.46 as compared to the coefficient 0.50. Maslen,[26] and more recently Probstein (private communication), consider $Pr = 1$ and $T_w/T_o \to 0$, and obtain 0.45 and 0.44, respectively. Ferri and co-workers[27] give their results in terms of a parameter $\omega/\sqrt{2ARe_F}$ which may be closely identified with Ω_*. However, the vorticity effect predicted by them appears to be 30 to 50% larger than the above results.

There is an apparent inconsistency between Eq. (3.5) and the earlier result of Hayes and Probstein[4] who gave a coefficient of 0.19 instead of 0.50. Their calculation was made for $Pr = 0.71$, and a low value of T_w/T_o. Instead of the linear viscosity-temperature relation, as used in most other analyses, the Sutherland law is used. Clearly, the discrepancy results from the difference in the viscosity law. In order to compare the two results, one must use the appropriate reference temperature in the linear viscosity law, which in this case can be taken, according to the study of Ref. 45 as

$$T_* = \frac{T_s + T_w}{2} \approx \frac{T_o}{2} \tag{4.1a}$$

and one must remember that, implicit in Hayes and Probstein's parameter Ω of Eq. (1.2), the wall temperature is taken as a reference temperature. Allowing for a low value of T_w/T_o, the relatively small numerical coefficient given by Hayes and Probstein can actually be accounted for.[42] The apparent discrepancy should not be taken, however, to indicate inadequacy of the linear

---

*In this example with a cold surface, the effects associated with curvatures and displacement are very small. The ambiguity resulting from the arbitrary division of the vorticity and displacement effects mentioned in Section 1 does not arise.

representation of the viscosity-temperature relation. Examples in Ref. 45 show in fact that with the proper reference temperature the linear relation is adequate for predicting the heat transfer rate, skin friction, shock stand-off distance and other quantities of interest. Rather, the discrepancy reflects the inappropriateness of using the wall temperature as a reference condition for the definition of Ω . In fact, Hayes and Probstein's results lead to an infinite rate of heat transfer in the limit of $\frac{T_w}{T_o} \to 0$.

Low Reynolds Number - Heat-transfer results pertaining to the merged-layer regimes have been obtained by Probstein and Kemp,[10] Levinsky and Yoshihara,[41] and the author.[42] For these regimes, the thin-shock-layer approach yields the first approximation consistent with Eq. (3.5) as

$$c_H = 3 \Big/ \left[\Gamma_{\frac{1}{3}}(k) + k^{-2/3} e^{-k} \right] \tag{4.2}$$

which approaches the free-molecule limit corresponding to a unit accommodation coefficient. One notes that the effect of the specific heat ratio γ will only appear as a correction to the value of c_H given above, which is a function only of k . Therefore, flows with different values of γ should correlate reasonably well in terms of the parameter K^2 in the merged-layer as well as in the viscous-layer regimes (see the numerical solutions given in Ref. 41 and 42). In fact, the heat-transfer rates based both on the solutions of Levinsky and Yoshihara[40] ($\gamma = \frac{5}{3}$) and that of Probstein and Kemp[10] (constant-density model with $\gamma = \frac{11}{9}$), agree reasonably well with Eq. (4.2). The corresponding shock stand-off distance (to be more precise, the thickness of the shock layer) predicted by Probstein and Kemp is, however, much higher than that obtained by the present approach,[41] primarily because of their constant-density assumption.

4.2 Experimental Results

Measurements of stagnation-point heat transfer have been made on spheres in hypersonic rarefied gas flow by Neice and co-worker,[46] Ferri and co-workers,[27,47,48] Wittliff and Wilson,[49,50] Varig,[51] Bloxsom and Rhodes,[52] and Hickman and Giedt (unpublished but reported in Ref. 12). Similar data for yawed and unyawed cylinders were also obtained by Vidal and Wittliff.[50] While discrepancies do exist among the data reported, as well as among analyses, the general trend of the data does bear out the theoretical predictions. The disagreement between theory and experiment is found mainly in the vorticity-interaction regime where the departure from the boundary-layer prediction is actually quite small.

In Fig. 4.1, the data for spheres of Ferri and co-workers[27,47] which encompasses both the high and low Reynolds number regimes, are reproduced along with theoretical predictions based on their analysis of Ref. 27. The data were taken in tests with a stagnation temperature T_o = 1280°K and test flow Mach numbers of 5 and 8. If one assumes vibrational equilibrium, the value of ε behind the shock should be about 0.13 to 0.14. The experimental data are presented as q/q_{BL} vs Re_F, where q is the stagnation-point heat-transfer rate measured on a small sphere and q_{BL} is the heat-transfer rate measured on a considerably larger sphere corresponding to vanishing vorticity. The Reynolds number Re_F may be related to K^2 as

$$Re_F \equiv \frac{\rho_t \sqrt{H_\infty}\, a}{\mu_t} \approx \frac{Re_b}{\sqrt{2}\,\varepsilon} = \frac{1}{\sqrt{2}}\left(\frac{T_o}{T_*}\cdot\frac{\mu_*}{\mu_o}\right)\frac{K^2}{\varepsilon^2} \qquad (4.3)$$

Included in the same figure for comparison is the theoretical curve based on the thin-shock-layer approach described in the last section (for both Regimes I and II) calculated for $Pr = 0.71$, T_w/T_o 0, and $\varepsilon = 0.13$. Also included in the figure are the relatively recent measurements of Vidal and Wittliff.[50] Their experiments, performed in a hypersonic shock tunnel, extend the measurement ot a range corresponding to the fully-merged-layer regime and beyond.* Although the shock-tunnel data of Vidal and Wittliff are obtained for a test section stagnation temperature as high as $T_o = 2500-3000°K$, chemical reaction is expected to be frozen both in the shock-layer as well as on the (noncatalytic) surface. There was nevertheless a considerable concentration of atomic species present in the test flow of the experiments due to freezing in the nozzle expansion. In the data correlation of Ref. 50 the energy associated with the frozen atomic species has been subtracted from the total enthalpy.

The general trend of agreement of these data with theory is quite evident from Fig. 4.1. In the higher Reynolds number range ($Re_F \geq 500$), there is a rise over the boundary-layer value due to the external-vorticity effect. In the lower Reynolds number range ($Re_F \leq 500$), the heat transfer ratio q/q_{BL} begins to decrease and soon goes below unity, approaching the free molecule limit. If one considers the scatter of the data and the degree of approximation in the analysis, the agreement is reasonable. Toward the high Reynolds number end, the data of Ferri and co-workers agree

*Only data in the range of $0.10 \leq K^2 \leq 1$ of Ref. 50 are included in Fig. 4.1.

well with their own theoretical prediction, but appear to be higher than that predicted by the thin-shock-layer approach (as well as the others). As far as the fractional increase in heat transfer $(q - q_{BL})/q_{BL}$ is concerned, measurements of Ferri and co-workers are consistently higher than the writer's prediction by 30 to 50%. The unsolved discrepancy suggests that effects of vibrational (and perhaps also rotational) relaxation in the experiments on the vorticity effect should be examined.

Heat-transfer data for sphere obtained by Hickman and Giedt (reported by Van Dyke) at Mach numbers from 2 to 6 in a low-density wind tunnel have been compared with the second-order boundary layer analysis by Van Dyke.[16] The measured departure from the boundary-layer theory is seen to exceed the prediction by a factor of two or more. It has been noted in Section 1 that the slip and temperature jump effects in Van Dyke's calculation are comparatively large. As indicated by Van Dyke himself, simply deleting them would bring better agreement with experiment.

Heat-transfer rates along the stagnation streamlines of yawed and unyawed cylinders have been measured in the low-density hypersonic shock tunnel and compared with the analysis of Cheng and Chang[45] by Wittliff and Vidal.[50] The comparison bears out the validity of the independence principle mentioned in Section 3.3.

PART II. EXTENSION OF THE THIN SHOCK LAYER APPROACH

The study in Part I reveals clearly that the thin-shock-layer approximation, appropriately modified to take account of the transport effects, simplifies and unifies analyses in both the low and high Reynolds number regimes. In Part II, this approach will be extended to study flow regions other than, or removed from, the stagnation region; a treatment of the shock-transition zone is included. In Section 5 below, the basic flow model will be developed, the problem formulated, and the adequacy as well as limitations of the approach discussed. Section 6 will present and discuss a numerical method based on a finite difference approximation for solving the shock-layer equations. The method is applied in Section 7 to study flows over wedge, paraboloid and other simple nonslender shapes. Finally, in Section 8, the thin-shock-layer approach is generalized to include nonequilibrium dissociation and specific analysis is made of the stagnation region.

5. THE THIN SHOCK LAYER APPROACH TO THE VISCOUS BLUNT BODY PROBLEM

In this section, the basic assumptions and the flow models underlying the thin-layer approach will be discussed; equations governing the shock layer and the shock-transition zone will be derived; and the initial-value problem formulated. As examples to demonstrate adequacy of the general formulation, solutions are tested against an exact numerical solution of Van Dyke[12] and Swigart[53] for a paraboloidal shock in the inviscid limit, and against the numerical solution of the stagnation region obtained by Levinsky and Yoshihara[40] in the merged-layer regime.

5.1 The Two-Layer Flow Model

For the purpose of the present analysis, the flow field around the body may be divided into an inner and an outer region as illustrated in Fig. 5.1: the shock layer and the shock-transition zone. For convenience, the surface separating the two regions will be referred to as the "shock interface". The compression ratio ρ/ρ_∞ across the shock-transition zone is assumed to be high. Both regions will be assumed to be thin in comparison with a typical dimension of the body (say the nose radius or a lateral dimension); this assumption is consistent with high compression ratio assumed.

With the exception of the study of Section 7 which deals with the nonequilibrium dissociation, an ideal gas with constant specific heats is assumed.* In the subsequent analyses, a linear viscosity-temperature relation may be adopted. The formulation presented applies to plane and axisymmetric steady flows around smooth, nonslender bodies.** Applications are made mainly to highly cooled surfaces with low wall-to-stagnation temperature ratios.

Let x denote the distance along the body surface and y the distance along the outward normal from the surface; x and y form a pair of orthogonal curvilinear coordinates (refer Fig. 5.1). It is assumed that both the shock layer and the shock-transition region are thin so that $\frac{\partial}{\partial x} \ll \frac{\partial}{\partial y}$.

---

*Implicit in the assumption of constant specific heats is the assumption that internal degrees of excitation, such as molecular vibration and dissociation do not undergo the processes of relaxation. Under this condition, one may assume a zero "bulk viscosity".[6,80]

**The nonslender bodies admissible for the present study can be pointed, but the surface angle must not be small and (except the apex of a pointed body) the surface curvature must be finite.

The Navier-Stokes equations governing the compressible, viscous, heat-conducting flow[4, 24] may then be reduced to the following form, neglecting the transverse and longitudinal curvature effects and retaining only the highest-order derivatives with respect to y in the transport terms.

$$\left.\begin{aligned}
&(\rho u z^{\nu})_x + (\rho v z^{\nu})_y = 0 \\
&p_x - \rho \kappa_c u v + \rho\left(u \frac{\partial}{\partial x} + v \frac{\partial}{\partial y}\right) u = (\mu u_y)_y \\
&p_y + \rho \kappa_c u^2 + \rho\left(u \frac{\partial}{\partial x} + v \frac{\partial}{\partial y}\right) v = \frac{4}{3}(\mu v_y)_y \\
&\rho\left(u \frac{\partial}{\partial x} + v \frac{\partial}{\partial y}\right)\left(h + \frac{u^2 + v^2}{2}\right) = \left[\mu\left(\frac{h}{P_r} + \frac{u^2}{2} + \frac{2}{3} v^2\right)_y\right]_y
\end{aligned}\right\} \quad (5.1)$$

Here u is the velocity component along x ; v , velocity component along y ; ρ , the density, p , the pressure; h , the specific enthalpy; μ , the coefficient of viscosity; z the distance of the body surface from the axis of symmetry; κ_c , the longitudinal curvature of the surface $\frac{d\beta}{dx}$. The index ν is zero for plane flow and unity for axisymmetric flow. P_r is the Prandtl number. These flow variables are further related through the equation of state $p = R\rho T$, $h = c_p T$, and the relation between μ and T . In the above equations, both the transverse curvature effect, as well as the higher-order longitudinal curvature effects, have been neglected.

The system of Eq. (5.1) which has been given previously by Hayes and Probstein[4] is valid in the shock layer and in the shock-transition zone to within errors of the order Δ/a and δ_s/a , respectively. To the same degree of accuracy, the coordinates (x , y), and the corresponding velocity components (u , v), in the system of Eq. (5.1) may also be interpreted as the coordinates and velocities parallel and normal to the shock interface instead of to the body surface. The terms $-\rho \kappa_c u v$ in the second of Eq. (5.1) and

the term $\rho u \frac{\partial v}{\partial x}$ in the third of Eq. (5.1) actually belong to the higher orders and can be neglected. One may note that the system of Eq. (5.1) is parabolic.* To be more precise, Eq. (5.1) has a degenerated characteristic pair $dy/dx = \pm\infty$, similar to the boundary-layer equations of compressible flow. Equations (5.1) can, however, be simplified further in the shock-layer region and in the shock-transition zone.**

5.2 Governing Equations in the Shock Layer

Because of the high compression ratio across the shock-transition zone, one has in the shock layer, in addition to the simplification $\frac{\partial}{\partial x} \ll \frac{\partial}{\partial y}$,

$$\rho_\infty/\rho \ll 1 \tag{5.2}$$

This implies that the normal velocity component within the shock layer is small, or more specifically,

$$\frac{v}{U_\infty \sin\beta} \ll 1 \tag{5.2a}$$

One notes that the ratio v/u is usually small in the shock layer, but there is no requirement that it has to remain small. This observation is essential with respect to the validity of the following equations in the stagnation region. Anticipating that p is of the order of $\rho_\infty U_\infty^2 \sin^2\beta$, and u is of the order $U_\infty \cos\beta$ and less within the shock layer, Eq. (5.1) can be further simplified to

---

*If terms of order $(\Delta + \delta_s)/a$ in the Navier-Stokes equations were also retained, the partial differential equations would contain such terms as u_{xy}, v_{xy}, etc. and would therefore appear to be hyperbolic. One still has an initial-value problem, however.

**The subsequent formulations of the problem in the two flow regions are comparable to solving Eq. (5.1) by a procedure of inner and outer expansion under the assumption of high compression ratio across the shock.

$$
\left.
\begin{aligned}
&(\rho u z^{\nu})_x + (\rho v z^{\nu})_y = 0 \\
&p_x + \rho\left(u\frac{\partial}{\partial x} + v\frac{\partial}{\partial y}\right)u = (\mu u_y)_y \\
&p_y + K_c \rho u^2 = 0 \\
&\rho\left(u\frac{\partial}{\partial x} + v\frac{\partial}{\partial y}\right)H = \left\{\frac{\mu}{P_r}\left[H - (1-P_r)\frac{u^2}{2}\right]_y\right\}_y
\end{aligned}
\right\} \qquad (5.3)
$$

where H is the total enthalpy. The system Eq. (5.3) which is to be applied in the shock layer is subject to a fractional error of the order Δ/a, or ε. This system differs from the boundary-layer equations only in one respect, namely, the pressure variation across the layer is no longer negligible and is, in fact, accounted for here by the same equation as for the inviscid shock layer. One may note that in the present formulation the tangential pressure gradient p_x, which has been generally regarded as a higher-order term in the existing inviscid theory, is retained. As has been observed,[41] this term will be important near the body surface when the Reynolds number is high, since the flow speed near the base of the shock layer is of the order $\sqrt{\varepsilon}\, U_\infty$ instead of U_∞ according to inviscid theory. The term p_x is therefore retained as a principal term in order to insure uniform validity of the equation at the higher Reynolds numbers. This is essential for a correct description of the boundary-layer phenomena under the present formulation.

Before turning to the shock-transition zone, one should recall that there are two well recognized shortcomings of the inviscid shock-layer theory which would also appear to affect the present approach. One is the breakdown of the approximation at a certain critical region on a convex body, corresponding to the shock-layer "separation" at the zero-pressure point.[4,18-21] This difficulty

is not found, however, with certain shapes such as the cones, paraboloids and hyperboloids to be studied. In any case, the viscous effect tends to reduce the flow speed, thus the centrifugal action, and delay the separation. The second difficulty has to do with the slow convergence of the Newtonian series, familiar from the work of Chester,[54] which renders the leading approximation worthless. This shortcoming, however, is not applicable to the present formulation. As is apparent from a discussion by Van Dyke,[4,55] the inaccuracy may be traced back to the tangential-pressure-gradient term p_x disregarded in the leading approximation. The present formulation, which has included p_x as a principal term, averts this difficulty as will be demonstrated by subsequent examples in Section 5.6.

5.3 Governing Equations in the Shock-Transition Zone

From the existing analyses of the shock-wave structure in one dimension,[55-57] one may anticipate the normal velocity component v to vary more or less in an anti-symmetric manner with respect to y between the two limits

$$O(\varepsilon) \leq \frac{v}{U_\infty \sin\beta} \leq 1 \tag{5.4}$$

It follows that, excluding a layer of thickness $\varepsilon \delta_s$ near the shock interface (see Fig. 5.1), one has in the shock-transition zone

$$\frac{v}{u} \geq O(1) \tag{5.5}$$

Anticipating $\rho v \sim \rho_\infty U_\infty \sin\beta$, it also follows from Eq. (5.4) that in the shock-transition zone (again excluding the region near the shock interface)

$$\frac{\rho}{\rho_\infty} = O(1) \tag{5.6}$$

That is, the density in the shock-transition zone is generally at the (low) free-

stream level. One must note the fact that an anti-symmetric normal-velocity profile will give a highly asymmetric density profile for high compression ratio, since $\rho \propto \frac{1}{v}$. This explains why the average density through the shock-transition zone is so low compared to the density at the interface. In any case, the assumptions related to Eqs. (5.5) and (5.6) are readily verified a posteriori.

For the study of the shock-transition zone, it will be more convenient to employ the system of orthogonal coordinates in which the surface $y = 0$ coincides with the shock interface.

Using Eqs. (5.5) and (5.6) and the thin-layer assumption, the system of Eq. (5.1) is then reduced simply to

$$\left.\begin{aligned} &(\rho v)_y = 0 \\ &\rho v u_y = (\mu u_y)_y \\ &p_y + \rho v v_y = \tfrac{4}{3}(\mu v_y)_y \\ &\rho v\left(h + \frac{u^2+v^2}{2}\right)_y = \left\{\mu\left[\frac{h}{Pr} + \frac{u^2}{2} + \frac{2}{3}v^2\right]_y\right\}_y \end{aligned}\right\} \qquad (5.7)$$

which can be simply integrated to yield a system of first-order ordinary differential equations governing the shock-transition zone

$$\left.\begin{aligned} &\rho v = \rho_1 v_1 \\ &p + \rho_1 v_1 v - \tfrac{4}{3}\mu v_y = \rho_1 v_1^2 \\ &\rho_1 v_1 u - \mu u_y = \rho_1 v_1 u_1 \\ &\rho_1 v_1\left(h + \frac{u^2+v^2}{2}\right) - \mu\left(\frac{h}{Pr} + \frac{u^2}{2} + \frac{2}{3}v^2\right)_y = \rho_1 v_1\left(h_1 + \frac{u_1^2+v_1^2}{2}\right) \end{aligned}\right\} \qquad (5.8)$$

where the subscript 1 refers to the upstream condition, with $\rho_1 = \rho_\infty$, $h_1 = h_\infty$, $u_1 = U_\infty \cos\beta$ and $v_1 = -U_\infty \sin\beta$.

Noting that, immediately behind the shock, $v \ll v_1$, the system of equations Eq. (5.8) after neglecting terms of order v is seen to include the modified Rankine-Hugoniot shock relations of Refs. 41 and 42:

$$\left.\begin{aligned} \rho_2 v_2 &= \rho_1 v_1 \\ p_2 &= \rho_1 v_1^2 \\ \rho_1 v_1 (u_2 - u_1) &= (\mu u_y)_2 \\ \rho_1 v_1 (H_2 - H_1) &= \left\{ \frac{\mu}{Pr} \left[H - (1 - Pr) \frac{u^2}{2} \right]_y \right\}_2 \end{aligned} \right\} \qquad (5.9)$$

where the subscript 2 refers to the condition at the shock interface.

If the alternative coordinate system is used in which the surface $y = 0$ coincides with the body instead of with the interface, the first of the system of Eq. (5.7) should be written as $\left[\rho \left(v - \frac{d\Delta}{dx} u\right)\right]_y = 0$. The term $\frac{d\Delta}{dx} u$ accounts for the fact that maximum gradients do not occur in the same direction as the normal to the body-surface, and is important near the interface where v becomes small and of order εU_∞. The appearance of this term does not materially complicate the matter. The whole system of the governing equations can be written, without increasing the degree of inaccuracy, in a form identical to Eq. (5.7) with v replaced by $\left(v - \frac{d\Delta}{dx} u\right)$.

The simplified Eq. (5.7) is not strictly valid in the neighborhood of the shock interface, i.e., in the shaded region of Fig. 5.1. However, the equations after integration with respect to y (the distance along the normal to the interface), that is Eqs. (5.8) as well as shock relations Eqs. (5.9), are valid uniformly. The remainder in each of these integrated equations causes an error in the solution, which is at most of the order

$$\frac{\int (\rho u)_x \, dy}{\rho v} \sim \frac{\delta_s}{a} \ln \frac{\rho}{\rho_\infty} \qquad (5.10)$$

where the integral is taken over the shock-transition zone.

One should note that the modified Rankine-Hugoniot shock relation Eq. (5.9) does not contain any information on the shock-wave structure. A

similar set of shock relations has been proposed previously by Sedov, Michailova and Chernyi[56] for the case in which the transport effects are weak. The theoretical basis for neglecting the shock thickness-curvature effects has not been provided, however. It is interesting to note that, in view of the appearance of the velocity and enthalpy gradients in these modified shock relations, the tangential velocity and the total enthalpy will change across the shock in a manner quite similar to the slip and temperature jump across the Knudsen layer next to a body surface. With Eq. (5.9) as an outer boundary condition, the shock-layer region can be analyzed independently of the shock-transition zone. Before formulating the shock-layer problem, however, thetreatment of the shock-transition zone will be further simplified.

5.4 Treatment of the Shock-Transition Zone

The equations governing the shock-transition zone have been reduced, in a manner consistent with the thin-shock-layer approximation, to a system of first-order ordinary differential equations, namely, Eq. (5.8). One notes that that system has satisfied the flow condition upstream of the shock, and that the boundary conditions for this first-order system are to be furnished by the shock-layer solution at the interface. In the following, the shock-transition zone problem will be further reduced under the assumption of a Prandtl number of 3/4 to the solution of a single first-order differential equation.

It is convenient to introduce the nondimensional quantities

$$\left.\begin{aligned} &\bar{u} \equiv \frac{u}{u_1} \quad , \qquad \bar{v} \equiv \frac{v}{v_1} \quad , \\ &\bar{p} \equiv \frac{p}{\rho_1 v_1^2} \quad , \qquad \bar{T} \equiv \frac{T}{T_0} \quad , \qquad \bar{\rho} \equiv \frac{\rho}{\rho_1} \end{aligned}\right\} \tag{5.11}$$

To eliminate the viscosity μ , one introduces the transformation

$$\bar{\eta} \equiv \frac{3}{4} \sin\beta \, \rho_\infty U_\infty \int_{y_2}^{y} \frac{dy}{\mu} \tag{5.12}$$

or

$$\bar{\eta} \equiv \frac{3}{4} \sin\beta \, Re_b \int_{y_2}^{y} \left(\frac{\mu_0}{\mu}\right) d\left(\frac{y}{a}\right)$$

where y_2 gives the location of the shock interface. In terms of this new variable $\bar{\eta}$ and the dimensionless variables $\bar{u}$, $\bar{v}$, etc., the system Eq. (5.9) is reduced to

$$\left.\begin{aligned} &\bar{\rho}\bar{v} = 1 \\ &\bar{p} + \bar{v} + \bar{v}_{\bar{\eta}} = 1 \\ &\bar{u} + \frac{3}{4}\bar{u}_{\bar{\eta}} = 1 \\ &\bar{H} + \frac{3}{4\,Pr}\left[\bar{H} + (Pr-1)\cos^2\beta\,\bar{u}^2 + \left(\frac{4}{3}Pr - 1\right)\sin^2\beta\,\bar{v}^2\right]_{\bar{\eta}} = 1 \end{aligned}\right\} \tag{5.13}$$

where

$$\bar{H} \equiv \bar{T} + \cos^2\beta\,\bar{u}^2 + \sin^2\beta\,\bar{v}^2$$

To complete this system of differential equations, one requires the equation of state in terms of the new variables

$$\bar{p} = \varepsilon \frac{\bar{\rho}\bar{T}}{\sin^2\beta} \tag{5.14}$$

Note that the equations governing the tangential velocity $\bar{u}$ can be integrated independently of the rest of Eq. (5.13) to give

$$\bar{u} = 1 - (1 - \bar{u}_2)\, e^{-\frac{4}{3}\bar{\eta}} \tag{5.15}$$

where $\bar{u}_2$ is the boundary value for $\bar{u}$ to be furnished by the shock-layer solution at the shock interface. For a Prandtl number of 3/4, having determined $\bar{u}$, the last of Eq. (5.13) governing the total enthalpy $\bar{H}$ can also be

simply integrated, giving

$$\bar{H} = 1 - (1 - \bar{H}_2) e^{-\bar{\eta}} + 2 \cos^2\beta (1 - \bar{u}_2) e^{-\bar{\eta}} \left(1 - e^{-\bar{\eta}/3}\right) - \frac{2}{5} \cos^2\beta (1 - \bar{u}_2)^2 e^{-\bar{\eta}} \left(1 - e^{-5\bar{\eta}/3}\right) \tag{5.16}$$

where $\bar{H}_2$ is the boundary value for $\bar{H}$.

In passing, one may note that the requirement of continuity of the tangential velocity u and total enthalpy H across the interface, as is implicit in the provision of $\bar{u}_2$ and $\bar{H}_2$ by the shock-layer solution, also guarantees the continuity of the gradients u_y and H_y in the present formulation.

To eliminate $\bar{p}$ in the second of Eq. (5.13), one makes use of the equation of state (5.14). With the help of the definition of $\bar{H}$ and the continuity relation $\bar{\rho} = \frac{1}{\bar{v}}$, the analysis of the problem is finally reduced to

$$\frac{d\bar{v}}{d\bar{\eta}} + (1 - \varepsilon)\bar{v} + (\csc^2\beta)(\bar{H} - \cos^2\beta\, \bar{u}^2) \frac{\varepsilon}{\bar{v}} = 1 \tag{5.17}$$

where $\bar{H}$ and $\bar{u}$ have been determined by Eqs. (5.15) and (5.16). Note that the magnitude of $\bar{v}$ varies from unity at upstream infinity $(\bar{\eta} \to \infty)$ to order ε near the shock interface $(\bar{\eta} \to 0)$. Concerning the term associated with $\varepsilon/\bar{v}$ in Eq. (5.17), one must notice two essential facts. First, as the interface is approached, this term (being inversely proportional to $\bar{v}$) becomes the most important one in the equation and cannot be dropped even though it is proportional to ε . Second, with this term retained, the condition of continuity of the normal velocity at the interface is automatically satisfied (to the leading approximation) by the solution to Eq. (5.17). This follows from the observation that, when $\bar{v}$ becomes of order ε , Eq. (5.17) gives

$$\bar{v} \approx \varepsilon \csc^2\beta \left(\bar{H}_2 - \cos^2\beta\, \bar{u}_2^2\right) + O(\varepsilon^2)$$

which is essentially the same value provided by the shock-layer solution at the shock layer's outer edge.

Taking advantage of the first-order continuity of v, one may prescribe $\bar{v}_{\bar{\eta}}$ at $\bar{\eta} = 0$ as the boundary condition for Eq. (5.17). This will thus insure continuity (matching) in both v and v_y within the degree of approximation considered.

The boundary condition for Eq. (5.17) may now be written as

$$\frac{d\bar{v}}{d\bar{\eta}} = -\frac{4a}{3Re_b U_\infty \sin\beta}\left(\frac{\mu}{\mu_0}\right)_2\left(\frac{\partial v}{\partial y}\right)_2 \qquad (\bar{\eta} = 0) \qquad (5.18)$$

where $(\mu/\mu_0)_2$ and $(\partial v/\partial y)_2$ are to be provided by the solution to the shock-layer equations.*

It may be noted, however, that if one were to prescribe $\bar{v}$ instead of $d\bar{v}/d\bar{\eta}$ at the shock interface, the continuity in both $\bar{v}$ and its first derivative could not be generally achieved. This is because, on account of the term $\varepsilon/\bar{v}$ in Eq. (5.17), even a change of order ε^2 in $\bar{v}$ at $\bar{\eta} = 0$ will critically affect the leading approximation of $d\bar{v}/d\bar{\eta}$ at $\bar{\eta} = 0$.

After determining $\bar{v}$ from Eq. (5.17) and (5.18), $\bar{\rho}$ can be obtained from $1/\bar{v}$, $\bar{T}$ from the definition of $\bar{H}$, and $\bar{p}$ from the equation of the state. The coordinate y corresponding to $\bar{\eta}$ may finally be determined

*In the stagnation region, $(\partial v/\partial y)_2$ on the right-hand side of Eq. (5.18) can be evaluated from (refer to List of Symbols) $\left(\frac{\partial v}{\partial y}\right)_2 = -\frac{U_\infty}{a}(1+\nu)\bar{u}_2\left[1+\frac{\partial}{\partial\bar{r}}\ln\bar{T}\right]_2$, if the normal velocity v determined from the shock-layer solution is based on a coordinate system with $y = 0$ coincide with the body surface, $\left(\frac{\partial v}{\partial y}\right)_2$ in Eq. (5.18) should be replaced by $\left(\frac{\partial v}{\partial y}\right)_2 - \left(\frac{d\Delta}{dx}\right)\left(\frac{\partial u}{\partial y}\right)_2$.

from the inverse of the transform Eq. (5.17).

Finally, one notes that, in the limit of infinite Reynolds number the Rankine-Hugoniot relations hold, and $\bar{u}_2 \longrightarrow \bar{H}_2 \longrightarrow 1$. In this limit, the solutions given by Eqs. (5.15) and (5.16) degenerate to $\bar{u} \longrightarrow 1$ and $\bar{H} \longrightarrow 1$; and Eqs. (5.17) and (5.18) reduce to

$$\left.\begin{aligned} &\frac{d\bar{v}}{d\bar{\eta}} + (1-\varepsilon)\bar{v} + \frac{\varepsilon}{\bar{v}} = 1 \\ &\frac{d\bar{v}}{d\bar{\eta}} = 0 \qquad (\bar{\eta} = 0) \end{aligned}\right\} \tag{5.19}$$

The solution for $\bar{v}$ may then be obtained by a separation of variables and corresponds to that of Becker and others.[57,58,59] In the general case, a simple quadrature of Eqs. (5.17) does not seem to be obvious in view of the dependence of $\bar{H}$ and $\bar{u}$ on $\bar{\eta}$.* The numerical integration of Eq. (5.17) is, however, rather straightforward. An example is given and discussed in Section 5.6.

In passing, it may be pointed out that the present analysis of the shock-transition zone differs from the usual one-dimensional analysis only in the boundary condition at the inner edge. It provides a generalization to include downstream nonuniformity under the assumption of $\delta_s/a \ll 1$.

5.5 Formulation of the Shock-Layer Problem

To complete the description of the shock-layer region, one has to specify the boundary conditions at the body surface. The velocity slip and temperature

*A "uniformly valid approximation" to the solution of Eq. (5.17) is nevertheless possible in which Eq. (5.17) is solved with $\bar{H}$ and $\bar{u}$ taken as constants evaluated at $\bar{\eta} = 0$.

jump at the surface, according to the theories of Maxwell and Smoluchowski (see, for example, Ref. 60), are proportional to the local mean-free path and the gradients of velocity and temperature at the surface. These effects have been investigated by many within the framework of the boundary-layer theory (see Section 1 of Part I). Making use of expressions for the momentum and energy fluxes provided by the Navier-Stokes equations, one arrives at the following estimates, in terms of the skin-friction and heat-transfer coefficients c_f and c_H

$$\left.\begin{aligned} \frac{T-T_w}{T_0} &\sim \frac{\mu_w c_p}{\rho_w \sqrt{\gamma R T_w}\, k T}\left(k \frac{\partial T}{\partial y}\right)_w \sim \sqrt{\varepsilon \frac{T_w}{T_0}}\left(1-\frac{T_w}{T_0}\right) c_H \\ \frac{u}{U_\infty} &\sim \frac{\left(\mu \frac{\partial u}{\partial y}\right)_w}{U_\infty \rho_w \sqrt{\gamma R T_w}} \sim \sqrt{\varepsilon \frac{T_w}{T_0}}\, \frac{u_1}{U_\infty} \cdot c_f \end{aligned}\right\} \qquad (5.20)$$

The magnitudes of c_H and c_f are small in most flow regimes and cannot exceed unit order. Hence, for a thin shock layer ($\varepsilon \ll 1$) and a cold surface $\left(\frac{T_w}{T_0} \ll 1\right)$, the velocity slip and temperature jump at the surface are small. In the present study, non-slip boundary conditions will be used. A correction for these effects can be made afterwards, if necessary.

For the present approach, it is advantageous to use the von Mises coordinates (x , ψ), where ψ is the stream function defined by

$$\frac{\partial \psi}{\partial x} = -(2\pi \bar{z})^{\nu} \rho v, \qquad \frac{\partial \psi}{\partial y} = (2\pi \bar{z})^{\nu} \rho u \qquad (5.21)$$

The equations governing the thin shock layer, Eq. (5.3), may then be recast into the form

$$\left.\begin{aligned} \frac{\partial p}{\partial \psi} &= -\frac{k_c u}{(2\pi \bar{z})^{\nu}} \\ u \frac{\partial u}{\partial x} &= (2\pi \bar{z})^{2\nu}\, u \frac{\partial}{\partial \psi}\left(\mu \rho u \frac{\partial u}{\partial \psi}\right) - \frac{1}{\rho}\frac{\partial p}{\partial x} \\ \frac{\partial H}{\partial x} &= (2\pi \bar{z})^{2\nu} \frac{\partial}{\partial \psi}\left\{\frac{\mu}{P_r} \rho u \frac{\partial}{\partial \psi}\left[H + (P_r - 1)\frac{u^2}{2}\right]\right\} \end{aligned}\right\} \qquad (5.22)$$

The inner boundary condition is, at $\psi = 0$,

$$u = 0 , \qquad H = H_w \tag{5.23}$$

and the outer boundary condition is provided by the modified Rankine-Hugoniot shock relations, Eq. (5.9), as

$$\left.\begin{aligned} p &= \rho_\infty U_\infty^2 \sin^2\beta \\ u &= U_\infty \cos\beta - (2\pi\bar{z})^{\nu} \frac{\mu\rho u}{\rho_\infty U_\infty \sin\beta} \frac{\partial u}{\partial \psi} \\ H &= H_\infty - (2\pi\bar{z})^{\nu} \frac{\mu\rho u}{Pr\,\rho_\infty U_\infty \sin\beta} \frac{\partial}{\partial\psi}\left[H + (Pr-1)\frac{u^2}{2}\right] \end{aligned}\right\} \tag{5.24}$$

These equations are to be applied at the shock interface where $\psi = \rho_\infty U_\infty \bar{z}(\pi\bar{z})^{\nu}$. Note that under the present approximation, $\bar{z}$ can be taken as either the shock surface or the body surface. The system of Eqs. (5.22), (5.23) and (5.24) completely determines the flow quantities u, H and p in terms of the variables x and ψ for a given surface $\bar{z} = \bar{z}(x)$. The normal velocity v, the coordinate y corresponding to ψ, as well as the location of the shock interface, can be determined through Eq. (5.21).

Of interest is the behavior of the solution to Eqs. (5.22) to (5.24) in the formal limit of zero Reynolds number. On account of the predominance of the transport effects at this limit, solutions to Eq. (5.22) will be characterized by a uniform distribution of v, T, p, $\mu\frac{\partial u}{\partial y}$, and $k\frac{\partial T}{\partial y}$ across the shock layer. Hence, the values of the last three quantities at the body surface will be provided by the shock relations Eq. (5.24), giving

$$p_w = p_2 = \rho_\infty U_\infty^2 \sin^2\beta$$

$$\tau_w = \left(\mu \frac{\partial u}{\partial y}\right)_2 = \rho_\infty U_\infty^2 \sin\beta\cos\beta$$

$$Q_w = \left(k \frac{\partial T}{\partial y}\right)_2 = \rho_\infty U_\infty (H_\infty - H_w) \sin\beta$$

These limiting values are no more nor less than the pressure, stress and heat-transfer rate in a hypersonic, free-molecule flow for unit surface accommodation coefficients.*

The errors introduced in the application of Eqs. (5.22) to (5.24) belong, respectively, to the orders Δ/a , $\sqrt{\varepsilon\, T_w/T_o}$ and $\delta \ln \varepsilon/a$. In the present study, only cold surfaces will be considered. The analyses will be further limited to regimes where the shock cannot be thicker than the shock layer, i.e. $\delta_s \leq O(\Delta)$. Under these restrictions, the errors in the analyses may be kept at essentially the same order as ε , or, at most, $\varepsilon \ln \varepsilon$.

The above condition, $\delta_s \leq O(\Delta)$, may be expressed with the help of estimates based on the Navier-Stokes equations in terms of the parameter K^2 previously introduced. The essential requirements for the present formulation may then be written as**

$$\varepsilon \ll 1 \quad , \qquad K^2 \geq O(1)$$

which are consistent with Eq. (3.2) of Part I. Implicit herein, of course, is also the hypersonic condition $\varepsilon M_\infty^2 \gg 1$. With some sacrifice in accuracy, the present formulation could also be extended to cover completely the fully-merged-layer regime of Probstein and Kemp.[10] At the lower Reynolds-number end of the latter regime $(\delta_s \sim \sqrt{\varepsilon}\, a)$, the errors in the present theory would become $\sqrt{\varepsilon} \ln \varepsilon$ instead of $\varepsilon \ln \varepsilon$.

---

*For the surface pressure to be correct, one requires, in addition to a unit surface accommodation coefficient for the normal component, that $T_w/T_o \ll 1$.

**For pointed bodies, the quantity a in $K^2 \equiv \varepsilon \frac{\rho_\infty U_\infty a}{\mu_*} \cdot \frac{T_*}{T_o}$ must be replaced of course by a length representative of the lateral dimension of the body.

Thus, using an approximation consistent with the thin-shock-layer concept, one can determine the hypersonic viscous flow field around a blunt body independent of the structure of the shock-transition zone, even though the shock and shock layer are comparable in thickness. The above formulation clearly indicates that insofar as the skin friction and heat-transfer characteristics are concerned, the shock-wave structure and related thickness-curvature effects are only secondary in importance. For purpose of analysis, the shock-transition zone may be treated as a surface of discontinuity located at the outer edge of the shock layer.

As do the boundary-layer equations, the partial differential equations Eq. (5.22) lead to an initial-value problem. With u , H and ρv specified at any station x , the solution can be continued downstream by a forward integration with respect to x , satisfying also the boundary conditions Eqs. (5.23) and (5.24). The method of solution to this system of equations will be discussed and developed in Section 6; the theory will be applied to study flows around simple blunt shapes in Section 7.

5.6 Assessment of the Accuracy

Before going on to the applications of Sections 6 to 8, some indication of the accuracy of the present approach is desirable particularly in view of its simplicity. For this purpose, certain results obtained by application of the present theory will be singled out for discussion here. Two comparisons are made with the results of previous, more exact analyses. In one, the shock-layer theory of the present formulation is applied in the inviscid limit to describe the hypersonic flow field and body supporting a paraboloidal shock; the results are then compared with the corresponding "exact" numerical solutions of Van Dyke[1] and

Swigart.[53] In the other, the present theory is compared with a numerical solution of Levinsky and Yoshihara[40] for the stagnation region in the merged-layer regimes. The comparison in the first case bears on the general criticism with regard to the poor degree of approximation of the Newtonian shock-layer theory,[1,4,12,55] as discussed in Section 5.2. The example chosen is particularly meaningful as it has a direct implication for accuracy of the subsequent examples of Section 7. The comparison in the second case provides a crucial test of the present two-layer model.

Paraboloidal Shock in the Inviscid Limit - The inviscid supersonic flow associated with a paraboloidal shock has been analyzed numerically, for $M_\infty \to \infty$, $\gamma = 1.40$, by Van Dyke[1] and Swigart.[53] For the assessment of the accuracy of the thin-shock-layer formulation based on Eqs. (5.22) to (5.24), the same problem has been analyzed in the limit of a vanishing viscosity $\mu \to 0$, using Eqs. (5.13) and (5.15). The non-slip boundary conditions Eq. (5.14) are not used, of course. The results of the analysis are presented in Fig. 5.2 along with the corresponding results of Van Dyke[1] and Swigart.[53] To avoid distraction from the basic point of interest here, the method employed to solve Eqs. (5.22) and (5.24) will not be discussed except to mention that it was similar to the finite difference scheme described in Section 6.

Figure 5.2(a) gives the streamline patterns and the body shapes supporting the paraboloidal bow shock. Figure 5.2(b) presents the pressure distributions along those body surfaces. Unlike the corresponding Newtonian theory (results not shown), the present formulation shows reasonably good agreement with the "exact" solution. The body surfaces predicted by both the exact method and the present approximation agree very well. The present calculation provides a

somewhat higher pressure at the surface; the difference of the two pressure distributions varies from 6% at the stagnation region to about 18% beyond the sonic region. Note that if the pressure were plotted in the form of the pressure ratio $p_B / p_{x=0}$, the agreement would be even better.

One notes in Fig. 5.2(a) a discrepancy in the location of sonic lines in the two analyses. This can, however, be explained by the observation that the changes in Mach number along the streamlines in the shock layer are generally quite slow (the changes being of the order $\sqrt{\varepsilon}$ according to the Newtonian theory). The differences in Mach number at the same point are actually quite small, being typically 15%.

The comparison given above shows that the present version of the thin-shock-layer analysis is reasonably adequate for the study of flow fields associated with a paraboloidal or similar shock. The results have also confirmed the importance of the tangential pressure gradient effect in the analysis of the hypersonic shock layer (cf. Section 5.2).

Merged-Layer Stagnation Region - The analysis of the hypersonic stagnation region in the merged-layer regimes by Levinsky and Yoshihara[40] has been discussed in Section 3 of Part I. The particular set of results of Ref. 40 singled out for the purpose of comparison here was calculated for the case of $M_\infty = 10$, $\gamma = 5/3$ and $Re_F = 100$, corresponding to $\varepsilon = 1/5$ and $K_0^2 = 5$. In their analysis, the Prandtl number was assumed to be 3/4, the wall temperature taken to be equal to the free-stream value, and the viscosity law $\mu \propto \sqrt{T}$ adopted. The results for the profiles of temperature, normal velocity and tangential velocity are reproduced in Fig. 5.3 as solid curves. To distinguish from their results, the corresponding analyses based on the two-layer model

described in Section 5.4 and 5.5 are represented in the same figure as circles and triangles. Considering the value $\gamma = 1.667$, the applicability of the thin-shock-layer theory to the present problem should be regarded as being critical.

The present analysis gives a shock interface at $y/a \approx 0.10$. The solution for $y/a \lesssim 0.10$ is obtained by numerical integration of the shock-layer equations of Eq. (5.22) to (5.24) in the stagnation region, and the solution for $y/a \gtrsim 0.10$ is obtained from the transition-zone solution of Eqs. (5.15) to (5.18). The value of $\bar{u}_2$, $\bar{H}_2$ and $(d\bar{v}/d\bar{\eta})_2$ are provided by the shock-layer solution. In addition to the profiles of the normal velocity $\bar{v}$, the temperature $\bar{T}$ and the tangential-velocity gradient $\bar{u}$ which are reproduced from Ref. 40, the corresponding density distribution ρ/ρ_∞ in the shock-transition zone is also calculated and presented in Fig. 5.3 for comparison.

As is evident from the figure, the analysis of Levinsky and Yoshihara and the considerably simplified treatment based on the present formulation agree in all essential details both in the shock layer and in the shock-transition zone. The small difference between the two analyses is somewhat surprising, when one notes that the specific-heat ratio 1.667 is rather far from unity. One notes, however, that the profiles of normal velocity and temperature given by the present analysis are discontinuous at the shock interface $y/a \approx 0.10$. These discontinuities are unavoidable in the present formulation which matches the derivatives of $\bar{v}$ at the interface. However, they are rather small, being of order ϵ^2 as compared to unity, and are indeed consistent with the assumption of the theory (see discussion of the preceding section).

It may be noted that if one were to interpret the length "a" in the shock-

layer solution as the shock radius instead of the body nose radius, as was done in the preceding paraboloidal-shock problem, the abscisa of the circles and triangles in Fig. 5.3 would increase by 10% and result in a better agreement with the solid curves. This interpretation is permissable within the present thin-layer approximation and also implies that the shock and the body are concentric. The latter assumption is in fact implicit in the analysis of Ref. 40.

It must be pointed out that the reasonably good agreement revealed in Fig. 5.3 is by no means an indication of the accuracy of present formulation in the absolute sense, since the analysis of Levinsky and Yoshihara also involves certain approximations. The small differences do demonstrate convincingly, however, the validity and adequacy of the two-layer concept underlying the present formulation. The result of the comparison implies, of course, that the most important aspect of the flow phenomena affecting the aerodynamics and heat transfer in the merged-layer regimes is not the direct effects related to the shock-thickness and the shock-wave structure but rather the slip-like transport effects immediately behind the shock.

6. METHOD FOR SOLVING THE VISCOUS SHOCK LAYER EQUATIONS

With the basic problem formulated and the adequacy of the flow model assessed, the thin-shock-layer theory will now be applied to study hypersonic viscous flows over wedge, paraboloid and other simple blunt shapes. To do so, we must first develop a method which is capable of obtaining nonsimilar solutions to the partial differential equations Eqs. (5.22) to (5.24) governing the shock layer. The present solution to the dissimilar problem requires the combined use of two methods; a forward-integration method based on the finite-

difference approximation, and the solution by series in the vicinity of the leading edge or the stagnation point. The latter solution is required to produce valid initial data for calculation by the finite-difference method.

6.1 Discussion of General Treatment

For the analysis of the shock layer, it is convenient to work with the dimensionless quantities $\bar{u}$, Θ and $\bar{p}$

$$\left.\begin{aligned} \bar{u} &\equiv \frac{u}{U_\infty \cos\beta} \\ \Theta &\equiv \frac{H - H_w}{H_\infty - H_w} \\ \bar{p} &\equiv \frac{p}{\rho_\infty U_\infty^2 \sin^2\beta} \end{aligned}\right\} \qquad (6.1)$$

Introduce the variables

$$\left.\begin{aligned} \lambda &= 2\,\frac{x'}{a} \\ \zeta &= \sqrt{\psi/\rho_\infty U_\infty (r z)^\nu z} \end{aligned}\right\} \qquad (6.2)$$

Note that x' is the distance measured along the axis of symmetry (cf Fig. 5.1) related to x through $(dx)^2 = (dx')^2 + (dz)^2$, and that $\bar{u}$ and Θ behave like $\sqrt{\psi}$ near the body surface and therefore will be regular in ζ . In terms of the new variables of Eq. (6.1) and (6.2), the system of differential equations Eqs. (5.22) is transformed to

$$
\begin{aligned}
\bar{u}\,\bar{u}_\lambda &= \tan\beta\,\frac{d\beta}{d\lambda}\cdot\bar{u}^2 - \varepsilon\left[\frac{T_w}{T_o}+\left(1-\frac{T_w}{T_o}\right)\Theta-\bar{u}^2\cos^2\beta\right]\left(\frac{2\tan\beta}{\sin^2\beta}\frac{d\beta}{d\lambda}+\frac{\bar{p}_\lambda}{\cos^2\beta}\cdot\frac{1}{\bar{p}}\right)\\
&\quad+\left(\frac{1+\nu}{2}\right)\left(\frac{1}{\bar{z}}\frac{d\bar{z}}{d\lambda}\right)\frac{\bar{u}}{\zeta}\,\bar{u}_\zeta-\left(\frac{1+\nu}{2}\right)\sigma^3\cos\beta\frac{d\beta}{d\lambda}\frac{N}{K^2}\frac{\bar{u}^3}{\zeta}\,\bar{u}_\zeta\\
&\quad+\left(\frac{1+\nu}{2}\right)^2\left(\frac{\sigma}{\cos\beta}\right)^2\frac{\bar{p}\,\bar{u}}{2K^2\zeta}\left[N\frac{\bar{u}}{\zeta}\,\bar{u}_\zeta\right]_\zeta\\
\Theta_\lambda &= \left(\frac{1+\nu}{2}\right)\left[\left(\frac{1}{\bar{z}}\frac{d\bar{z}}{d\lambda}\right)\zeta\,\Theta_\zeta-\sigma^3\cos\beta\frac{d\beta}{d\lambda}\frac{N}{PrK^2}\frac{\bar{u}^2}{\zeta}\Theta_\zeta\right.\\
&\quad\left.-2\sigma^3\cos^3\beta\frac{d\beta}{d\lambda}\frac{\cos^2\beta N}{K^2}\frac{\left(1-\frac{1}{Pr}\right)}{\left(1-\frac{T_w}{T_o}\right)}\frac{\bar{u}^3}{\zeta}\,\bar{u}_\zeta\right]\\
&\quad+\left(\frac{1+\nu}{2}\right)^2\left(\frac{\sigma}{\cos\beta}\right)^2\frac{\bar{p}}{2PrK^2\zeta}\left[N\frac{\bar{u}}{\zeta}\Theta_\zeta\right]_\zeta+\left(\frac{1+\nu}{2}\right)^2\frac{\sigma^2}{K^2}\frac{\left(1-\frac{1}{Pr}\right)}{\left(1-\frac{T_w}{T_o}\right)}\frac{\bar{p}\,\bar{u}}{\zeta}\left[N\frac{\bar{u}}{\zeta}\,\bar{u}_\zeta\right]_\zeta\\
\bar{p}_\zeta &= -\left(\frac{2}{1+\nu}\right)2\sigma\cos^3\beta\frac{d\beta}{d\lambda}\cdot\bar{u}\cdot\zeta
\end{aligned}
\qquad (6.3)
$$

where

$$N \equiv \frac{\mu}{\mu_*}\cdot\frac{T_*}{T} \qquad \text{and} \qquad \sigma \equiv \frac{\sin\beta\cos\beta}{\bar{z}/a}$$

The subscripts λ and ζ denote partial derivative with respect to λ and ζ. As before, the parameter K^2 is defined as

$$K^2 \equiv \varepsilon\frac{\rho_\infty U_\infty a}{\mu_o}\left(\frac{\mu_o}{\mu_*}\frac{T_*}{T_o}\right) = \varepsilon\,Re_b\left(\frac{\mu_o}{\mu_*}\cdot\frac{T_*}{T_o}\right)$$

where T_* and μ_* are the reference temperature and the corresponding viscosity respectively. If the linear representation $\mu/\mu_* = T/T_*$ is adopted, the factor N in the above equations becomes unity. The boundary conditions at the surface $\zeta = 0$, Eq. (5.23), becomes

$$\bar{u} = \Theta = 0 \qquad (6.4)$$

The shock relations at the outer edge of the shock layer, Eq. (5.24), become

$$\left.\begin{aligned} \bar{u} &= 1 - \left(\frac{1+\nu}{2}\right)\frac{\sigma N}{K^2}\,\frac{\bar{u}\,\bar{u}_\zeta}{\zeta}\,, \qquad \bar{p} = 1 \\ \Theta &= 1 - \left(\frac{1+\nu}{2}\right)\frac{\sigma N}{P_r K^2}\,\frac{\bar{u}\,\Theta_\zeta}{\zeta} - 2\cos^2\beta\,\frac{\left(1-\frac{1}{P_r}\right)}{\left(1-\frac{T_w}{T_0}\right)}\,\bar{u}\,(1-\bar{u}) \end{aligned}\right\} \quad (6.5)$$

These relations are now to be satisfied at $\zeta = 1$. The relation between the physical distance y from the body surface and ζ can be determined from

$$\frac{y}{\varepsilon Z} = \left(\frac{2}{1+\nu}\right)\frac{1}{\sigma \sin\beta}\left\{\int_0^\zeta \left[\frac{T_w}{T_0} + \left(1-\frac{T_w}{T_0}\right)\Theta\right]\frac{\zeta\, d\zeta}{\bar{p}\,\bar{u}} - \cos^2\beta \int_0^\zeta \frac{\bar{u}\,\zeta\, d\zeta}{\bar{p}}\right\} \quad (6.6)$$

The local skin friction and the local heat-transfer rate at the surface can be calculated from $\bar{p}$, $\bar{u}_\zeta$ and Θ_ζ at $\zeta = 0$:

$$\left.\begin{aligned} c_f &\equiv \frac{\left(\mu\frac{\partial u}{\partial y}\right)_w}{\frac{1}{2}\rho_\infty U_\infty^2} = \frac{1+\nu}{K^2}\,\sigma^2\left(\frac{x}{z}\right)\bar{p}\,(\bar{u}_\zeta)^2 \\ c_H &\equiv \frac{\left(k\frac{\partial T}{\partial y}\right)_w}{\rho_\infty U_\infty (H_\infty - H_w)} = \frac{1+\nu}{2P_r K^2}\,\sigma(\sin\beta)\,\bar{p}\cdot\bar{u}_\zeta\cdot\Theta_\zeta \end{aligned}\right\} \quad (6.7)$$

Aside from the dependence of the solution on the shock or body shape through β and σ, the system Eqs. (6.3) to (6.5) is governed by the parameters: K^2, ε, T_w/T_0 and P_r. Clearly, K^2 is the most important parameter and controls the transport effects in the shock layer. Following the classification for the stagnation region, Eq. (3.2) of Part I, one may also divide the general shock-layer problem into two regimes. In one, defined by $O(1) \leq \varepsilon K^2 < \infty$, the inviscid shock relations hold, i.e. $\bar{u} \to \Theta \to \bar{p} \to 1$ at $\zeta = 1$. In the other, where $O(\varepsilon) \leq \varepsilon K^2 \leq O(1)$, the speed and enthalpy changes across the shock-transition zone are important.

As noted before, the thin-shock-layer approximation has reduced the governing differential equations to the parabolic type. This makes forward integration in the downstream direction possible. One may note, however,

that the great simplification found in the analysis of the stagnation region cannot be found in the general case. Specifically, an analytical treatment in the merged-layer regimes (Regime II) is not generally possible. Although the differential equations themselves admit a separation of variables (after neglecting the tangential-pressure-gradient term), a self-similar solution does not exist owing to the outer boundary condition Eq. (6.5).

For analysis in the higher Reynolds number regime (Regime I), Eqs. (6.3) to (6.5) may best be handled by transformation to the coordinate system (ξ , η), familiar in boundary-layer theory. However, vorticity-interaction theory based on the boundary-layer approximation can no longer be extended, as is permissible for the stagnation region, to treat the non-linear vorticity effect in the viscous-layer regime. This is because the solution in the more general case cannot be simply described in terms of the asymptotic property of the boundary-layer solution, as in the case of the stagnation region (or, at least, the possibility of such a simple description is not obvious). Of course, for small departures from the boundary-layer limit, the second-order boundary-layer theory is valid. In fact, Hayes' original matching condition, Eq. (1.1)

$$f_\eta^2 = 1 + 2\Omega f \qquad \eta \longrightarrow \infty$$

is consistent with the thin-shock-layer approach and should be generally applicable.* A treatment of the vorticity-interaction theory based on Eq.

---

*Presumably, the alternative condition Eq. (1.3) $f_{\eta\eta}(\infty) = \Omega$ may also apply. To the writer's knowledge, the equivalence of Eqs. (1.1) and (1.3) has not been proved in the general case, however.

(1.1) (which also requires the use of a numerical method to handle the non-similar solution), though not carried out here, may be considered as complementary to the method presently to be described, whose range of validity covers the merged-layer as well as the viscous-layer regimes.

Before passing to the discussion of the two methods employed in the present procedure, the possibility of using momentum-integral methods[4,29,61] as well as other methods familiar from the boundary-layer theories,[62,63] should not be completely overlooked. The main objection to the use of momentum-integral methods which also involve stepwise numerical integration for the present study is its limited range of applicability. This shortcoming is related to the fact that the velocity and temperature profiles of the shock layer in the low and high Reynolds number ranges considered are radically different, and do not permit the simple description characteristic of most integral methods.

6.2 Series Expansion Near Axis of Symmetry

For flow regions not far removed from the axis of symmetry, solution by a series in ascending power of the distance from the axis is possible. Thus for the stagnation region, one may assume a development in $(x/a)^2$ for $\bar{u}$, Θ and $\bar{p}$. In terms of the variables λ and ζ, one has, for the stagnation region of a smooth blunt body (considering only positive λ).

$$\bar{u} = \bar{u}_0 + \lambda \bar{u}_1 + \lambda^2 \bar{u}_2 + \cdots \tag{6.8}$$

with similar developments for Θ and $\bar{p}$. The leading terms $\bar{u}_0$, Θ_0 and $\bar{p}_0$, together with $\bar{p}_1$, determine the solution in the stagnation region for which Eqs. (6.3) to (6.5) reduce to the following system of ordinary differential equations

$$\left.\begin{aligned}
&\bar{u}_o^2 - \left(\frac{1+\nu}{2}\right)\zeta\,\bar{u}_o\bar{u}_o' = \left(\frac{1+\nu}{2K}\right)^2 \frac{\bar{u}_o}{\zeta}\left(N\,\frac{\bar{u}_o\bar{u}_o'}{\zeta}\right)' + 2\varepsilon\left(1-\bar{p}_1\right)\left[\frac{H_w}{H_\infty} + \left(1-\frac{H_w}{H_\infty}\right)\Theta_o\right], \\
&-\zeta^2\Theta_o' = \frac{1+\nu}{2PrK^2}\left(N\,\frac{\bar{u}_o\,\Theta_o'}{\zeta}\right)', \\
&\bar{p}_o' = 0 \\
&\bar{p}_1' = (2-\nu)\,\bar{u}_o\,\zeta
\end{aligned}\right\} \tag{6.9}$$

$$\bar{u}_o(0) = \Theta_o(0) = 0 \tag{6.10}$$

$$\left.\begin{aligned}
&\bar{p}_o(1) = 1, \qquad \bar{p}_1(1) = 0 \\
&\bar{u}_o(1) = 1 - \frac{1+\nu}{2K^2}\,N\,\bar{u}_o(1)\,\bar{u}_o'(1) \\
&\Theta_o(1) = 1 - \frac{1+\nu}{2PrK^2}\,N\,\bar{u}_o(1)\,\Theta_o'(1)
\end{aligned}\right\} \tag{6.11}$$

where the prime ( )' denotes differentiation with respect to ζ . The appearance of $\bar{p}_1$ in the first equations signifies the tangential-pressure-gradient effect. Eqs. (6.9) to (6.11) constitute a two-point boundary-value problem. This analysis of the stagnation region has been discussed in Section 3 of Part I. More detailed results are given in Refs. 42-44.

By collecting terms of the next power of λ in the Eqs. (6.3) to (6.5), one obtains a system of ordinary differential equations governing u_1 , Θ_1 , and $\bar{p}_2$. These equations, given in the Appendix, lead to a two-point boundary-value problem involving a system of linear ordinary differential equations. By virtue of their linearity, however, solution to this two-point boundary-value problem can be obtained simply by superposition of the particular solutions. This considerably simplifies the task of numerical analyses.

The systems of equations governing the coefficients for the higher powers

of λ, $\bar{u}_2$, Θ_2 and $\bar{p}_3$, etc. are similar, but more complex. In the following study of the problems of paraboloidal and hyperboloidal shapes, only the coefficients $\bar{u}_1$, Θ_1 and $\bar{p}_2$ have been determined. The range of validity of the solution based on the two-term representation, $\bar{u}_0 + \lambda \bar{u}_1$, etc., is of course rather limited, but the roles of the coefficients $\bar{u}_1$, Θ_1 and $\bar{p}_2$ are nevertheless crucial for the numerical solution of the downstream flow field, as will be discussed subsequently.

The series solution of the type of Eq. (6.8) is applicable only for a body with finite nose radius. For a pointed body, the appropriate series solutions take the form

$$\begin{aligned} \bar{u} &= \bar{u}_0 \lambda^{1/2} + \bar{u}_1 \lambda + \bar{u}_2 \lambda^{3/2} + \cdots \\ \Theta &= \Theta_0 \lambda^{1/2} + \Theta_1 \lambda + \Theta_2 \lambda^{3/2} + \cdots \\ \bar{p} &= 1 + \bar{p}_1 \lambda^{1/2} + \bar{p}_2 \lambda + \cdots \end{aligned} \tag{6.12}$$

The leading terms for $\bar{u}$ and Θ are simply proportional to ζ. In this case, the successive coefficients $\bar{u}_1$, $\bar{u}_2$, $\bar{u}_3$, etc. can also be determined in explicit analytical form. These developments will be used in the study of wedge and cone flows in Section 7.1.

6.3 Finite-Difference Method

Numerical methods for solving the parabolic and hyperbolic partial differential equations by finite-difference approximations have been quite extensively studied in recent years (for example, see Refs. 64 and 65). The methods have been applied to viscous-flow problems within the context of the boundary-layer theory by a number of investigators.[66-69]

Singularities in the Difference Equations - In the finite-difference approximation, the derivatives are replaced by the quotients of the differences,

and the partial differential equations are satisfied approximately at a finite number of grid or lattice points. For an initial-value problem such as the present one, a forward integration is possible; the solution to the difference equations may then be determined in terms of values obtained at preceding stations or grid lines. That is, the difference approximation is used to evaluate $\partial\bar{u}/\partial\lambda$, $\partial\Theta/\partial\lambda$ in terms of quantities given on the right-hand side of Eq. (6.3). The quantities $\bar{u}$ and Θ are then obtained by integrating with respect to λ. Strictly speaking, this procedure is not applicable to Eq. (6.3) at $\lambda = 0$ and $\zeta = 0$, because some of the terms on the right-hand side of the first and second of Eqs. (6.3) are proportional to

$$\left(\frac{\sigma}{\cos\beta}\right)^2 \frac{\bar{u}}{\zeta^2} \sim \frac{1}{\lambda\zeta}$$

Hence in the limit of either $\lambda \to 0$ or $\zeta \to 0$, the values of $\partial\bar{u}/\partial\lambda$, etc. become indeterminate, or even infinite (in the case of pointed bodies). This leads to two important observations. First, in order to achieve forward integration correctly in the vicinity of the stagnation point $\lambda = 0$, it is most essential to provide the coefficients $\bar{u}_1$, etc. in the series solution of Eq. (6.8), which are in fact the correct expressions for $\partial\bar{u}/\partial\lambda$, etc. at $\lambda = 0$. Starting the integration procedure merely with the knowledge of $\bar{u}_0$, etc., as has been proposed in some previous work,[66,67] cannot yield the correct solution. Second, in view of the factor $1/\lambda\zeta$, errors resulting from the difference approximations will be greatly amplified in the vicinity of the "leading edge" $\lambda = 0$ and at the body surface $\zeta = 0$. As far as the method of difference is concerned, the lines $\lambda = 0$ and $\zeta = 0$ may therefore be regarded as singularities of the equations. It is clear that application of the difference equations must exclude these lines.

The manner in which the difference quotients are formed and in which the equations are approximated gives rise to a variety of difference methods. The best known are the standard explicit and implicit scheme and, in addition, that introduced by Dufort and Frankel.[64,65,70] Near the singularities, the conditions for stability and convergence, together with the small truncation-error requirement, are so stringent that the explicit schemes become hardly practical for the present application.* The implicit scheme, which is subject to none of these restrictions, not only is superior as has been demonstrated by Flugge-Lotz and Blottner for the boundary-layer analyses,[67] but is necessary in the present analysis. This is quite clearly brought out by the conclusion of a recent study of A. L. Chang and the writer,[71] in which the relative merit and efficiency of all three schemes are examined for the case of a cone (the result of which is to be presented in Section 7).

In view of the critical nature of the singularities in amplifying the truncation errors, the regions near $\lambda = 0$ and $\zeta = 0$ will both be excluded. The system of difference equations considered applies therefore only in the domain

$$\left.\begin{aligned} \lambda_0 &\le \lambda \\ \zeta_0 &\le \zeta \le 1 \end{aligned}\right\} \tag{6.13}$$

The boundary condition originally at $\bar{u}(0) = \theta(0) = 0$ can be simply transformed to the new boundary $\zeta = \zeta_0$ by the Taylor theorem

$$0 = \bar{u} - \bar{u}_\zeta \zeta_0 + \bar{u}_{\zeta\zeta} \zeta_0^2 + \cdots \tag{6.14}$$

---

*The stability for the standard explicit scheme would require $\Delta\lambda \le 0\left[\lambda\zeta(\Delta\zeta)^2\right]$, the convergence of the Dufort-Frankel scheme would require $(\Delta\lambda)^2 \ll \lambda\zeta(\Delta\zeta)^2$. Whereas small trunction errors would require $\left[\Delta\lambda + (\Delta\zeta)^2\right]/\lambda\zeta \ll 1$

where $\bar{u}$, $\bar{u}_\zeta$ and $\bar{u}_{\zeta\zeta}$ are evaluated at $\zeta = \zeta_o$. If one applies the first-order correction in the Taylor series, as is done below, the error incurred by shifting the boundary from $\zeta = 0$ to $\zeta = \zeta_o$ will be of the order ζ_o^2 . In the following, the initial data for $\bar{u}$, etc. will be prescribed at $\lambda = \lambda_o$ by the two-term development $\bar{u}_o + \lambda \bar{u}_1$, etc.* The exclusion of $\lambda = \zeta = 0$ in this manner will therefore introduce an error of the order $\left(\lambda_o^2 + \zeta_o^2\right)$. (In most calculations performed λ_o and ζ_o are taken as 0.10.) With the exclusion of the region close to $\lambda = \zeta = 0$, the truncation errors in the difference equations are still very large; solution with acceptable accuracy will require increments $\Delta\lambda$ and $\Delta\zeta$ considerably smaller than λ_o and ζ_o . (In subsequent applications, $\Delta\lambda$ and $\Delta\zeta$ are taken in most cases as 1/100.)

Difference Quotients and Difference Equations - In the implicit scheme (see the sketch on Fig. 6.1) the unknown values of $\bar{u}$ and Θ at point e along a new grid line (column m) are to be solved simultaneously with values at points d, f, etc. along the same grid line using known data from the preceding stations. The difference quotients for $\bar{u}$ derivatives which define the present scheme, are the first terms in the following development

$$\left.\begin{aligned}
\left(\frac{\partial \bar{u}}{\partial \lambda}\right)_e &= \frac{3\bar{u}_e - 4\bar{u}_b + \bar{u}_g}{2(\Delta\lambda)} - \frac{1}{6}(\Delta\lambda)^2\, \bar{u}_{\lambda\lambda\lambda} + \cdots \\
\left(\frac{\partial \bar{u}}{\partial \zeta}\right)_e &= \frac{\bar{u}_f - \bar{u}_d}{2(\Delta\zeta)} - \frac{1}{6}(\Delta\zeta)^2\, \bar{u}_{\zeta\zeta\zeta} + \cdots \\
\left(\frac{\partial^2 \bar{u}}{\partial \zeta^2}\right)_e &= \frac{\bar{u}_f - 2\bar{u}_e + \bar{u}_d}{(\Delta\zeta)^2} - \frac{(\Delta\zeta)^2}{12}\, \bar{u}_{\zeta\zeta\zeta\zeta} + \cdots
\end{aligned}\right\} \qquad (6.14)$$

*To be more precise, the following formulation requires initial data along $\lambda = \lambda_o$ as well as along $\lambda = \lambda_o - \Delta\lambda$.

The difference quotients for θ derivatives are similar. One must note that the difference approximations for $\partial\bar{u}/\partial\lambda$ have been carried out to within an error of order $(\Delta\lambda)^2$ instead of $(\Delta\lambda)$. With these quotients, the partial differential equations Eqs. (6.3) are approximately satisfied at the grid point e. The difference equations can be linearized without sacrificing accuracy by expressing the values of the coefficients of $\frac{\partial\bar{u}}{\partial\zeta}$, $\frac{\partial^2\bar{u}}{\partial\zeta^2}$, etc. in the differential equations at point e in terms of their corresponding values at b and g of the preceding station (refer to Fig. 6.1). This is accomplished through the relation

$$X_e = (2X_b - X_g) - \frac{(\Delta\lambda)^2}{2}(X_e)_{\lambda\lambda} + \cdots \qquad (6.15)$$

where X may be any of the dependent variables. To eliminate the pressure as an unknown in the difference equation, one can replace $\partial\bar{p}/\partial\lambda$ in terms of values of $\bar{p}$ at the preceding three stations b, g and h (see sketch) through

$$\left(\frac{\partial p}{\partial\lambda}\right)_e = 2\left(\frac{\partial p}{\partial\lambda}\right)_b - \left(\frac{\partial p}{\partial\lambda}\right)_g - \frac{(\Delta\lambda)^2}{2}(\bar{p}_e)_{\lambda\lambda\lambda} + \cdots$$
$$= \frac{5\bar{p}_b - 8\bar{p}_g + 3\bar{p}_h}{2(\Delta\lambda)} + O(\Delta\lambda)^2 \qquad (6.16)$$

The pressure $\bar{p}$ can always be obtained after $\bar{u}$ is determined by integrating the third of Eq. (6.3) with respect to ζ. The error resulting from the integration by Simpson's rule is of the order $(\Delta\zeta)^3$. Application of Eqs. (6.14) to (6.16) to the system of differential equations Eqs. (6.3) gives rise to twice as many algebraic equations as the number of points between $\zeta = \zeta_0$ and $\zeta = 1$ along a grid line.

To complete the formulation, one must convert the boundary condition at $\zeta = 1$, Eq. (6.5), and the boundary condition at $\zeta = \zeta_0$, Eq. (6.13), to

two linear algebraic relations among the unknown values of $\bar{u}$ and Θ without introducing new unknowns corresponding to points beyond $\zeta_0 < \zeta < 1$. This can be accomplished by the typical relation

$$\left(\frac{\partial \bar{u}}{\partial \zeta}\right)_f = \frac{1}{2(\Delta\zeta)}\left[3\,\bar{u}_f - 4\bar{u}_e + \bar{u}_g\right] + O(\Delta\zeta)^2 \qquad (6.17)$$

and relations similar to Eq. (6.15). The difference equations at all grid points along the same grid, together with the boundary conditions, form a linear algebraic system sufficient for determining $\bar{u}$ and Θ at all grid points between $\zeta = \zeta_0$ and $\zeta = 1$. The complete system of equations is given in the Appendix. It sufficies to say that the matrix of this system is the tri-diagonal type, and the solution can be obtained by following the standard procedure, e.g. Gauss' elimination method.[65]

Truncation Error - One may now examine more closely the truncation errors in the difference equations. Only the truncation errors associated with the first of Eq. (6.3) need be considered. A similar conclusion applies to the other equations. There are two terms in the remainders of the difference equations which are most critically affected by the singularity $\lambda = 0$ and $\zeta = 0$: one associated with the tangential pressure gradient and the other with the tangential stress term. With the knowledge of the remainders given in Eqs. (6.14) to (6.16), and of the fact that near $\lambda = \zeta = 0$, $\cos\beta \sim \frac{z}{a} \sim \lambda$ and $\bar{u} \sim \zeta$, the fractional error in $\bar{u}$ caused by these two terms may be estimated as

$$\left[\varepsilon \frac{T_w}{T_o} \frac{(\Delta\lambda)^2}{\lambda\zeta^2}\right] \bar{p}_{\lambda\lambda\lambda} + \frac{1}{\lambda\zeta^2}\left[\frac{(\Delta\zeta)^2}{K^2}\,\bar{u}_{\zeta\zeta\zeta\zeta} + \frac{(\Delta\lambda)^2}{K^2}\,\bar{u}_{\zeta\zeta}\,\bar{p}_{\lambda\lambda\lambda}\right]$$

The factors $\bar{u}_{\zeta\zeta\zeta\zeta}/K^2$ and $\bar{u}_{\zeta\zeta}/K^2$ are not large numbers, especially

at $K^2 = O(1)$, because $\bar{u}$ is essentially proportional to ζ for small λ (refer to the discussion in Section 3, Part I). In the merged-layer regimes, at least, the fractional error in $\bar{u}$ cannot exceed

$$\frac{\delta \bar{u}}{\bar{u}} \sim \varepsilon \frac{T_w}{T_o} \frac{(\Delta \lambda)^2}{\lambda_o \zeta_o^2} + \frac{(\Delta \zeta)^2 + (\Delta \lambda)^2}{\lambda_o \zeta_o} \quad ,$$

since

$$\lambda \geq \lambda_o \quad , \quad \zeta \geq \zeta_o$$

Taking $\lambda_o \sim \zeta_o \sim \frac{1}{10}$, and $\Delta\lambda \sim \Delta\zeta \sim \frac{1}{100}$, and $\varepsilon \frac{T_w}{T_o} \leq \frac{1}{10}$, the fractional error $\delta \bar{u} / \bar{u}$ is seen to remain at the level of one percent.

7. STUDY OF FLOWS OVER SIMPLE NONSLENDER SHAPES

The method of solution formulated in the preceding section will now be applied to study hypersonic flow around wedge, cone, paraboloid and hyperboloid shapes at low Reynolds number. Only solutions to the shock-layer region will be discussed below. The flow structure in the shock-transition zone, in each case, can be determined by simply integrating the first-order ordinary differential equations, Eq. (5.13), after the shock-layer solution is obtained.

7.1 Nonslender Cone and Wedge

As examples of flows around pointed bodies, the shock layers on cones and wedges will first be studied. The analysis may provide a basis for assessing the low-density aerodynamic and heat-transfer characteristics of flat surface at high incidence, which could be meaningful to the current lifting re-entry studies.[72-74] From the viewpoint of present approach based on the two-layer concept, the cases considered are interesting in that the curvature of shock above the wedge and cone surfaces is generally

small, and, therefore, the formulation developed in Section 5.5, which has neglected the shock curvature effect, could possess a regime of validity even beyond the limit

$$\frac{\delta_s}{z} \leq O(\varepsilon)$$

On the other hand, the solution will break down in the vicinity of the leading edge because of its singularity at the apex. This will be discussed later.

One may also note that the problem of a flat-plate at zero incidence has been the subject of both theoretical and experimental studies of recent years.[43,50,75-77] Generally speaking, the problem is complicated by the presence of both the boundary-layer displacement and surface-slip effects. However, in the present problem which considers thin shock layers over highly cooled, nonslender cones and wedges, these two effects can be regarded as unimportant compared to the slip-like velocity and enthalpy changes across the shock.

The problem under the present framework is also attractive in that for the case of a linear viscosity law the analysis is reduced to the solution of a single parabolic differential equation governing the velocity. It may therefore serve as a testing ground for the various methods and schemes of solving the shock-layer equations.[71] In this case, the first of Eqs. (6.3) can be alternatively written for $W = \bar{u}^2/2$ as,

$$\bar{x}\frac{\partial W}{\partial \bar{x}} = (1+\nu)\bar{\psi}\frac{\partial W}{\partial \bar{\psi}} + (1+\nu)^2\frac{\sqrt{2W}}{\bar{x}}\frac{\partial^2 W}{\partial \bar{\psi}^2} \qquad (7.1)$$

The boundary conditions, Eqs. (6.4) and (6.5), are

$$\left.\begin{aligned} W &= 0 && (\bar{\psi} = 0) \\ \sqrt{2W} &= 1 - \frac{1+\nu}{\bar{\varkappa}} \frac{\partial W}{\partial \bar{\psi}} && (\bar{\psi} = 1) \end{aligned}\right\} \tag{7.2}$$

Note Eq. (7.1) contains none of parameters K^2, ε, P_r and T_w/T_o. The effects of gas rarefaction and surface incidence, as well as the variation of the reference temperature with respect to $\varkappa$, are all contained in, and therefore can all be correlated by, the variable

$$\bar{\varkappa} \equiv \varepsilon \frac{\rho_\infty U_\infty \varkappa}{\mu_o} \left(\frac{\mu_o}{\mu_*} \frac{T_*}{T_o}\right) \sec\beta \tag{7.3}$$

The appearance of the factor $\sec\beta$ in $\bar{\varkappa}$ signifies the influence of the oblique-shock angle on the local Reynolds number. This is particularly evident, if one considers a linear viscosity-temperature relation and high Reynolds number; in that case, the local velocity varies like $\cos\beta$, and the viscosity like $\cos^2\beta$. To relate the variable $\bar{\varkappa}$ to the Reynolds number based on the free-stream condition, say Re_b, one may use the reference temperature T_*

$$\frac{T_*}{T_o} = \frac{1}{\bar{u}(1)} \int_0^{\bar{u}(1)} \frac{T}{T_o}\, d\bar{u} = \frac{T_w}{T_o} + \left(1 - \frac{T_w}{T_o}\right) \frac{\bar{u}(1)}{2} - \cos^2\beta \frac{[\bar{u}(1)]^2}{3} \tag{7.4}$$

After the velocity field is determined, the other flow quantities can in turn be found. For a unit Prandtl number, the total enthalpy may be obtained simply from the Crocco relation

$$\Theta = \bar{u} = \sqrt{2W} \tag{7.5}$$

As observed in Section 6.2, the solution of $\bar{u}$ may be developed as a series in the form

$$\bar{u} = \bar{u}_o \bar{\varkappa}^{1/2} + \bar{u}_1 \bar{\varkappa} + \bar{u}_2 \bar{\varkappa}^{3/2} + \cdots \tag{7.6}$$

of which the coefficients can be analytically determined, for $\nu = 0$ and 1, respectively, as

$$\bar{u}_0 = \sqrt{2}\,\zeta\,,\quad \bar{u}_1 = -\zeta\,,\quad \bar{u}_2 = \frac{5\sqrt{2}}{12}\zeta - \frac{\sqrt{2}}{15}\zeta^4\,,\ \text{etc.}\qquad (\nu = 0)$$

$$\bar{u}_0 = \zeta\,,\quad \bar{u}_1 = -\frac{5}{12}\zeta - \frac{1}{30}\zeta^4\,,\quad \bar{u}_2 = \frac{1}{1440}\left(187\,\zeta - 20\zeta^4 + \frac{11}{5}\zeta^7\right),\ \text{etc.}\qquad (\nu = 1)$$

The appearance of the argument $\bar{x}^{1/2}$ clearly indicates that the solution to the shock-layer equations in this case is singular at the apex $\bar{x} = 0$. As in the classical boundary-layer theory, the immediate vicinity of the leading edge of a cone or flat plate has to be excluded from the present analysis.

With the initial data provided by the series Eq. (7.6), the numerical solutions to Eq (7.1) are obtained for the wedge and cone. The procedure used follows essentially that discussed in the preceding section, which is based on an implicit difference scheme. The advantage of using the variables W, $\bar{x}$ and $\bar{\psi}$ rather than $\bar{u}$, $\bar{x}$ and ζ is that in these new variables the truncation errors of the difference scheme for this particular problem become less critical with respect to the singularity at the surface mentioned previously. Consequently, the increment $\Delta\bar{\psi}$ used is not required to be as small as $\Delta\zeta$. Strictly speaking, the use of W and $\bar{\psi}$ requires certain corrections to the difference quotients shown in Eq. (6.14), because W is not strictly regular, but behaves like*

$$W = a\,\bar{\psi} + b\,\bar{\psi}^{3/2} + O(\bar{\psi}^4)$$

near the surface where $\bar{\psi} = 0$. Examination shows, however, that the corrections are numerically small and not necessary, at least for the present

---

*The singularity is more critical when $p_x \neq 0$. In this more general case, $W = a\,\bar{\psi} + b(\bar{\psi})^{3/2} + 0$.

problem.[43]

The results of skin friction and heat-transfer rate on cones and on wedges for $Pr = 1$ are presented in Fig. 7.1 as $\frac{c_H}{\sin\beta}\left(= \frac{c_f}{\sin 2\beta}\right)$ vs. $\bar{\chi}$. As shown, the values of c_H and c_f approach, respectively, $\sin\beta$ and $\sin 2\beta$ as $\bar{\chi} \longrightarrow 0$, as required by the free-molecular-flow theory for unit accommodation coefficients. Fig. 7.1 indicates that, as far as the heat-transfer rate and skin friction on cones and wedges are concerned, appreciable departure from the boundary-layer theory does not occur until $\bar{\chi} \approx 1$. For $\bar{\chi} < 1$, the analytical development (6-term expansion for $\nu = 0$, 4-term for $\nu = 1$) appears to be adequate. The calculation performed begins at $\bar{\chi} = 0.01$ and uses $\Delta\bar{\psi} = 1/10$ and $\Delta\bar{\chi} = 1/1000$ for $.01 \leq \bar{\chi} \leq .2$ and $\Delta\bar{\chi} = 1/100$ for $.2 \leq \bar{\chi} \leq 10$. The total computation time (including print-out) on an IBM 704 digital computer is approximately 2 minutes.

The corresponding velocity profile tends to a linear distribution in ζ in the limit of $\bar{\chi} \longrightarrow 0$, as is also revealed by the coefficients $\bar{u}_o$ in the development of Eq. (7.5). As $\bar{\chi}$ increases, the velocity gradient increases near the surface, tending to form a boundary layer, and decreases at the outer edge, thus reducing the velocity change across the shock. The value of $\bar{u}$ immediately behind the "shock" is also given in Fig. 7.1. It is rather interesting to observe in this respect that, even at $\bar{\chi}$ as low as 3, the flow field can already be represented very closely by the classical boundary-layer limit, in spite of the fact that the velocity at the outer edge is still quite far from the inviscid value and that the viscous layer is still a major fraction of the shock layer. To bring out clearly this observation, the velocity profiles at various $\bar{\chi}$ stations are correlated in terms of the similarity variable

$$\eta \equiv \sqrt{\frac{3\bar{x}}{3+\nu}} \int_0^{\bar{y}} \frac{d\bar{y}}{\sqrt{2W}} \tag{7.7}$$

The good correlation and the excellent agreement with the Blasius profile, as revealed in Fig. 7.2, also provide a check on the accuracy of the method.

Finally, from the local skin-friction of the wedge surface, one can determine the lift/drag ratio for a flat plate at incidence in the low Reynolds number regime. This ratio corresponding to a 46° incidence angle, which is calculated on the basis of one surface on the compression side, is included at the lower part of Fig. 7.1 as a function of $\bar{x}$. Though not presented in the figure, the L/D ratio at β = 30° and 60° does not differ a great deal from that for β = 45°. The L/D ratio at $\bar{x}$ = 1.0 is about 0.35, becomes lower for $\bar{x} < 1$, and tends to zero as $\bar{x} \longrightarrow 0$. Once again, the present analysis yields the correct free-molecule limit for unit accommodation coefficients. It may be noted that using boundary-layer theory would lead to a negative L/D at low Reynolds number.

As a check on the internal consistency of the analysis, one can examine the solutions to determine whether or not the shock layer remains thin in comparison with the lateral dimension of the body. Examination of the solution obtained shows that the particular assumption of equating the shock slope with the body slope may not be strictly satisfactory for a flat plate at less than 25° incidence in the range of $\bar{x} < 1$. (The case of a cone is less critical.) An interesting question arises, in this respect, that is, whether and when the viscous shock layer will also detach from the surface, as it does in the inviscid limit, when the wedge or cone angle becomes too high.

7.2 Paraboloid and Hyperboloid

As examples of flows around bodies of revolution having finite nose radii, the shock layers around a paraboloid and a hyperboloid will now be studied, applying the full method developed in Section 6.

The principal reason for selecting this class of bodies is that the zero-pressure point[4,19] does not occur on these bodies, and the shock-layer theory should be valid. The comparison provided at the end of Section 5 for the paraboloidal shock in the inviscid limit has further indicated that the present version of the thin-shock-layer approximation may be used to describe the flow field with fair accuracy. It is reasonable to expect that the approximation will remain adequate in the corresponding viscous problem. The degree of approximation in the case of the hyperboloidal shape may presumably be better, because of its smaller surface curvature. Here, the distinction between a shock and body geometry should not be essential, so long as the shock-layer approximation is valid, since the two are equivalent in the leading approximation. To provide a flexible interpretation of the present analysis, one may regard either the body shape or the shape of the "shock interface" as specified.

The following study concerns highly cooled bodies of uniform surface temperature with $\frac{T_w}{T_o} = \frac{1}{8}$, $\varepsilon = \frac{1}{8}$ and $Pr = .71$. To simplify the matter, the linear viscosity-temperature relation $\mu/\mu_* = T/T_*$ is assumed. The constant (μ_*/T_*) can be evaluated in the manner described in Section 4.1 of Part I, using the reference temperature given in Eq. (4.1a) for the stagnation region.*

*This linear representation may perhaps be somewhat improved by taking into account the effect of flow speed on the mean temperature of the shock layer, in a manner similar to that provided in Eq. (7.4).

In the present study concerning flow regions not very far from the blunt nose, such idealization should be sufficient. In terms of the variable λ, the shock or body shape considered can be described as

$$\frac{z}{a} = \sqrt{\lambda + \frac{b}{4}\lambda^2} \tag{7.8}$$

where b is zero for a paraboloid, and is positive for a hyperboloid. The analyses to be discussed are obtained for $b = 0$ and $b = 1$. The latter corresponds to a hyperboloid which approaches a 45° cone at infinity -- (ideally the hyperboloid may be regarded as a blunted cone). For each geometry, values of $K^2 = 0.3$, 1, 3, 10 and 30 are considered, encompassing the viscous-layer, the incipient-merged layer as well as the fully-merged layer regimes.

The method of series expansion is first employed to determine u_0, Θ_0, $\bar{p}_1$, $\bar{u}_1$, Θ_1, and $\bar{p}_2$ which provides initial data for the difference method. The solutions are carried out for each value of K^2 from $\lambda = 0.1$ near the axis of symmetry to $\lambda = 3$ (about 2 to 3 times the nose radius), with a step size of $\Delta\lambda = 1/100$ and $\Delta\zeta = 1/100$. To avoid excessive amplification of the truncation error near $\zeta = 0$, the inner boundary is shifted from $\zeta = 0$ to $\zeta = \zeta_0$, as previously discussed. The value of ζ_0 used is 0.15 for the cases then $K^2 = 0.3$, 1, and 3, and 0.10 for the less critical cases where $K^2 = 10$ and 30. Instability is not detected, except for a bounded oscillation of small amplitude which is found in the case of $K^2 = 0.30$ over the range of $0.1 \lesssim \lambda \lesssim 0.30$. For each value of K^2, the total computation time (including print out) on an IBM 704 digital computer is about 27 minutes. The results of the calculation are presented in Figs. 7.3 to 7.11.

The profiles of velocity, enthalpy, pressure and temperature at three successive stations $\frac{x}{a}$ = .59, 1.24 and 2.82 downstream of the stagnation point are presented in Figs. 7.3 to 7.5 for various values of K^2. The profiles for the paraboloidal case which are essentially similar are not presented. The particular features of these profiles which should be emphasized are the reductions of tangential velocity and total enthalpy at the outer edge from their respective upstream values as a result of the transport effects behind the shock. The reductions increase, of course, with decreasing density, i.e., decreasing K^2, and decrease generally with increasing distance x from the axis of symmetry. As in the solution for shock layers on the wedge and cone, the gradients $\partial u/\partial y$, $\partial T/\partial y$, etc. near the body surface increase with distance x, and a boundary layer is seen to emerge gradually at the base of the shock layer, as one moves downstream. At the higher Reynolds numbers, K^2 = 10 and 30, the temperature profiles at the downstream stations attain maximum values inside the shock layer, as in a boundary layer with surface cooling. The profile of the total-enthalpy function Θ also reveals similar characteristics, though to a lesser degree. In fact, for the case of K^2 = 30, the function Θ, thus the total enthalpy itself, overshoots slightly its free-stream value at the station $\frac{x}{a}$ = 2.82. This overshoot results from the mutual compensation of the viscous dissipation and heat conduction (from the higher-temperature region inside the shock layer), with the former overbalanced by the latter. This feature is peculiar only for the Prandtl number 0.71 assumed, and is absent for $P_r \geq 1$. The similar overshoot in total enthalpy has also been found previously in Van Driest's calculations of laminar boundary

layer over a flat plate.[78] One may also note from these results that there is very little variation of pressure across the shock layer for all Reynolds numbers. This property is, of course, only incidental to the particular configuration studied.

From the velocity, temperature and pressure, the streamline pattern describing the flow field around a blunt body can be determined. Results are presented in Figs. 7.6 and 7.7 for $K^2 = 1$ and 30 for both the paraboloid and the hyperboloid. In order to provide a closer comparison with the inviscid case previously presented in Fig. 5.2 of Part I,* the results presented in Figs. 7.6 and 7.7 have been interpreted as solutions to the inverse problem, that is, the flow fields and body surface supporting paraboloidal and hyperboloidal shocks. To be more specific, by the term "shock" one is referring to the "shock interface" discussed in Section 5, which is also the location of the outer edge of the shock layer in the present two-layer model. Consider first Fig. 7.6 at $K^2 = 1.0$, which represents the flow fields in the merged-layer regimes. Comparing the results of the paraboloidal shock in Fig. 7.6(a) with the corresponding results in Fig. 5.2, one sees that far from the axis of symmetry the inviscid and viscous shock layers are comparable in thickness, but that, near the stagnation region, the thickness in the viscous case studied is noticeably smaller. The results are understandable through the observation that the high rate of surface cooling effectively increases the density level, and hence the mass flux, ρu, near the stagnation region. Away from the stagnation region, the

*Strictly speaking, the particular example given in Fig. 5.2 which assumes $\epsilon = 1/7$ does not correspond to the inviscid limit of the example considered here, which assumes $\epsilon = 1/8$. The difference however is rather small.

heat conduction to the cooled body is offset and even overbalanced by the viscous dissipation. For an insulated body, one may anticipate a substantial thickening of the shock layer downstream of the stagnation point. Comparing the flow pattern of the paraboloidal (Fig. 7.6a), with the hyperboloidal shocks (Fig. 7.6b), the latter is seen to be generally thinner. The relative difference between the inviscid and the "fully viscous" shock layers observed for the paraboloid case also applies for the hyperboloidal case.

The flow patterns at a higher Reynolds number, $K^2 = 30$, is presented in Fig. 7.7. It is of interest to observe that the shock-layer thicknesses around the bodies have not changed much from those of the preceding figure, in spite of the considerably larger difference in Reynolds number. The main reason is presumably that, at $K^2 = 30$, a good fraction of the shock layer near the stagnation point still belongs to the region where viscous and heat-conducting effects are important.

It may be remarked that the results presented in Figs. 7.6 and 7.7, as well as in the other figures, do not provide the complete flow picture, since they describe only the pattern within the shock layer. As pointed out before, solution to the shock-transition zone can be easily obtained from the information provided here. The streamline pattern in the shock-transition zone may be constructed by working backward.

The surface pressures on the paraboloid and hyperboloid, non-dimensionalized by the pressure behind the shock, are provided in Fig. 7.8. Although not corresponding to the exact inviscid limit for $\varepsilon = 1/8$, the inviscid results calculated previously for $\varepsilon = 1/7$ are also included for comparison. The results obtained show a continuous transition between the

inviscid limit and free-molecule limit (which is $\bar{p} = 1$). As already noted, $\bar{p}$ is practically unity for the hyperboloid. Also included in Fig. 7.8 are the distribution of the thickness of the shock layer around bodies for the five cases of K^2 analyzed. Except for the case of $K^2 = 0.30$, the results for all K^2's compare closely one with another, confirming the relative insensitivity of the shock-layer thickness with respect to change in Reynolds number previously observed.

Finally, the local skin friction and surface heat-transfer rate are presented respectively in Figs. 7.8 and 7.9 for both the paraboloid and hyperboloid. Also included are the distributions corresponding to the free-molecule limit (for unit accommodation coefficients). The smooth transition to the free-molecule limit is quite evident from the results presented for successive values of K^2. Generally, the value of c_H falls off as one moves away from the stagnation point. Similar is the value of c_f, after reaching a maximum. One notes that the rate of this falling-off increase generally with increasing Reynolds number, also that the distributions of the higher K^2's are remarkably similar. To study the heat-transfer characteristics more closely and to make comparison with the boundary-layer limit possible, the results of Fig. 7.10 are reproduced in Fig. 7.11 in the form of $q/q_{MAX.}$ vs. x/a, where $q_{MAX.}$ is the heat-transfer rate at the stagnation point. One sees that for both paraboloid and hyperboloid, the heat-transfer distributions at $K^2 = 30$, 10, as well as 3, are reasonably close to one another. While the rate of falling-off from the stagnation-point value is seen to increase with increasing K^2 as in the preceding figure, Fig. 7.11 reveals that there is a reversal of this trend for $q/q_{MAX.}$ at

K^2 = 10 for both paraboloid and hyperboloid. That is, at the same x/a, the ratio $q/q_{MAX.}$ is slightly higher for K^2 = 30 than for K^2 = 10. This reversed trend is further confirmed by the boundary-layer limit estimated on the basis of the local-similarity method (using the inviscid solution obtained from the present theory for the outer flow), also included in Fig. 7.11.* The reversal in the trend of heat-transfer distribution at K^2 = 10 can be explained by the vorticity effect. Since the external vorticity effect generally decreases in the downstream direction, the effect may tend to decrease on q/q_{MAX} ratio from the corresponding boundary-layer prediction, in agreement with the reversed trend observed.

From the above discussion, one should note that the distribution of the heat-transfer ratio is relatively independent of Reynolds number over a very wide range. In particular, the variation of the heat-transfer ratio in the range K^2 = 3-30 is remarkably small. This, together with the fact that the vorticity interaction is itself not a predominantly large effect, suggests that the heat-transfer distributions on a smooth blunt body should remain essentially unchanged in the boundary-layer through the incipient-merged-layer regimes. A similar conclusion is applicable to the skin-friction characteristics.** The insensitivity of the distribution of the measured heat-transfer rate with respect to Reynolds number has been reported in Refs. 50 and 52 for low-density hypersonic flows over spheres.

---

*The accuracy of the local-similarity method for the boundary-layer analysis is taken for granted here.

**In this instance, one shall consider the distribution of the ratio of τ to $\lim_{x\to 0} x \frac{d\tau}{dx}$.

8. STUDY OF NONEQUILIBRIUM DISSOCIATION IN SHOCK LAYER AT LOW REYNOLDS NUMBER

Thus far, only an ideal gas with constant specific heats has been considered. A more realistic analysis of the low-density hypersonic flow must include nonequilibrium flow chemistry. The following section will discuss briefly an extension of the thin-layer approach to study dissociation and species diffusion in the viscous shock layer, assuming a single dissociation-recombination reaction. The stagnation region in the viscous layer and merged-layer regimes will be analyzed.

8.1 Relation to Previous Work

The stagnation region with nonequilibrium dissociation has been studied by Chung,[36] on the basis of a viscous-layer model. His analysis assumes a binary mixture of diatomic molecules with a unit Lewis number and a linear viscosity-temperature relation, for a noncatalytic surface. Very significant effects of surface cooling on the flow chemistry have been revealed. The following analysis assumes a similar chemical kinetic model but will be conducted from a viewpoint more consistent with the general approach developed in the preceding sections. The present flow model allows for changes in the tangential velocity, total-enthalpy, and species concentration across the shock and therefore possesses a regime of validity larger than the viscous-layer model. The influence of the wall catalycity on the species diffusion and flow chemistry will also be studied.

In considering nonequilibrium flow of rarefied gases, questions naturally arise as to the importance of the effects associated with the vibrational (also perhaps rotational) relaxation.[79] Although not being accounted for in the

present study, the basic flow model developed here may provide a simple framework for studying these as well as other more complex high-temperature real-gas effects.

Before passing to the specific analysis of the stagnation region, the general problem of the shock layer with species diffusion and nonequilibrium chemistry will be discussed.

8.2 General Discussion

Consider a binary mixture of diatomic molecules and dissociated atoms. The diffusion velocity of the atomic species V' may be written for the present study as[6,80]

$$V' = -D_{12}\left[\frac{\partial}{\partial y}\ln\alpha + \left(\frac{1-\alpha^2}{2}\right)\frac{\partial}{\partial y}\ln p - \left(\frac{K_T}{6}\right)(1+\alpha)^2(1-\alpha)\frac{\partial}{\partial y}\ln T\right] \qquad (8.1)$$

where α is the atomic concentration in mass fraction, and D_{12} the binary diffusion coefficient. The thermal diffusion has been generally neglected in boundary layer analysis ($\frac{K_T}{6} \approx 1/10$ for air) but may be quite significant for nonequilibrium flow with a highly cooled surface.

Of particular significance is the second term on the right of Eq. (8.1) corresponding to the pressure diffusion. This term is not present in boundary-layer analysis which assumes a uniform pressure across the layer, but is important in the present study because the pressure variation is not generally negligible in the shock layer (as well as in the shock-transition zone). In fact, in the merged-layer regimes, the contribution of the pressure diffusion can be as important as that due to any other processes, and should therefore be included in the general formulation of the problem. In the stagnation region, however, the pressure gradient is small and the pressure diffusion effect can

also be neglected. From Eq. (8.1), one may infer that pressure diffusion tends to increase the flux of the (lighter) atomic species toward the (convex) surface in region downstream of the stagnation point.

Consistent with Eq. (8.1) is the expression for the energy flux[6,77]

$$q = -k\frac{\partial T}{\partial y} + (h_1 - h_2 + Q)\,\rho\alpha V' - \mu\frac{\partial u}{\partial y}\,u \tag{8.2}$$

where Q is the heat of formation per unit mass of the atoms, and h_1 and h_2 the specific enthalpies of the atoms and molecules, respectively.* The differential equations governing the shock layer Eq. (5.3) remain unchanged except for the last equation governing the total enthalpy. The equations governing the total enthalpy H and the atomic concentration α in the shock-layer region are

$$\left.\begin{aligned}
\rho\left(u\frac{\partial}{\partial x} + v\frac{\partial}{\partial y}\right)H &= \frac{\partial}{\partial y}\frac{\mu}{Pr}\frac{\partial}{\partial y}\left[H + (Pr-1)\frac{u^2}{2}\right] \\
&+ \frac{\partial}{\partial y}(\mathcal{L}e - 1)\frac{\mu}{Pr}(h_1 - h_2 + Q)\frac{\partial \alpha}{\partial y} \\
&+ \frac{\partial}{\partial y}\mathcal{L}e\,\frac{\mu}{Pr}(h_1 - h_2 + Q)\alpha\left[\left(\frac{1-\alpha^2}{2}\right)\frac{\partial \ln p}{\partial y} - \frac{K_T}{6}(1+\alpha)^2(1-\alpha)\frac{\partial \ln T}{\partial y}\right], \\
\rho\left(u\frac{\partial}{\partial x} + v\frac{\partial}{\partial y}\right)\alpha &= -\frac{\partial}{\partial y}\rho\alpha V' + w\,,
\end{aligned}\right\} \tag{8.3}$$

where w is the rate of production of the atomic species in mass per unit volume.** Consistent with the present two-layer model, and with Eqs. (8.1) and (8.2), are the two equations relating total-enthalpy drop and concentration

---

*The assumption of $\frac{K_T}{3}R_2 T \ll h$, h_2 and Q has been used.

**To complete the system of differential equation, one has $p = R_2(1+\alpha)\rho T$, where R_2 is the gas constant for the molecule, as well as h_1 and h_2 as function of T, μ as function of T and α, etc.

jump across the shock-transition zone.

$$\left.\begin{aligned} \rho_1 v_1 (H_2 - H_\infty) &= -q_2 \\ \rho_1 v_1 (\alpha_2 - \alpha_\infty) &= -(\alpha V')_2 \end{aligned}\right\} \tag{8.4}$$

The finite atom concentration at the outer edge of the shock layer, α_2, is a result of upstream diffusion of the atomic species which are produced inside the shock layer. Implicit in the last of Eqs. (8.4), which resemble a concentration-jump across the Knudsen layer, is the assumption that the gas-phase reaction is frozen within the shock-transition zone, i.e. w is negligible. The assumption may be justified on the basis of the relatively low collision frequency in the transition zone. Because of the temperature maximum reached inside the transition zone however, a domain (corresponding to a flight speed and altitude much higher than contemplated) does exist in which excitations of modes of vibration and dissociation within the shock can be important.

The boundary condition governing the species concentration at the surface, assuming a first-order recombination rate[78] and neglecting dissociation at the surface, is

$$-(\alpha V') = \frac{\gamma_w}{2(2-\gamma_w)} \sqrt{\frac{8RT}{\pi}}\, \alpha \,, \qquad (y = 0) \tag{8.5}$$

where γ_w is the recombination efficiency (the probability for each atom to recombine after reading the surface) and $(\alpha V')$ is provided by Eq. (8.1) including the pressure diffusion. To see more clearly the manner in which the recombination efficiency γ_w affects surface catalycity in the regimes considered, one may express Eq. (8.5) in terms of the variable ζ,

$$\alpha = \frac{1+\nu}{2K_0^2} \frac{\mathcal{L}e}{Pr} \left(\frac{2-\gamma_w}{2\gamma_w}\right) \sqrt{\pi \varepsilon_\infty \frac{T_0}{T_w}}\, \frac{\mu_w}{\mu_0} \frac{\bar{u}}{\zeta} \frac{\partial \alpha}{\partial \zeta} \tag{8.6}$$

One sees that as K_0 decreases, for a fixed recombination efficiency γ_w, the wall-catalycity effect reduces. In the range of $K_o^2 = 0(1)$, the question of whether or not a fully catalytic wall (i.e. $\alpha \approx 0$) can be realized will depend on whether

$$\frac{1}{\gamma_w}\frac{\mu_w}{\mu_o}\sqrt{\frac{T_o}{T_w}} \ll 1 \tag{8.6a}$$

Since $\mu \propto T^{\omega}$, and ω is not much larger than 1/2, it seems that a fully catalytic surface would require comparatively high value of γ_w at $K^2 = 0(1)$.

Assuming a single dissociation-recombination reaction of the type $X_2 + M \rightleftharpoons X + X + M$, the rate of production w/ρ may be written in the familiar form[28,29,79]

$$\frac{w}{\rho} = 2(2k_r')T^{-s}\left(\frac{p}{RT}\right)^2\left[\frac{K_p}{4p}(1-\alpha) - \frac{\alpha^2}{1+\alpha}\right] \tag{8.7}$$

where K_p is the "equilibrium constant" which may be related to the constant ρ_D of Lighthill[19] through

$$\rho_D \equiv \frac{K_p e^{D/RT}}{4R_2T} \tag{8.8}$$

Lighthill finds ρ_D remains practically constant for pure oxygen and pure nitrogen for a temperature as high as 8000°K. Examination shows that at higher temperature, large departure of ρ_D from the nearly constant value will occur for nitrogen because of the excitation of certain highly degenerated electronic states of the nitrogen atoms. In his study of the viscous shock layer, Chung[36] assumed "unexcited electronic state" (apparently meaning the high-lying levels to be unexcited). Presumably, his ρ_D does not differ a great deal from its value at 8000°K.

Another point of importance with regard to the reaction rate is the relatively weak recombination in the gas phase at low density. As observed by

Gibson,[84] the recombination rate based on the three-body process becomes negligible as density level decreases. In boundary-layer studies,[29,30,82] the recombination is important because the ambient density level is sufficiently high and increases further towards a highly cooled surface. In the low Reynolds number regimes studied here, the ambient density is too low to make the three-body processes effective, even with a highly cooled surface. The recombination in the gas phase may therefore be expected to be negligible. The range of validity of this simplification can be easily established by an order-of-magnitude analysis based on Eq. (8.7). A direct consequence of neglecting the three-body processes is the binary scaling law, which permits correlations of nonequilibrium flow fields of different body scale and ambient density by preserving the product (ρa) in the same manner as in the Reynolds-number similitude.[84] It is evident that this scaling law may apply to both inviscid and viscous flows. In case of viscous flow, however, in order to preserve similarity in the boundary condition, the binary scaling law requires the nonslip surface condition, and a noncatalytic ($\frac{\partial \alpha}{\partial y} = 0$) or a fully catalytic surface ($\alpha = 0$). In the following, nonequilibrium dissociation in the stagnation region will be analyzed on the basis of the model described. In passing, it may be pointed out that the procedure of solution developed in the previous section for shock layers around nonslender bodies can be extended to study nonequilibrium dissociation, including species diffusion in the shock-transition zone.

8.3 Nonequilibrium Dissociation and Species Diffusion in the Stagnation Region

In the following study, the perfect-gas value of c_p for the atom species and molecular species will be assumed to be, respectively,

$$\left.\begin{aligned} c_{p_1} &= \left(\frac{3}{2}+1\right) R_1 = \frac{5}{2} R_1 \\ c_{p_2} &= \left(\frac{7}{2}+1\right) R_2 = \frac{9}{2} R_2 \end{aligned}\right\} \tag{8.10}$$

Thus the molecules in the shock layer are assumed to possess, in a classical sense, the full rotational as well as vibrational degrees of freedom. Implicit is the assumption that excitation of the electronic states of the atoms and molecules does not contribute to the internal energy of the particle. Thus, associated with the atomic and molecular species are two specific heat ratios $\gamma = 5/3$ and $\gamma = 9/7$. To make the temperatures in the following analysis dimensionless, one introduces a "free-stream stagnation temperature":

$$T_0 \equiv \frac{U_\infty^2}{2 c_{p_2}} = \varepsilon_\infty \frac{U_\infty^2}{R_2} \tag{8.11}$$

where $\varepsilon_\infty = \frac{\gamma_\infty - 1}{2\gamma_\infty} = \frac{1}{7}$, corresponds to a specific ratio of $\gamma_\infty = 7/5$.

It will be convenient to introduce the following parameters

$$\left.\begin{aligned} \theta_d &\equiv D/kT_0 \\ \chi &\equiv \frac{2R_2^s (2k_r')(\rho_d')(\rho_\infty a)}{\varepsilon_\infty^{1+s} M_2^2 U_\infty^{1+2s}} \\ \sigma &\equiv \rho_\infty / \varepsilon_\infty \rho_d' \end{aligned}\right\} \tag{8.12}$$

where ρ_d' is a reference value for ρ_D and will be taken for the present purpose as 122 gm/cc.

The system of differential equations governing the shock layer in the stagnation region in terms of the variable ζ, becomes

$$\left.\begin{aligned} \bar{u}^2 - \zeta \bar{u}\bar{u}' &= \frac{1}{K_0^2}\frac{\bar{u}}{\zeta}\left[\frac{\bar{u}\bar{u}'}{\theta^{1-\omega}\zeta(1+\alpha)}\right]' + \frac{1}{7}(1-\bar{p}_1)(1+\alpha)\theta \\ -\zeta \bar{u}\alpha' &= \frac{\mathcal{L}e}{Pr K_0^2}\frac{\bar{u}}{\zeta}\left[\frac{\bar{u}\alpha'}{\theta^{1-\omega}\zeta(1+\alpha)}\right]' + \frac{\chi}{\theta^{1+s}}\left[\frac{\rho_D}{\rho_d'} e^{-\theta_d/\theta}(1-\alpha) - \frac{\bar{\sigma}}{\theta}\left(\frac{\alpha^2}{1+\alpha}\right)\right] \\ -\zeta \bar{u}\bar{H}' &= \frac{1}{Pr K_0^2}\frac{\bar{u}}{\zeta}\left[\frac{\bar{u}\bar{H}'}{\theta^{1-\omega}\zeta(1+\alpha)}\right]' + \varepsilon_\infty \frac{(\mathcal{L}e-1)\bar{u}}{Pr K_0^2 \zeta}\left[\frac{(\theta+2\theta_d)\bar{u}\alpha'}{\theta^{1-\omega}\zeta(1+\alpha)}\right]' \\ \bar{p}_1' &= \left(\frac{2}{1+\nu}\right)\bar{u}\zeta \end{aligned}\right\} \tag{8.13}$$

where $\bar{H} \equiv H/\frac{1}{2}U_\infty^2$ and $\theta \equiv T/T_0$ are respectively the dimensionless enthalpy and temperature, which are related through

$$\theta = \frac{2}{9+\alpha}\left(\frac{7}{2}\bar{H} - \theta_d \alpha\right) \tag{8.14}$$

Note that $K_0\left(=\varepsilon_\infty \frac{\rho_\infty U_\infty a}{\mu_0}\right)$ is the same parameter as defined previously. In the above equations, a viscosity law $\mu \propto T^\omega$ has been used, and the thermal diffusion neglected.

The boundary condition on the surface becomes, at $\zeta = 0$

$$\left.\begin{aligned} &\bar{u} = 0 \\ &\theta = T_w/T_0 \\ &\alpha - \frac{\mathcal{L}e\,\Gamma}{Pr\,K_0^2}\,\bar{u}'\alpha' = 0 \end{aligned}\right\} \tag{8.15}$$

where

$$\Gamma \equiv \frac{2-\gamma_w}{2\gamma_w}\sqrt{\gamma \varepsilon_\infty}\left(\frac{T_w}{T_0}\right)^{\omega-\frac{1}{2}}$$

The boundary condition at the outer edge of the shock layer becomes, at $\zeta = 1$

$$\left.\begin{aligned} &\bar{u} + \frac{\bar{u}\,\bar{u}'}{K_0^2\,\theta^{1-\omega}(1+\alpha)} = 1, \qquad \bar{p}_1 = 0, \\ &\alpha + \frac{\mathcal{L}e}{Pr\,K_0^2}\,\frac{\bar{u}\alpha'}{\theta^{1-\omega}(1+\alpha)} = \alpha_\infty, \\ &\bar{H} + \frac{1}{Pr\,K_0^2}\,\frac{\bar{u}\,\bar{H}'}{\theta^{1-\omega}(1+\alpha)} + \frac{\varepsilon_\infty(\mathcal{L}e-1)(\theta+2\theta_d)\,\bar{u}\,\alpha'}{Pr\,K_0^2\,\theta^{1-\omega}(1+\alpha)} = 1 + 2\varepsilon_\infty\,\theta_d\,\alpha_\infty \end{aligned}\right\} \tag{8.16}$$

Eqs. (8.13) to (8.16) constitute a standard two-point boundary-value problem. The above formulation includes the frozen atomic species in the free stream.

In the following examples, the above formulation is applied to an idealized mixture* of "air molecules" and air "atom" as in Refs. 29 and 79, thus one uses a value of $T_D = D/k$ = 101,300°K, which is a weighted average between 59,000°K (oxygen) and 113,200°K (nitrogen), based on the composition

*This idealization may lead to oversimplification of the chemical rate equation.

in the free stream. To make the present calculations comparable with Chung's analysis, the same values of U_∞, $2k'_r$, s, a, T_w and α_∞ (=0), are used and are listed in Fig. 8.1. Differing from Chung's however are the values $\omega = 1/2$ and $\mathcal{L}e = 1.40$, also $\rho_D/\rho'_d = 1$. These differences should not be considered to be critical. The value $U_\infty = 26,000$ ft/sec used corresponds to re-entry from satellite speed.

Numerical integrations have been performed for $K_o^2 = 0.473$, 1.97, 5.79, 16.24 and 35.2, corresponding to a one-foot nose radius at altitudes of 350,000 ft., 320,000 ft., 300,000 ft., 280,000 ft. and 265,000 ft., respectively. Throughout the whole series of calculations, the values of $\gamma\sigma/\theta^{2+s}$ which controls the recombination rate are of the order of 10^{-2} or much less, and one may use the binary-scaling rule to apply the present results to bodies of other dimension. The table given on top of Fig. 8.1 provides the correspondence between the value of K_o^2 and the altitude for nose radius smaller and greater than one foot, according to this rule.

The solutions by numerical integration are presented in Fig. 8.1 to 8.3. As typical results, the atom concentration profiles of the shock layer are presented in Fig. 8.1 for both noncatalytic as well as fully catalytic surfaces for $K_o^2 = 16.24$. This value of K_o^2 falls in the viscous-layer regime and corresponds to the highest altitude considered by Chung (280,000 ft.). Included in Fig. 8.1 for comparison is the corresponding profile in the inviscid limit ($K_o^2 \to \infty$), as well as a solution for unit Lewis number. The difference in solution due to the Lewis number is clearly small, at least for the noncatalytic case considered, whereas the departure of the solutions from the inviscid limit is clearly very large.

An important feature of the profiles obtained is the finite value of atom concentration at the outer edge, which is absent in the corresponding solution of Chung. The present results show that the concentration jump is not negligible even in the viscous-layer regime where changes in tangential velocity and enthalpy across the shock may be neglected. Chung's solution (not shown) follows the inviscid profile near the shock and becomes comparable with the present result (for the noncatalytic case) near the surface. The large influence of the wall catalycity on the composition in the inner portion of the shock layer is clearly indicated by the large difference between the two extreme cases shown in Fig. 8.1. However, the temperature profiles corresponding to these extreme cases (not shown) reveal indistinguishable difference throughout the entire shock layer. The negligible difference in temperature profile is explained by the fact that for this as well as other values of K_o^2 considered (and for the speed of 23,000 ft/sec or lower) dissociation takes place mainly in the outer portion of the shock layer where the temperature is highest. The composition in the inner portion of the shock layer is controlled by diffusion as in a frozen boundary layer. Since there is practically no heat release from chemical reaction in the inner part of the layer, the change in composition resulting from the change in wall catalycity will not introduce appreciable change in temperature.

The profiles of concentration, velocity, enthalpy and temperature at other values of K_o^2 corresponding to successive degrees of rarefaction are presented in Fig. 8.2 for the case of noncatalytic surface. The corresponding results for a fully catalytic surface will not be presented, except to mention that the conclusion drawn from the study of Fig. 8.1 with respect to the large

influence of the wall catalycity on atom concentration profile and the small effect on temperature remains the same. According to Fig. 8.2, at a higher value of K_o^2, say $K_o^2 = 35.2$, the concentration jump across the shock is still appreciable and reduction of atom concentration level by surface cooling is still significant. At the lower values of K_o^2, say $K_o^2 \leq 5$, the temperature is reduced (because of the combined effect of surface cooling and enthalpy drop across the shock) to such a low level that the effect of dissociation is hardly distinguishable.

The stagnation-point heat-transfer coefficient C_H as well as the standoff distance, Δ, corresponding to the solutions discussed are presented in Fig. 8.3. As anticipated, the use of a non-catalytic surface to reduce heat transfer becomes less and less effective as the degree of rarefaction increases, i.e. K_o^2 decreases, since the difference in heat-transfer characteristics of the two extreme surface conditions depend on the amount of atomic particles present. At K_o^2 below 5, the difference in heat transfer vanishes. Also included is the C_H value for a $\gamma = 9/7$, corresponding to the case of completely frozen chemistry. The stand-off distance, that is, the thickness of the shock layer (obtained for a noncatalytic surface) is seen to vary with density rather slowly. The relatively high degree of dissociation taking place in the outer portion of the shock layer at higher K_o's reduces the temperature and increases the density, causing a reduction in the standoff distance from the ideal-gas value, as shown in Fig. 8.3.

CONCLUSION

In this paper, the problem of hypersonic flow of a rarefied gas around blunt bodies is studied within the framework of the continuum theory. The existing theories and experiments on the stagnation region are discussed; the approach based on the thin-shock-layer approximation is extended to study flow fields removed from the stagnation region as well as in the shock-transition zones. Particular problems are analyzed to illustrate aerodynamic and heat-transfer characteristics of blunt as well as pointed nonslender bodies at low Reynolds number. Also studied is nonequilibrium dissociation with species diffusion in the shock layer under the influence of strong surface cooling.

Attempts to analyze the stagnation region based on the continuum theory have resulted in three main approaches. One approach treats vorticity and other effects under the assumption of small departure from the boundary-layer limit. The theories of Van Dyke[24] and others[25, 26] based on this approach have been most systematically and elegantly developed, and, in fact, can be extended to study flow regions removed from the stagnation point. In a second approach, applicable to regimes of low density, transport effects are considered throughout the shock layer, and a system of simplified Navier-Stokes equations is integrated along the axis of symmetry. However, in order to make the partial differential equations tractable in this approach, one has to assume a constant density or a thin shock layer. The third approach makes consistent use of the thin-shock-layer model. Without sacrificing the essential features of the problem, the thin-shock-layer approach simplified the analyses of the

stagnation region in both the high and low Reynolds number regimes. Within the degree of approximation used, it embraces both of the other approaches.

As a result of the more systematic studies,[24-26] much of the controversy and disagreement in results of vorticity, displacement and other effects has been resolved during recent years. Unresolved, however, remains the variance between the predicted and measured values of heat-transfer rates. One may cite in particular that the rise of heat-transfer rate predicted by Maslen,[26] Van Dyke[24] and others[45] is consistently lower than the values deduced from the experimental measurement of Ferri, Zakkay and Ting,[27] and some other sources. Unresolved also remains the difference among results for the slip and temperature-jump effects. Maslen[26] shows that these effects are not important for heat-transfer studies, as opposed to the conclusion of Rott and Lenard[26] and also of Van Dyke.[24] Disagreement appears to be less critical among results for the lower Reynolds number regime. Experimental heat-transfer data measured by Ferri and Zakkay,[47] and by Vidal and Wittliff[50] appear to follow the theoretical trend of the thin-shock-layer analysis rather well in this regime. There exists also reasonable correlation among heat-transfer predictions of Probstein and Kemp,[10] Levinsky and Yoshihara[40] and Cheng[41] in the merged-layer regimes.

The new development with the thin-shock-layer approach includes an extension of the thin-layer concept to formulate the problem in the shock-transition zone, and development of a finite-difference method for solving the shock-layer equations without similarity assumptions.

The basic flow model consists of an outer layer and an inner layer,

identifiable as the shock-transition zone and the shock layer, respectively. Across the shock-transition zone, the compression ratio is assumed to be high. In the shock-transition zone, the density is assumed to be generally at the low free-stream level, implying that the high compression ratio across the shock is not achieved except in the vicinity of the interface of the two layers.

Because of the thin-layer approximations, the thickness-curvature effects which generally appear in the higher-order boundary layer or Navier-Stokes equations do not appear. Also, the slip and temperature-jump effects can be separately treated as higher-order effects of the shock-layer theory. The system of partial differential equations governing the shock layer is of parabolic type, for which a forward integration in the downstream direction is possible. The corresponding system for the shock-transition zone is reducible to one of ordinary differential equations, very similar to that of the one-dimensional shock wave. This system gives rise to a set of modified shock conservation relations which account for the transport efforts immediately behind the shock. According to these modifications, the total enthalpy and tangential velocity will change across the shock in a manner similar to the surface slip and temperature jump across the Knudsen layer near the body surface. With these shock relations, which do not involve any detail of the shock-wave structure, the flow field in the shock layer can be determined independently of the shock-transition zone. An interesting general property of the present formulation is that the solution always has the correct values for skin friction and heat-transfer rate in the free-molecule limit (for unit accommodation coefficients).

The shock-wave structure can be determined by simply integrating the ordinary differential equations with boundary conditions at the inner edge furnished by the shock-layer solution. The analysis provides, in essence, a generalization to include downstream nonuniformity under the condition $\delta_s/a \ll 1$.

Unlike the existing Newtonian shock-layer theories for inviscid flow around blunt bodies, the present analysis, which treats the tangential pressure gradient as a principal term, possesses reasonably good accuracy, as has been revealed in the comparison with Van Dyke's inviscid solution[1] for a paraboloidal shock. The rather detailed agreement with the merged-layer solution of Levinsky and Yoshihara[40] confirms the validity of the two-layer concept underlying the present formulation, it also shows the surprising accuracy of the thin-layer approximation even for a monatomic gas.

The method for solving the dissimilar problem of the shock layer has been developed mainly for the viscous layer and the merged-layer regimes. It provides step-wise integration in the downstream direction, using a finite-difference approximation. The difference equations are singular at the axis of symmetry and at the body surface. On account of the singularity, it is necessary to develop a series solution in the vicinity of axis of symmetry to produce valid initial data at a station downstream of the axis of symmetry. Because of the singularity, it is also necessary to resort to the use of an implicit scheme for the difference approximation, which is free from the usual handicap of the stability and convergence requirements. With this implicit scheme, and allowing the truncation error of an order of one per-cent, solutions to the shock-layer problems can be brought within the normal

capacity of a standard high-speed digital computer (IBM 704).

With the method of analysis developed, the present theory is applied to analyze flows over a wedge, cone, paraboloid and hyperboloid for a perfect gas of constant specific heat. Generally, the solutions obtained reveal substantial changes in total enthalpy and tangential velocity across the shock in the low Reynolds number regime corresponding to $\varepsilon K^2 \leq 0(1)$. They provide a smooth transition from the boundary-layer theory to free-molecule limit (for unit accommodation coefficients). The velocity and temperature gradients near the body surface increase with distance from the stagnation point or apex, indicative of boundary-layer developments.

For the nonslender wedge and cone studied, the local heat-transfer rate and skin friction are found to be governed by a single variable $\bar{x} \sim \varepsilon Re_x \sec\beta$, which contains the gas rarefaction as well as surface incidence effects. A remarkable feature revealed by the study is that the velocity profile can be represented very closely by the classical boundary-layer solution (at $\bar{x} \gtrsim 3$), even though the velocity immediately behind the shock is quite far from the inviscid value and the viscous layer is still a major fraction of the shock layer.

For the problems of paraboloidal and hyperboloidal shapes, five successive values of K^2 are considered in the range of $K^2 = 0.3 - 30$, encompassing the viscous layer and the merged-layer regimes. For these examples, $T_w/T_o = 1/8$, $Pr = 0.71$ and $\varepsilon = 1/8$. Except for the case of lowest Reynolds number, the distributions of the thickness of the shock layer around the body are relatively insensitive to the change of Reynolds number. Comparison with the inviscid solution shows however that the viscous cases

studied have a thinner shock layer near the nose region due to strong cooling by heat conduction to the low-temperature surface.

The results obtained reveal interesting heat-transfer characteristics of a smooth blunt body at low Reynolds numbers. The ratio of local heat-transfer rate at a fixed station x to the maximum rate at the nose decreases from the free-molecule distribution with increasing density. A reversal of this trend occurs however at $K^2 \approx 10$, corresponding to the viscous-layer regime. This reversal can be explained by the vorticity effect. One may recall from the discussion that the variations in the heat-transfer ratio in the range of $K^2 = 3\text{-}30$ are remarkably small. This, together with the fact that the vorticity interaction is itself not a large effect, suggests that there is a very wide range of Reynolds number (corresponding to the boundary-layer through the incipient-merged-layer regimes) in which the heat-transfer distribution on a smooth blunt body remains essentially unchanged. Similar behavior has also been observed for the skin friction characteristics.

In the study of nonequilibrium dissociation and species diffusion in the stagnation region, an example is carried out for an idealized binary mixture of "air molecules" and "air atoms", and a cold body surface at near-satellite speed, comparable to the previous analysis of Chung.[36] The results reveal that the "concentration jump" across the shock resulting from the upstream diffusion of the atomic species is appreciable even in the viscous-layer regime where changes in the total enthalpy and tangential velocity across the shock may be neglected. In the merged-layer regimes, as a result of the combined effect of surface cooling and enthalpy drop across the shock, the gas-phase chemistry is practically frozen. Even in the

viscous-layer regime, dissociation takes place only in the outer part of the shock layer near interface. In these low-density regimes, the surface catalycity has a predominant influence over the composition in the inner portion of the shock layer, as is expected. However, there is very little change in the temperature profile associated with change in surface catalycity, because of the frozen gas-phase chemistry in the inner part of the shock layer.

The discussion has also brought out the importance of pressure diffusion in shock layers removed from the stagnation region.

ACKNOWLEDGMENT

The research on which this report is based was carried out mainly under the sponsorship of the U. S. Navy through the Office of Naval Research under Contract Nonr 2653(00). A portion of the investigation with the wedge and cone problems was originally carried out for the U.S. Air Force through the Office of Scientific Research, under Contract AF 49(638)-952.

The author would like to thank many of his colleagues in the Aerodynamic Research Department for their valuable discussion and generous assistance. He is pleased to acknowledge the contribution of Mrs. A. L. Chang in many parts of the present study, particularly in the development of a method for integrating the shock-layer equations. He would like to thank also Mr. H. Selib of the Systems Research Department for programming all problems for computation, as well as for helpful suggestions.

APPENDIX

In the following, important details of the present method of numerical solution to the shock-layer equations described in Section 6 will be provided.

A.1 The System of Ordinary Differential Equations Governing the Coefficients $\bar{u}_1$, Θ_1, and $\bar{p}_2$.

For blunt bodies with finite nose radii, Z is expressible as

$$\left(\frac{Z}{a}\right)^2 = \lambda + \frac{b}{4}\lambda^2 + \cdots\cdots$$

The function $\bar{u}$, Θ and $\bar{p}$ may assume the form

$$\bar{u} = \bar{u}_0 + \lambda\,\bar{u}_1 + \cdots\cdots$$

$$\Theta = \Theta_0 + \lambda\,\Theta_1 + \cdots\cdots$$

$$\bar{p} = 1 + \lambda\,\bar{p}_1 + \lambda^2\,\bar{p}_2 + \cdots\cdots$$

The system of equations governing $\bar{u}_0$, Θ_0 and $\bar{p}_1$ have been given in Section 6.2 of Part II. The system governing $\bar{u}_1$, Θ_1 and $\bar{p}_2$ are provided below.

$$\begin{cases}
3\bar{u}_1 - \dfrac{2\varepsilon}{\bar{u}_0}\left[\dfrac{H_w}{H_\infty} + \left(1 - \dfrac{H_w}{H_\infty}\right)\Theta\right]\left[(\bar{p}_1 - 1)^2 - 2\bar{p}_2 + b\left(\bar{p}_1 + \dfrac{1}{2}\right)\right] \\
\quad + \dfrac{2\varepsilon}{\bar{u}_0}(\bar{p}_1 - 1)\left[\left(1 - \dfrac{H_w}{H_\infty}\right)\left(\Theta_1 - \dfrac{\Theta_0\,\bar{u}_1}{\bar{u}_0}\right) - \dfrac{H_w}{H_\infty}\,\dfrac{\bar{u}_1}{u_0} - \bar{u}_0^2\right] = \left(\dfrac{1+\nu}{2}\right)\zeta\left(\bar{u}_1' + \bar{u}_0' + \dfrac{b}{2}\bar{u}_0'\right) \\
\quad + \dfrac{b}{2}\bar{u}_0 + \left(\dfrac{1+\nu}{2}\right)\dfrac{N}{K^2}\,\dfrac{\bar{u}_0^2\,\bar{u}_0'}{\zeta} + \left(\dfrac{1+\nu}{2}\right)^2\dfrac{N}{K^2\zeta^2}\left[\zeta\bar{p}_1\left(\dfrac{\bar{u}_0\bar{u}_0'}{\zeta}\right)' + (\bar{u}_0\bar{u}_1)'' - \dfrac{(\bar{u}_0\bar{u}_1')'}{\zeta}\right] \\
\Theta_1 = \dfrac{1+\nu}{4}\zeta\left[\Theta_1' + \Theta_0'\left(1 - \dfrac{\bar{u}_1}{\bar{u}_0} - \bar{p}_1\right) + \dfrac{b}{2}\Theta_0'\right] + \left(\dfrac{1+\nu}{2}\right)^2\dfrac{N}{K^2}\left(\dfrac{1 - \frac{1}{P_r}}{1 - \frac{T_w}{T_0}}\right)\dfrac{\bar{u}_0}{\zeta^2}\left[\left(-\dfrac{\bar{u}_0\bar{u}_0'}{\zeta}\right) + \bar{u}_0\bar{u}_0'' + 2(\bar{u}_0')^2\right] \\
\quad + \left(\dfrac{1+\nu}{2}\right)\dfrac{1}{2P_rK^2}\,\dfrac{N}{\zeta}\left[\left(\dfrac{\bar{u}_0}{\zeta}\Theta_1'\right)' + \dfrac{\Theta_0'}{\bar{u}_0}\left(\bar{u}_1' - \bar{u}_1\,\dfrac{\bar{u}_0'}{\bar{u}_0}\right)\right] + \left(\dfrac{1+\nu}{2}\right)\dfrac{N}{2P_rK^2}\,\dfrac{\bar{u}_0^2}{\zeta}\,\Theta_0' \\
\bar{p}_2' = (2-\nu)\zeta\left(\bar{u}_1 - \bar{u}_0 - \dfrac{7}{4}b\bar{u}_0\right)
\end{cases}$$

$$
\begin{cases}
\bar{u}_1(0) = \Theta_1(0) = 0 \\
\bar{p}\nu_2(1) = 0 \\
\bar{u}_1(1) = \bar{u}_0(1-\bar{u}_0)\left(1+\frac{b}{2}\right) - \left(\frac{1+\nu}{2}\right)\frac{N}{K^2}\,\frac{\bar{u}_0^2}{\zeta}\,\bar{u}_1' \\
\Theta_1(1) = (1-\Theta_0)\left(1-\frac{\bar{u}_1}{\bar{u}_0}+\frac{b}{2}\right) - \left(\frac{1+\nu}{2}\right)\frac{N}{Pr\,K^2}\,\frac{\bar{u}_0}{\zeta}\,\Theta' - 2\,\frac{\left(1-\frac{1}{Pr}\right)}{\left(1-\frac{T_w}{T_0}\right)}\,\bar{u}_0(1-\bar{u}_0)
\end{cases}
$$

A.2 The Implicit-Difference Formulation of the Shock-Layer Equations

The complete, final form of the finite-difference formulation of the shock-layer equations, based on the implicit scheme, are given below. For each point e, there are two algebraic equations

$$
\left.
\begin{aligned}
A\,\bar{u}_d + B\,\bar{u}_e + C\,\bar{u}_f &= G \\
D\,\Theta_d + E\,\Theta_e + F\,\Theta_f &= J
\end{aligned}
\right\} \qquad (A.1)
$$

which relate the values of $\bar{u}$ and Θ at the point e to the values at the neighboring points d and f.

The subscripts refer to grid points specified in the sketches below and in Fig. 6.1.

(a)

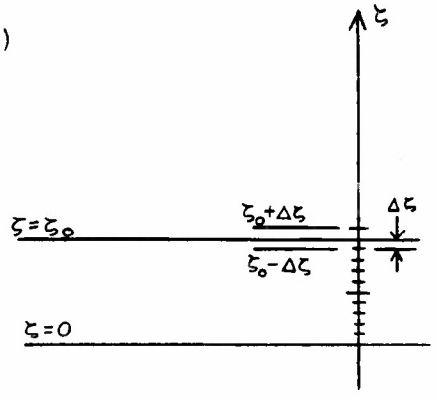

(b)

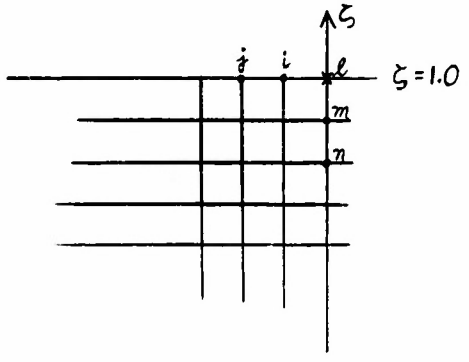

The coefficients A, B, C, D, E, F, G, and J in Eq. (A.1) are:

$$A=\left(\frac{\Delta\lambda}{\Delta\zeta}\right)\left\{\frac{1+\nu}{2}\left(\frac{1}{\bar{z}}\frac{d\bar{z}}{d\lambda}\right)\zeta-\left(\frac{1+\nu}{2}\right)\frac{1}{K^2}\sigma^3\cos\beta\frac{d\beta}{d\lambda}\frac{(2\bar{u}_b-\bar{u}_g)^2}{\zeta}\right.$$
$$\left.+\left(\frac{1+\nu}{2}\right)^2\frac{1}{2K^2}\left(\frac{\sigma}{\cos\beta}\right)^2\frac{1}{(\Delta\zeta)}\frac{(2\bar{p}_b-\bar{p}_g)}{\zeta}\cdot\frac{(2\bar{u}_b-\bar{u}_g)}{\zeta}\left[\frac{(\bar{u}_c-\bar{u}_a)}{(2\bar{u}_b-\bar{u}_g)}-\frac{\Delta\zeta}{\zeta}-2\right]\right\}$$

$$B=3+2\left(\frac{1+\nu}{2}\right)^2\frac{1}{K^2(\Delta\zeta)}\left(\frac{\sigma}{\cos\beta}\right)^2\left(\frac{\Delta\lambda}{\Delta\zeta}\right)\frac{(2\bar{p}_b-\bar{p}_g)}{\zeta}\cdot\frac{(2\bar{u}_b-\bar{u}_g)}{\zeta}$$

$$C=-\left(\frac{\Delta\lambda}{\Delta\zeta}\right)\left\{\frac{1+\nu}{2}\left(\frac{1}{\bar{z}}\frac{d\bar{z}}{d\lambda}\right)\zeta-\left(\frac{1+\nu}{2}\right)\frac{1}{K^2}\sigma^3\cos\beta\frac{d\beta}{d\lambda}\frac{(2\bar{u}_b-\bar{u}_g)^2}{\zeta}\right.$$
$$\left.+\left(\frac{1+\nu}{2}\right)^2\frac{1}{2K^2}\left(\frac{\sigma}{\cos\beta}\right)^2\frac{1}{\Delta\zeta}\frac{(2\bar{p}_b-\bar{p}_g)}{\zeta}\frac{(2\bar{u}_b-\bar{u}_g)}{\zeta}\left[\frac{(\bar{u}_c-\bar{u}_a)}{(2\bar{u}_b-\bar{u}_g)}-\frac{\Delta\zeta}{\zeta}+2\right]\right\}$$

$$G=\bar{u}_g+2(2\bar{u}_b-\bar{u}_g)\left\{1+(\Delta\lambda)\left[\tan\beta\frac{d\beta}{d\lambda}+2\varepsilon\cot\beta\frac{d\beta}{d\lambda}+\frac{\varepsilon}{2\bar{p}_b-\bar{p}_g}\left(\frac{\partial\bar{p}}{\partial\lambda}\right)_e\right]\right\}$$
$$-\left(\frac{1+\nu}{2}\right)^2\frac{1}{4K^2}\left(\frac{\sigma}{\cos\beta}\right)^2\left(\frac{\Delta\lambda}{\Delta\zeta}\right)\frac{(2\bar{p}_b-\bar{p}_g)}{(\Delta\zeta)}\frac{(\bar{u}_c-\bar{u}_a)^2}{\zeta^2}$$
$$-\frac{2\varepsilon(\Delta\lambda)}{(2\bar{u}_b-\bar{u}_g)}\left[\frac{T_w}{T_o}+\left(1-\frac{T_w}{T_o}\right)(2\Theta_b-\Theta_g)\right]\left[2\frac{\tan\beta}{\sin^2\beta}\frac{d\beta}{d\lambda}+\frac{(\partial\bar{p}/\partial\lambda)_e}{\cos^2\beta(2\bar{p}_b-\bar{p}_g)}\right]$$

$$D=\left(\frac{\Delta\lambda}{\Delta\zeta}\right)\left\{\frac{1+\nu}{2}\left(\frac{1}{\bar{z}}\frac{d\bar{z}}{d\lambda}\right)\zeta-\left(\frac{1+\nu}{2}\right)\frac{1}{PrK^2}\sigma^3\cos\beta\frac{d\beta}{d\lambda}\frac{\bar{u}_e^2}{\zeta}\right.$$
$$\left.+\left(\frac{1+\nu}{2}\right)\frac{1}{2PrK^2}\left(\frac{\sigma}{\cos\beta}\right)^2\frac{\bar{u}_e}{(\Delta\zeta)}\frac{(2\bar{p}_b-\bar{p}_g)}{\zeta^2}\left[\frac{\bar{u}_f-\bar{u}_d}{2\bar{u}_e}-\frac{\Delta\zeta}{\zeta}-2\right]\right\}$$

$$E=3+2\left(\frac{1+\nu}{2}\right)^2\frac{1}{PrK^2(\Delta\zeta)}\left(\frac{\sigma}{\cos\beta}\right)^2\left(\frac{\Delta\lambda}{\Delta\zeta}\right)\frac{2\bar{p}_b-\bar{p}_g}{\zeta}\cdot\frac{\bar{u}_e}{\zeta}$$

$$F=-\left(\frac{\Delta\lambda}{\Delta\zeta}\right)\left\{\frac{1+\nu}{2}\left(\frac{1}{\bar{z}}\frac{d\bar{z}}{d\lambda}\right)\zeta-\left(\frac{1+\nu}{2}\right)\frac{1}{PrK^2}\sigma^3\cos\beta\frac{d\beta}{d\lambda}\frac{\bar{u}_e^2}{\zeta}\right.$$
$$\left.+\left(\frac{1+\nu}{2}\right)^2\frac{1}{2PrK^2}\left(\frac{\sigma}{\cos\beta}\right)^2\frac{\bar{u}_e}{(\Delta\zeta)}\frac{(2\bar{p}_b-\bar{p}_g)}{\zeta^2}\left[\frac{\bar{u}_f-\bar{u}_d}{2\bar{u}_e}-\frac{\Delta\zeta}{\zeta}+2\right]\right\}$$

$$J=4\Theta_b-\Theta_g-\left(\frac{1+\nu}{2}\right)2\sigma^3\cos^3\beta\frac{d\beta}{d\lambda}\frac{\left(1-\frac{1}{Pr}\right)}{\left(1-\frac{T_w}{T_o}\right)}\left(\frac{\Delta\lambda}{\Delta\zeta}\right)\frac{\bar{u}_e^3}{\zeta}(\bar{u}_f-\bar{u}_d)$$
$$+2\cdot\left(\frac{1+\nu}{2}\right)^2\frac{\sigma^2}{K^2}\frac{\left(1-\frac{1}{Pr}\right)}{\left(1-\frac{T_w}{T_o}\right)}\frac{(2\bar{p}_b-\bar{p}_g)}{(\Delta\zeta)}\cdot\frac{\bar{u}_e^2}{\zeta^2}\left[\bar{u}_f-2\bar{u}_e+\bar{u}_d-\frac{\Delta\zeta}{2\zeta}(\bar{u}_f-\bar{u}_d)+\frac{(\bar{u}_f-\bar{u}_d)^2}{2\bar{u}_e}\right]$$

where $\left(\partial\bar{p}/\partial\lambda\right)_e$ is to be evaluated by the difference quotient (Refer to the sketch of Fig. 6.1), i.e. $\left(\frac{\partial\bar{p}}{\partial\lambda}\right)_e = \frac{1}{2(\Delta\lambda)}\left[5\bar{p}_b - 8\bar{p}_g + 3\bar{p}_k\right]$

The system of linear algebraic equations generated at all points between $\zeta = \zeta_o$ and $\zeta = 1$ by application of Eq. (A.1) is to be solved with the boundary conditions:

$$\left.\begin{aligned}
\bar{u}(\zeta_o) &= \frac{\zeta_o}{2}\left[\frac{\overline{\bar{u}(\zeta_o+\Delta\zeta)}}{\zeta_o+\Delta\zeta} + \frac{\overline{\bar{u}(\zeta_o-\Delta\zeta)}}{\zeta_o-\Delta\zeta}\right], \\
\Theta(\zeta_o) &= \frac{\zeta_o}{2}\left[\frac{\overline{\Theta(\zeta_o+\Delta\zeta)}}{\zeta_o+\Delta\zeta} + \frac{\overline{\Theta(\zeta_o-\Delta\zeta)}}{\zeta_o-\Delta\zeta}\right],
\end{aligned}\right\} \text{at } \zeta = \zeta_o$$

$$\left.\begin{aligned}
\bar{u}_\ell &= 1 - \left(\frac{1+\nu}{2}\right)\frac{\sigma}{K^2\zeta}\,\frac{(2\bar{u}_i - \bar{u}_j)}{2(\Delta\zeta)}\left[3\bar{u}_\ell - 4\bar{u}_m + \bar{u}_n\right], \\
\Theta_\ell &= 1 - \left(\frac{1+\nu}{2}\right)\frac{\sigma}{PrK^2\zeta}\,\frac{\bar{u}_\ell}{2(\Delta\zeta)}\left[3\Theta_\ell - 4\Theta_m + \Theta_n\right] \\
&\quad - 2\cos^2\beta\,\frac{\left(1-\frac{1}{Pr}\right)}{\left(1-\frac{T_w}{T_o}\right)}\,\bar{u}_\ell\left(1-\bar{u}_\ell\right)
\end{aligned}\right\} \text{at } \zeta = \zeta_\ell = 1$$

REFERENCES

1. Van Dyke, M. D., The Supersonic Blunt-Body Problem -- Review and Extension. Journal of the Aerospace Sciences, Vol. 25, No. 8, p. 485, August 1958.

2. Vaglio-Laurin, R., On the PLK Method and Supersonic Blunt-Body Problem. Journal of the Aerospace Sciences, Vol. 29, No. 2, p. 185, February 1962.

3. Belotserkovskii, O. M., Flow Past a Circular Cylinder with a Detached Shock Wave. Doklady Akad. Nauk SSSR, Vol. 113, No. 3, pp. 509-512, 1957 (Russian).

4. Hayes, W. D. and Probstein, R. F., Hypersonic Flow Theory. Academic Press, 1959.

5. Tsien, H. S., Super Aerodynamics, Mechanics of Rarefied Gases. Journal Aero. Sci., Vol. 13, No. 12, p. 653, December 1946.

6. Chapman, S. and Cowling, T. G., The Mathematical Theory of Non-uniform Gases. 2nd Ed., Chapter 15, Cambridge University Press, 1952.

7. Sherman, F. A., A Low-Density Wind-Tunnel Study of Shock-Wave Structure and Relaxation Phenomena in Gases. NACA TN 3298, 1955.

8. Schaaf, S. A., and Chambre, P. L., Flow of Rarefied Gases, Section H, Vol. 3 of High Speed Aerodynamics and Jet Propulsion, Fundamentals of Gas Dynamics. Edited by H. W. Emmons, Princeton University Press, Princeton, New Jersey, 1958.

9. Adams, M. C. and Probstein, R., On the Validity of Continuum Theory for Satellite and Hypersonic Flight Problems at High Altitudes. Jet Propulsion, Vol. 28, No. 2, p. 86, Feb. 1958.

10. Probstein, R. F. and Kemp, N., Viscous Aerodynamics Characteristics in Hypersonic Rarefied Gas Flow. Journal of the Aerospace Sciences, Vol. 27, No. 3, p. 174, March 1960.

11. Probstein, R. F., Shock-Wave and Flow Field Development in Hypersonic Re-entry. ARS Journal, Vol. 31, No. 2, p. 185, Feb. 1961.

12. Van Dyke, M., A Review and Extension of Higher Order Hypersonic Boundary Layer Theory. Paper presented at Third International Symposium on Rarefied Gas Dynamics, Paris, France, June 1962.

13. Lees, L., A Kinetic Theory Description of Rarefied Gas Flow. GALCIT Hypersonics Research Project Memo No. 51, 1959.

14. Willis, R., Comparison of Kinetic Theory Analysis of Linearized Couette Flow. Phys. Fluids, Vol. 5, No. 2, p. 127, Feb. 1962.

15. Talbot, L., Survey of the Shock Structure Problem. ARS Journal Vol. 32, No. 7, p. 1009, July 1962.

16. Liepman, H. W., Narasimha, R. and Chahine, M., The Structure of a Plane Shock Layer. Phys. Fluids, Vol. 5, No. 11, Nov. 1962.

17. Bhatnager, P. L., Gross, E. P. and Krook, M., A Model for Collision Processes in Gases. I. Small Amplitude Processes in Charged and Neutral One-Component Systems. Physical Review, Vol. 94, No. 3, p. 511, May 1954.

18. Busemann, A., Flussigleit und Gasbewegung. Handbuch der Naturwissenschafter Auflage, p. 275, Jena, Gustave Fischer, 1933.

19. Lighthill, J. J., Dynamics of Dissociating Gas. Part 2, Equilibrium Flow. J. Fluid Mech., Vol. 2, p. 1, January 1957.

20. Chester, N., Supersonic Flow Past a Blunt Body with a Detached Shock. Part I, Two-Dimensional Body. J. Fluid Mech., Vol. 1, Part 4, p. 353, October 1956.

21. Freeman, N. C., On the Theory of Hypersonic Flow Past Plane and Axially-Symmetric Bluff Bodies. J. Fluid Mech., Vol. 1, p. 366, October 1960.

22. Rott, N. and Lenard, M., Vorticity Effect on Stagnation-Point Flow of a Viscous Incompressible Fluid. Journal of the Aerospace Sciences, Vol. 26, No. 8, p. 542, August 1959.

23. Kemp, N. H., Vorticity Interaction at an Axisymmetric Stagnation Point in a Viscous Incompressible Fluid. Journal of the Aerospace Sciences, Vol. 26, No. 8, p. 543, August 1959.

24. Van Dyke, M., Second-Order Compressible Boundary-Layer Theory with Application to Blunt Bodies in Hypersonic Flow. Stanford University, SUDAER 112, Rept. No. AFOSR TN 61-1270, July 1961.

25. Lenard, M., Stagnation Point of a Variable Property Fluid at Low Reynolds Numbers. Ph.D. Thesis, Cornell University, Sept. 1961.

26. Maslen, S. H., Second-Order Effects in Laminar B oundary Layers. AIAA Journal, Vol. 1, No. 1, p. 33, January 1963.

27. Ferri, A., Zakkay, V. and Ting, L., Blunt-Body Heat Transfer at Hypersonic Speed and Low Reynolds Number. Journal of the Aerospace Sciences, Vol. 28, No. 12, p. 962, December 1961.

28. Hayes, W. D., On Laminar Boundary Layer with Heat Transfer. Jet Propulsion, Vol. 26, p. 270, 1956.

29. Moore, F. K., Hypersonic Boundary Layer Theory, Section E in Vol. 4 of High Speed Aerodynamics and Jet Propulsion, Theory of Laminar Flows. (Ed. by F.K. Moore), Princeton University Press, Princeton, New Jersey (to be published).

30. Lees, L., Laminar Heat Transfer Over Blunt-Nosed Bodies at Hypersonic Flight Speeds. Jet Propulsion, Vol. 26, No. 4, p. 259, 1956.

31. Moore, F. K., On Local Flat Plate Similarity in the Hypersonic Boundary Layer. Journal of the Aerospace Sciences, Vol. 28, No. 10, p. 753, October 1961.

32. Hoshizaki, H., Heat Transfer in Planetary Atmospheres at Super-Satellite Speeds. ARS Journal, Vol. 32, No. 10, p. 1544, Oct. 1962.

33. Oguchi, H., Blunt Body Viscous Layer with and without a Magnetic Field. Phys. Fluids, Vol. 3, No. 4, p. 567, August 1960.

34. Ho, H. T. and Probstein, R. F., The Compressible Viscous Layer in Rarefied Hypersonic Flow. Brown University Aeronaut. Research Laboratories Tech. Note ARL TN 60-132, August 1960.

35. Herring, T. K., The Boundary Layer Near the Stagnation Point in Hypersonic Flow Past a Sphere. J. Fluid Mech., Vol. 7, p. 257, 1960.

36. Chung, P. M., Hypersonic Viscous Shock Layer of Nonequilibrium Dissociating Gas. NASA TR R-109, 1961.

37. Goldberg, L. and Scala, S., Mass Transfer in the Hypersonic Low Reynolds Number Viscous Layer. Presented at the IAS 30th Annual Meeting, New York, January 1962.

38. Germain, P. and Guiraud, J. P., Conditions de Choc et Structure des Ondes de Choc dans un Ecoulement Stationnaire de Fluide Dissipatif. Recherche Aeronautique, No. 81, p. 11, 1961; also ONERA Publication No. 105, 1962.

39. Chow, R. R. and Ting, L., Higher-Order Theory of Curved Shock. Journal of the Aerospace Sciences, Vol. 28, No. 5, May 1961; also Polytechnic Institute of Brooklyn, PIBAL Rept. No. 609, August 1960.

40. Levinsky, E. S. and Yoshihara, H., Rarefied Hypersonci Flow Over a Sphere. Hypersonic Flow Research, Ed. F. R. Riddell, p. 81, Academic Press, 1962.

41. Cheng, H. K., Hypersonic Shock-Layer Theory of the Stagnation Region at Low Reynolds Number. Proc. Heat Transfer and Fluid Mechanics Institute, University of Southern California, Stanford University Press, p. 161, June 1961.

42. Cheng, H. K. and Chang, A. L., Hypersonic Shock Layer at Low Reynolds Number -- The Yawed Cylinder. U. S. Air Force, Office of Aerospace Research. Aeronautical Research Lab. Rept. ARL 62-453; also available as Cornell Aero. Lab. Rept. No. AF-1515-A-1, Oct. 1962.

43. Pan, Y. S. and Probstein, R. F., Shock Structure and the Leading Edge Problem. Abstract of paper presented at the Third International Symposium on Rarefied Gas Dynamics, Paris, France, June 1962.

44. Shidlovsky, V. P., The Problem of the Supersonic Flow of Slightly Rarefied Gas About a Sphere. Abstract of paper presented at Third International Symposium on Rarefied Gas Dynamics, Paris, France, June 1962.

45. Cheng, H. K. and Chang, A. L., Remarks on Stagnation Region in Rarefied High Mach-Number Flow. AIAA Journal, Vol. 1, No. 1, p. 231, January 1963.

46. Hosizaki, H., Neice, S. and Chan, K. K., Stagnation Point Heat Transfer Rates at Low Reynolds Number. IAS Paper No. 60-68, June 1960.

47. Ferri, A. and Zakkay, V., Measurement of Stagnation Point Heat Transfer at Low Reynolds Numbers. Journal of the Aerospace Sciences, Vol. 29, No. 7, p. 847, July 1962.

48. Ferri, A., Zakkay, V. and Ting, L., On Blunt-Body Heat Transfer at Hypersonic Speed and Low Reynolds Numbers. Journal of the Aerospace Sciences, Vol. 29, No. 7, p. 882, July 1962.

49. Wittliff, C. E. and Wilson, M. R., Low-Density Stagnation-Point Heat Transfer in the Hypersonic Shock Tunnels. ARS Journal, Vol. 32, pp. 275-276, 1962.

50. Vidal, R. J. and Wittliff, C. E., Hypersonic Low-Density Studies of Blunt and Slender Bodies. Paper presented at Third International Symposium on Rarefied Gas Dynamics, Paris, France, June 1962.

51. Varwig, R. L., Stagnation-Point Heat-Transfer Measurements in Hypersonic Low Reynolds Number Flow. Aerospace Corp. Rept. TDR-930(2230-11) TN-2 (DCAS-TDR-62-125) June 1962.

52. Bloxsom, D. E. and Rhodes, B. V., Experimental Effect of Bluntness and Gas Rarefaction on Drag Coefficients and Stagnation Heat Transfer on Axisymmetric Shapes in Hypersonic Flow. Journal of Aerospace Sciences, Vol. 29, No. 12, p. 1429, December 1962.

53. Swigart, R. J., A Theory of Asymmetric Hypersonic Blunt-Body Flows. IAS Paper No. 62-98, Presented at IAS National Summer Meeting, Los Angeles, California, June 1962.

54. Chester, W., Supersonic Flow Past a Bluff Body with a Detached Shock. Part 2, Axisymmetrical Body. J. Fluid Mech., Vol. 1, p. 490, November 1956.

55. Van Dyke, M. D., A Model of Supersonic Flow Past Blunt Axisymmetric Bodies with Application to Chester's Solution. Journal Fluid Mech., Vol. 3, p. 515, 1958.

56. Sedov, L. I., Michailova, M. P. and Chernyi, G. G., On the Influence of Viscosity and Heat Conduction on the Gas Flow Behind a Strong Shock Wave. Vestnik Moskovskovo Universiteta, No. 3, p. 95, 1953.

57. Becker, R., Stosswelle and Detonation. Z. Physik 8, p. 321, 1922.

58. Bush, W. B., The Hypersonic Approximation for the Shock Structure of a Perfect Gas with the Sutherland Viscosity Law. Calif. Inst. Tech. Firestone Flight Sci. Lab., Air Force Office of Scientific Res. Rept. AFOSR 2257, February 1962.

59. Sychev, V. V., On Hypersonic Flow of Viscous Heat-Conducting Gas. PMM, Vol. 25, No. 4, p. 600, 1961.

60. Kennard, E. H., Kinetic Theory of Gases. Chapter 8, 1st Ed., McGraw-Hill, New York and London, 1938.

61. Glick, H. S., Modified Crocco-Lees Mixing Theory for Supersonic Separated and Reattaching Flows. Jour. Aerospace Sci., Vol. 29, No. 10, p. 1238, October 1962.

62. Dorodnitsyn, A. A., Method of the Integral Relations for the Numerical Solution of Partial Differential Equations. Rep. Inst. of Exact Mechanics and Computing Technique, Akad. Nauk SSSR, 1958 (in English).

63. Pallone, A., Nonsimilar Solutions of the Compressible-Laminar Boundary-Layer Equations with Applications to the Upstream Transpiration Cooling Problem. Jour. Aerospace Sci., Vol. 28, No. 6, p. 449, June 1961.

64. Forsythe, G. E. and Wasow, W. R., Finite-Difference Methods for Partial Differential Equations. Wiley, 1960.

65. Richtmeyer, R. D., Difference Methods for Initial-Value Problems. Interscience Publishers, Inc., 1957.

66. Flugge-Lotz, I. and Yu, E. Y., Development of Finite-Difference Method for Computing a Compressible Laminar Boundary Layer with Interaction. Division of Engineering Mechanics, Stanford Univ. Tech. Rept. No. 127 (AFOSR TN 60-577), May 5, 1960.

67. Flugge-Lotz, I. and Blottner, F. G., Computation of the Compressible Laminar Boundary-Layer Flow Including Displacement Thickness Interaction Using Finite-Difference Methods. Division of Engineering Mechanics, Stanford Univ. Tech. Rept. No. 131, (AFOSR 2206) January 1962.

68. Kramer, R. F. and Lieberstein, H. M., Numerical Solution of Boundary Layer Equations without Similarity Assumptions. JAS 26, 8, 1959.

69. Der, J. and Raetz, G. S., Solution of General Three-Dimensional Laminar Boundary-Layer Problems by an Exact Numerical Method. Paper presented at IAS 30th Annual Meeting, January 1962.

70. Dufort, E. C. and Frankel, S., Stability Conditions in the Numerical Treatment of Parabolic Differential Equations. Math Tables and Other Aids to Computations, Vol. VII, No. 43, July 1953.

71. Chang, A. L. and Cheng, H. K., A Study of Finite-Difference Methods as Applied to Hypersonic, Viscous Shock-Layer Equations. Cornell Aero. Lab. Rept. AF-1285-A-9, March 1963.

72. Chapman, D. R., An Analysis of the Corridor and Guidance Requirements for Supercircular Entry into Planetary Atmospheres. NASA TR R-55, 1955.

73. Eggers, A. J., Hansen, C. F. and Cunningham, B. E., Stagnation-Point Heat Transfer to Blunt Shapes in Hypersonic Flight, Including Effects of Yaw. NACA TN 4229, April 1958.

74. Yoler, Y. A., Dyna-Soar: A Review of the Technology. Aerospace Eng., Vol. 20, No. 8, p. 9, August 1961.

75. Nagamatsu, H. T., Weil, J. A. and Sheer, R. E., Heat Transfer to Flat Plate in High Temperature Rarefied Ultrahigh Mach Number Flow. ARS Journ., Vol. 32, No. 4, p. 533, April 1962.

76. Oguchi, H., The Sharp Leading Edge Problem in Hypersonic Flow. Rarefied Gas Dynamics. Edited by L. Talbot, Academic Press, p. 501, 1961.

77. Oguchi, H., The Leading Edge Slip Effects in a Rarefied Hypersonic Flow. Paper presented at Third International Symposium on Rarefied Gas Dynamics, Paris, France, June 1962.

78. Van Driest, E. R., Investigation of Laminar Boundary Layer in Compressible Fluid Using the Crocco Method. NACA TN 2597, Jan. 1952.

79. Scala, S. M. and Talbot, L., Shock Wave Structure with Rotational and Vibrational Relaxation. Paper presented at Third International Symposium on Rarefied Gas Dynamics, Paris, France, June 1962.

80. Hirschfelder, J. O., Curtiss, C. F. and Bird, R. H., Molecular Theory of Gases and Liquid. John Wiley and Sons, 1954.

81. Glasstone, S., Laidler, K. J. and Eyring, H., The Theory of Rate Processes. McGraw-Hill Book Co., New York, 1941, pp. 339-400.

82. Fay, J. A. and Riddell, F. R., Theory of Stagnation Point Heat Transfer in Dissociated Air. Journ. Aerospace Sciences, Vol. 25, No. 2, p. 73, February 1958.

83. Hall, J. G., Eschenroeder, A. Q., and Marrone, P. V., Blunt-Nosed Inviscid Air-Flows with Coupled Nonequilibrium Processes. Jour. Aerospace Sci., Vol. 29, No. 9, p. 1038, September 1962.

84. Gibson, W. E., Dissociation Scaling for Nonequilibrium Blunt Nose Flow. ARS Journal, Vol. 32, No. 2, p. 285, February 1962.

85. Reshotko, E. and Beckwith, I. E., Compressible Laminar Boundary Layer Over a Yawed Infinite Cylinder with Heat Transfer and Arbitrary Prandtl Number. NACA Rept. 1379, 1958.

86. Eggers, A. J., Hansen, C. F. and Cunningham, B. E., Stagnation-Point Heat Transfer to Blunt Shapes in Hypersonic Flight, Including Effects of Yaw. NACA TN 4229, April 1958.

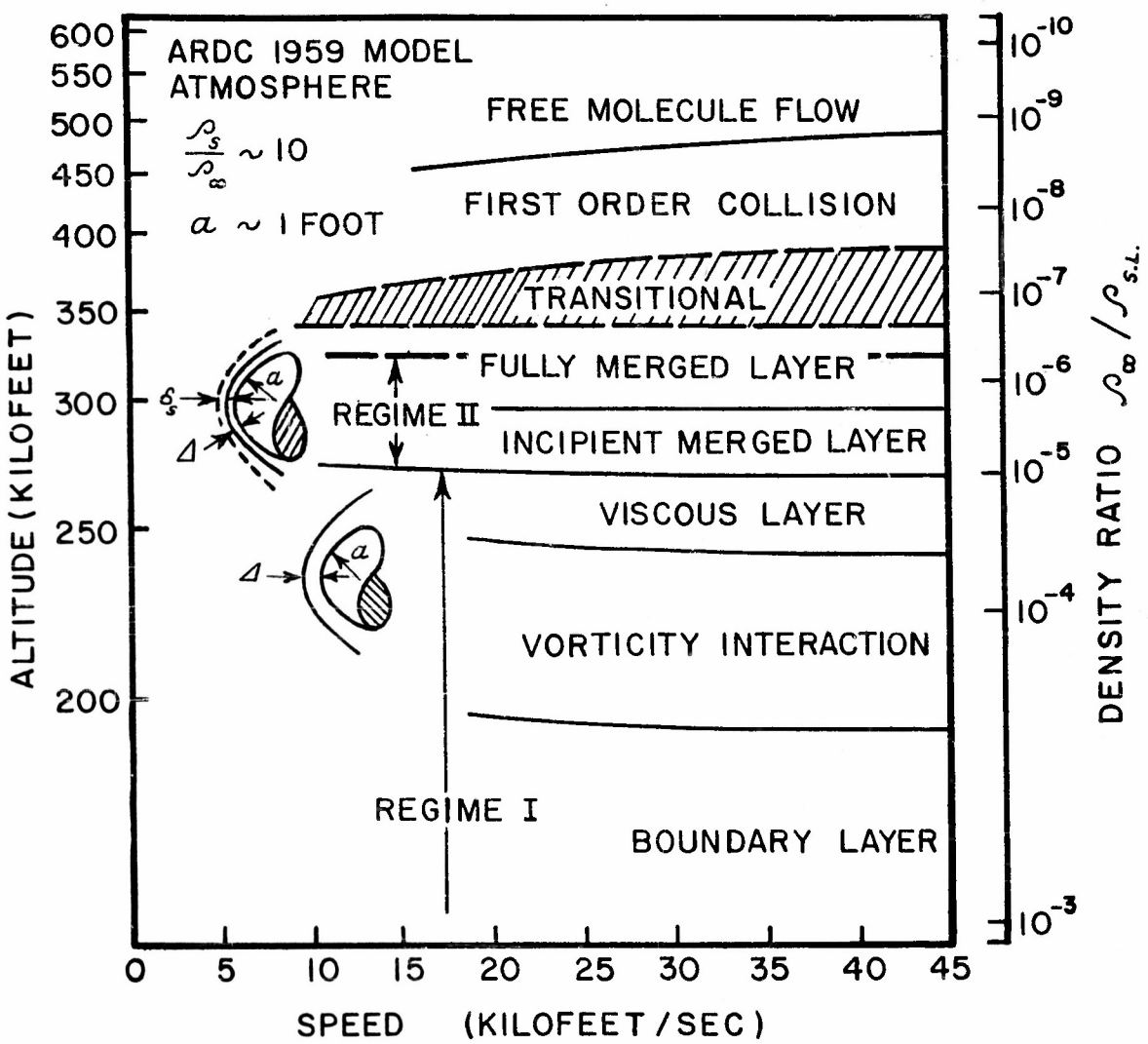

Figure 1.1 RAREFIED GAS-FLOW REGIMES OF A HIGHLY COOLED BLUNT BODY AT HYPERSONIC SPEED (BOUNDARIES BASED ON DATA OF PROBSTEIN)

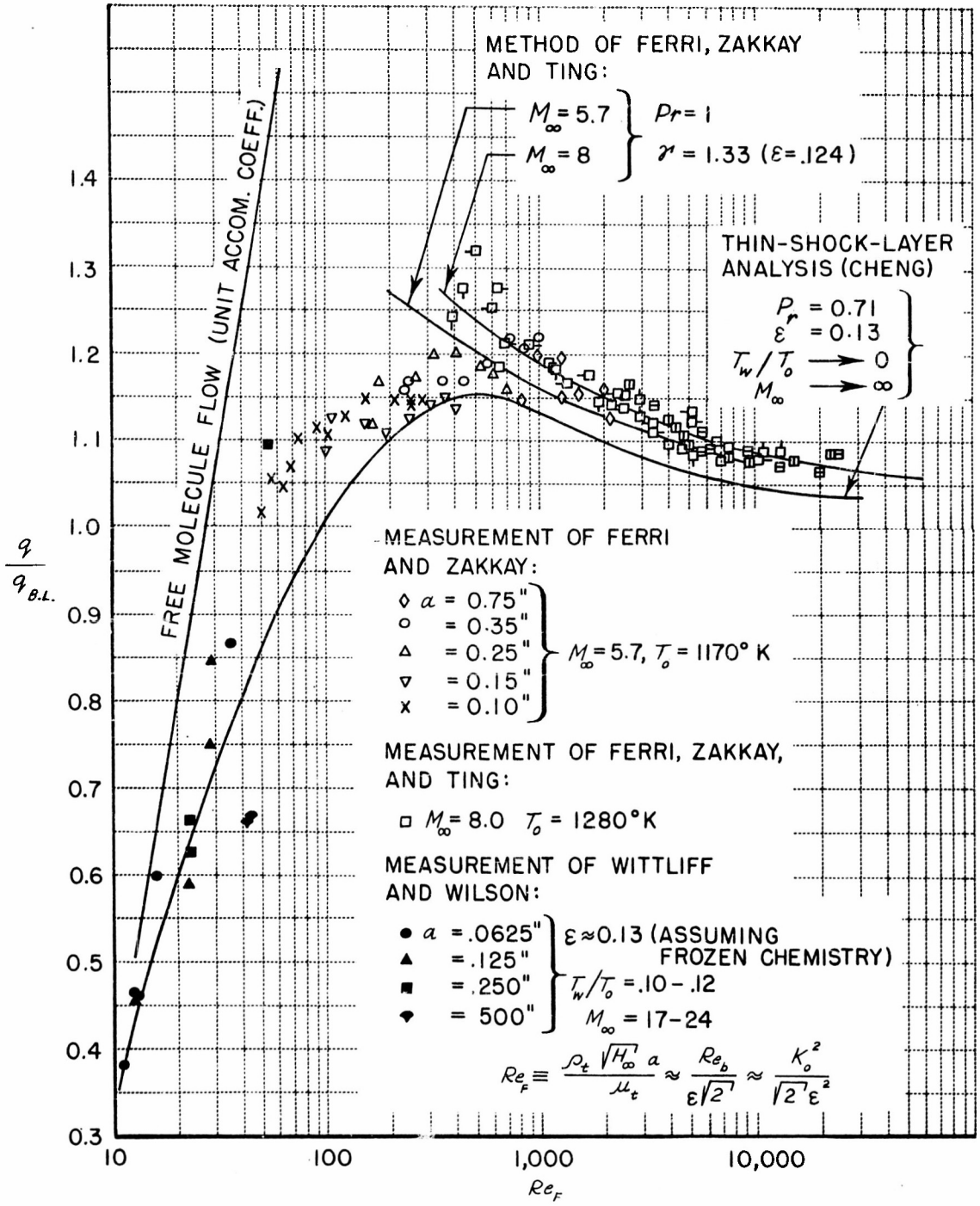

Figure 4.1 COMPARISON OF STAGNATION-POINT HEAT-TRANSFER MEASUREMENTS ON SPHERICAL BODIES WITH THEORIES

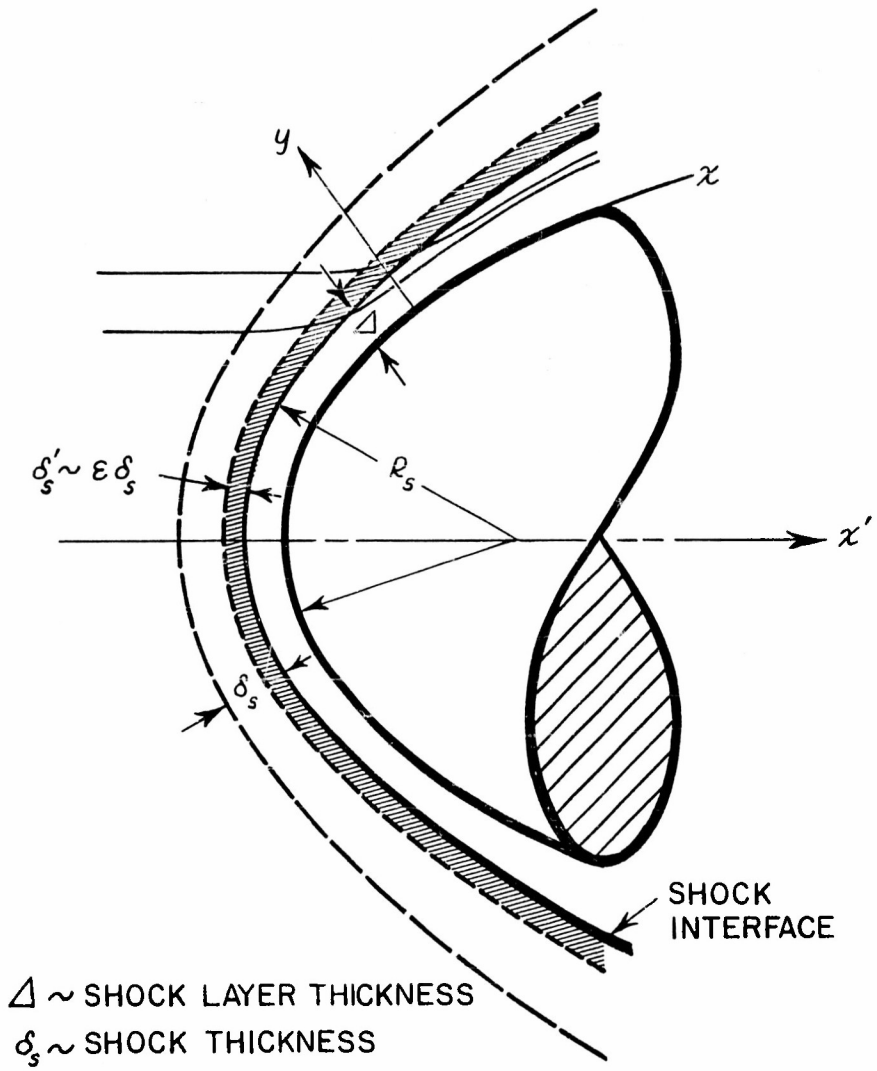

Figure 5.1 TWO-LAYER FLOW MODEL

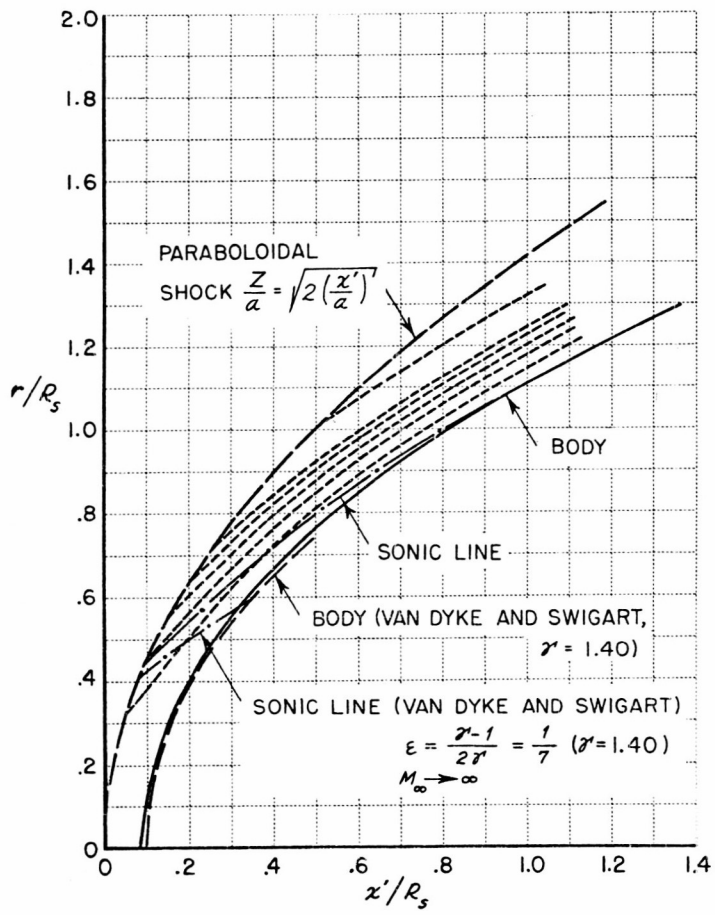

(a) STREAMLINE PATTERN AND BODY SHAPE

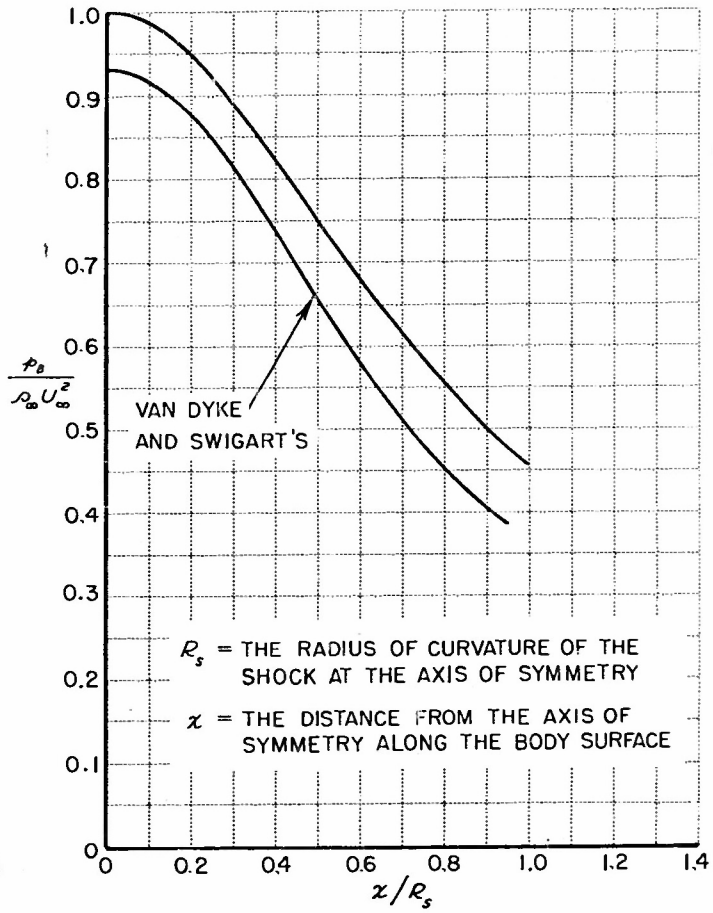

(b) SURFACE PRESSURE DISTRIBUTION

Figure 5.2 COMPARISON OF RESULTS BASED ON THE PRESENT THIN-SHOCK-LAYER APPROACH WITH THE EXACT NUMERICAL SOLUTION FOR THE FLOW AND BODY SUPPORTING A PARABOLOIDAL SHOCK IN THE INVISCID LIMIT

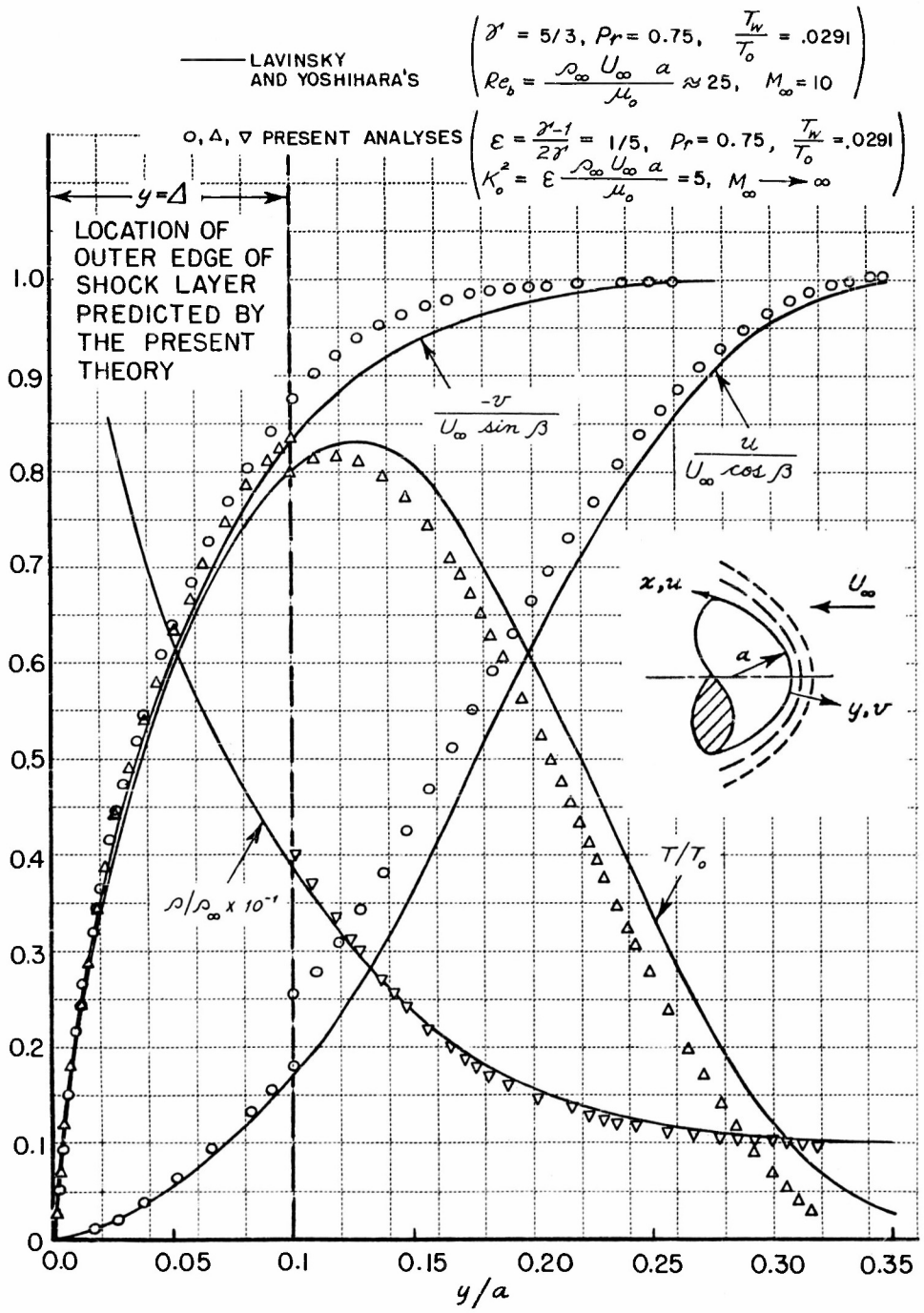

Figure 5.3 COMPARISON OF SOLUTION BASED ON TWO-LAYER MODEL WITH SOLUTION OF LEVINSKY AND YOSHIHARA FOR THE STAGNATION REGION AT LOW REYNOLDS NUMBER

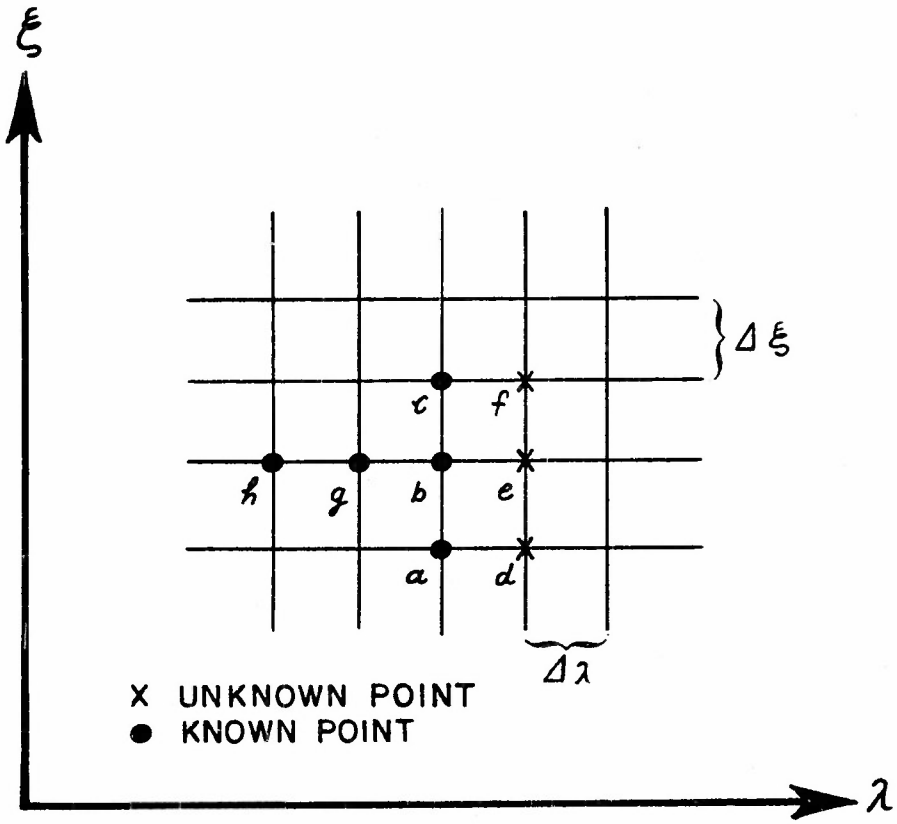

Figure 6.1 SKETCH OF GRID POINTS IN THE IMPLICIT DIFFERENCE SCHEME

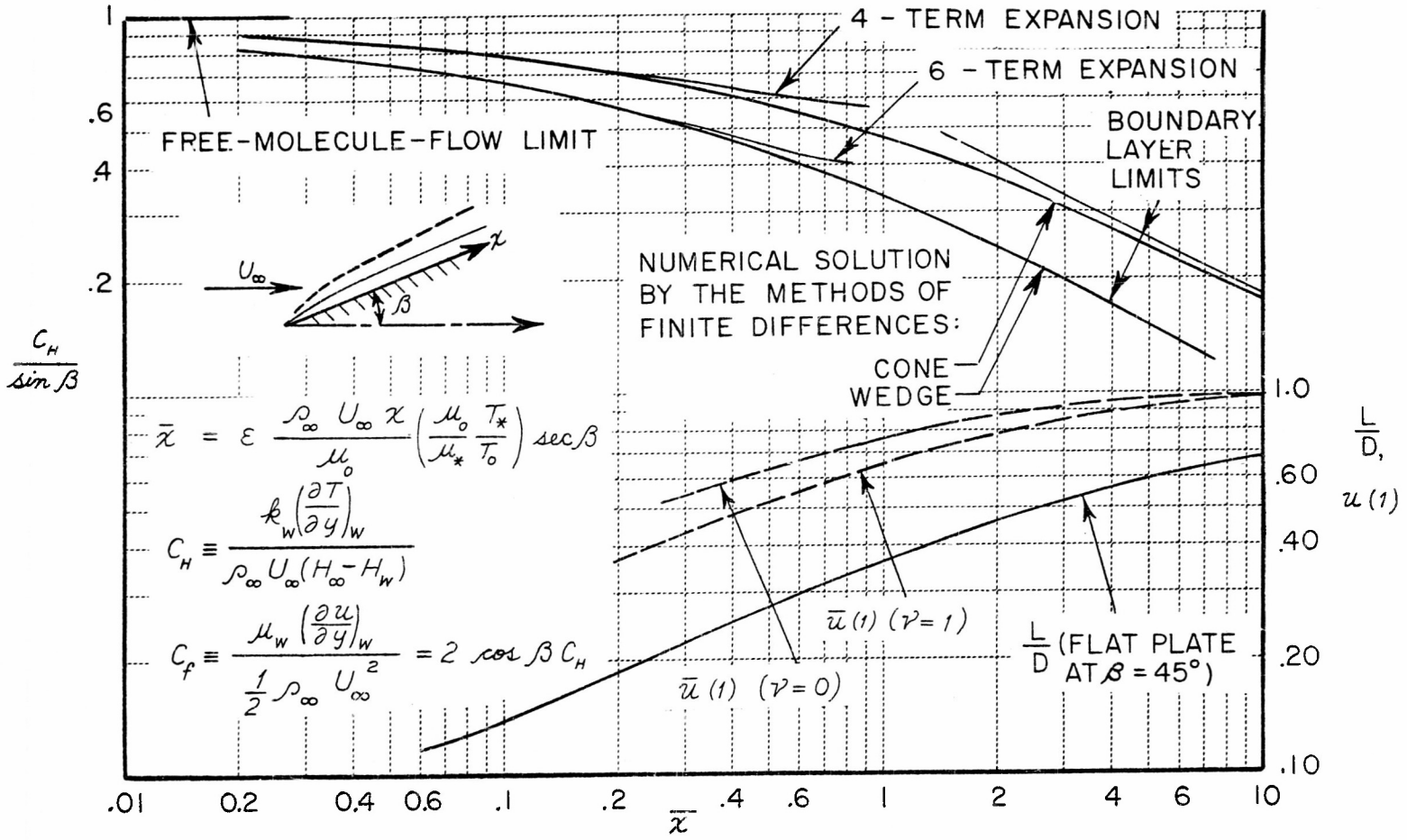

Figure 7.1 DISTRIBUTION OF SKIN FRICTION AND SURFACE HEAT-TRANSFER RATE ON CONE AND ON WEDGE IN HYPERSONIC FLOW AT LOW REYNOLDS NUMBER

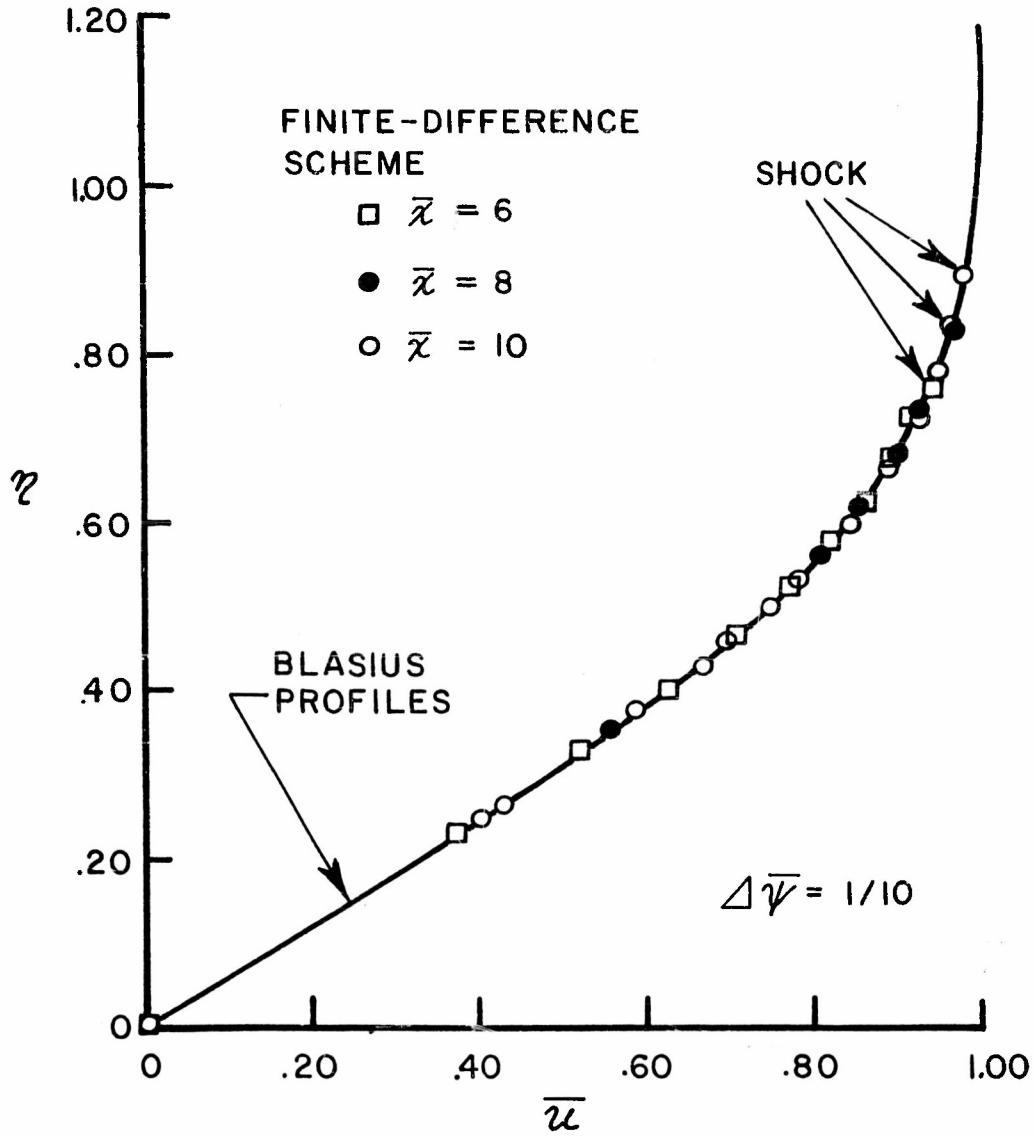

Figure 7.2 CORRELATION OF THE VISCOUS SHOCK LAYER SOLUTIONS FOR A WEDGE AT LARGE VALUE OF $\bar{x}$ WITH THE BLASIUS PROFILE

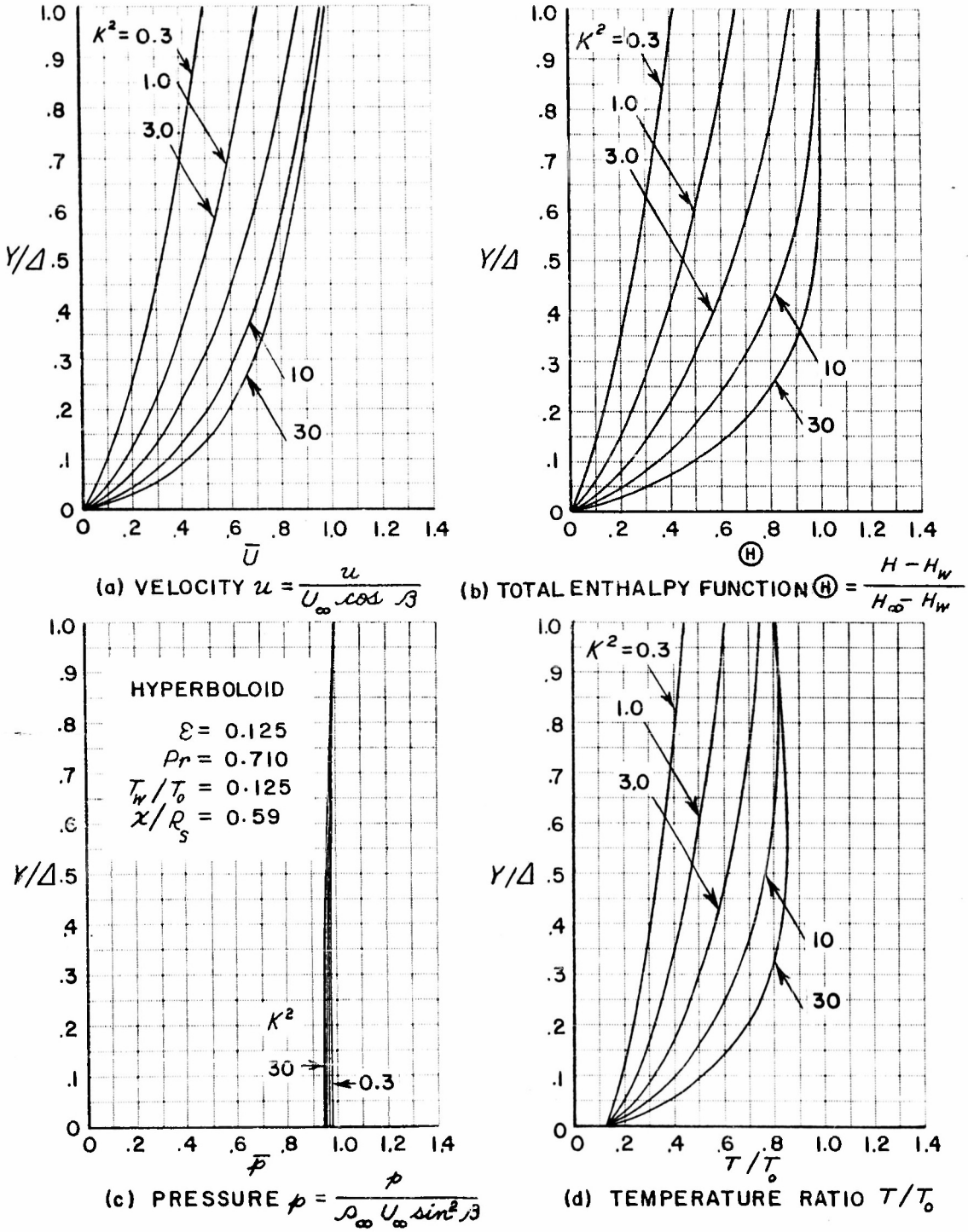

Figure 7.3 PROFILES OF VELOCITY, TOTAL-ENTHALPY FUNCTION, PRESSURE AND TEMPERATURE RATIO OVER THE BODY SUPPORTING A HYPERBOLOIDAL SHOCK AT x/R_s = 0.59

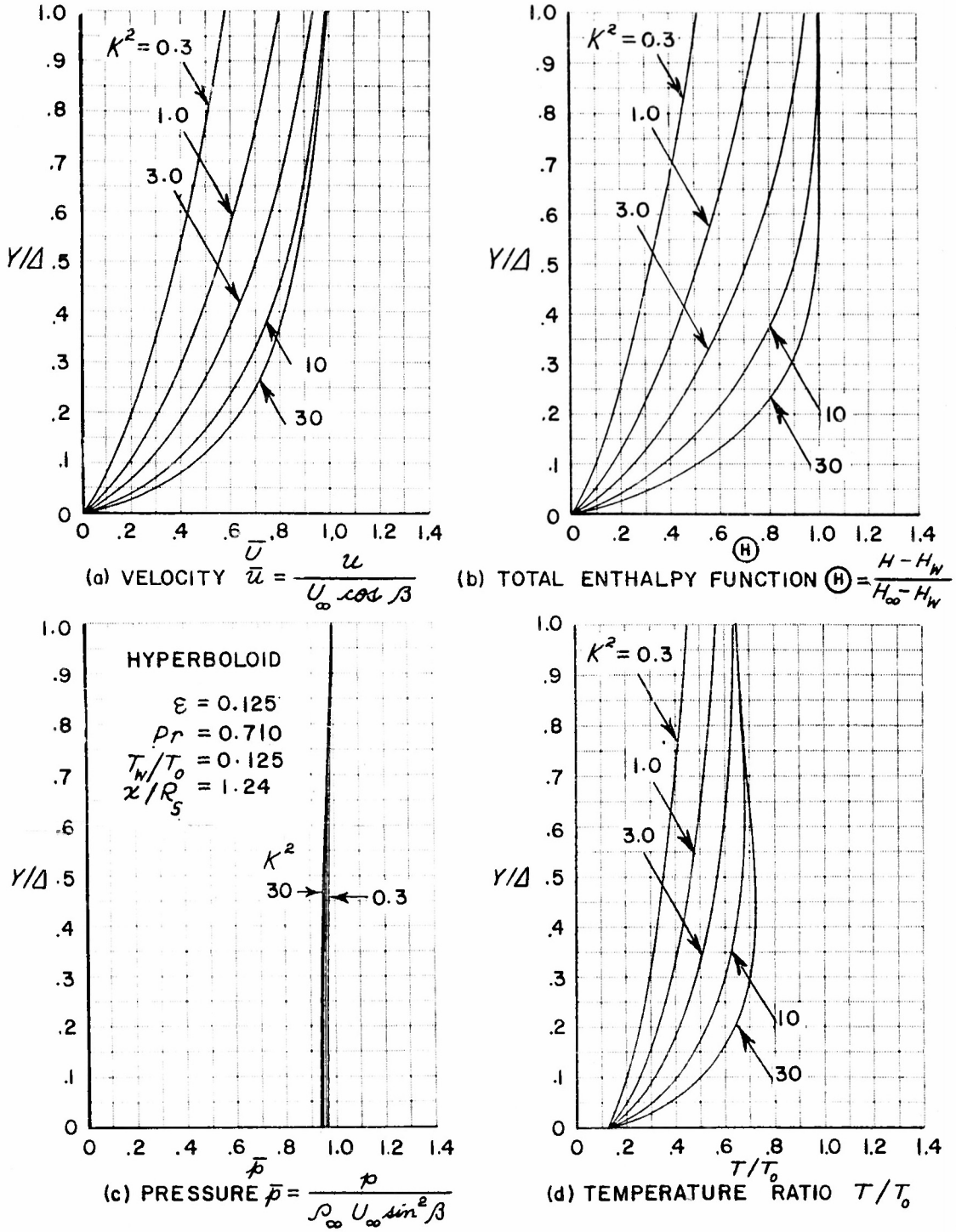

Figure 7.4 PROFILES OF VELOCITY, TOTAL-ENTHALPY FUNCTION, PRESSURE AND TEMPERATURE RATIO OVER THE BODY SUPPORTING A HYPERBOLOIDAL SHOCK AT $x/R_s = 1.24$

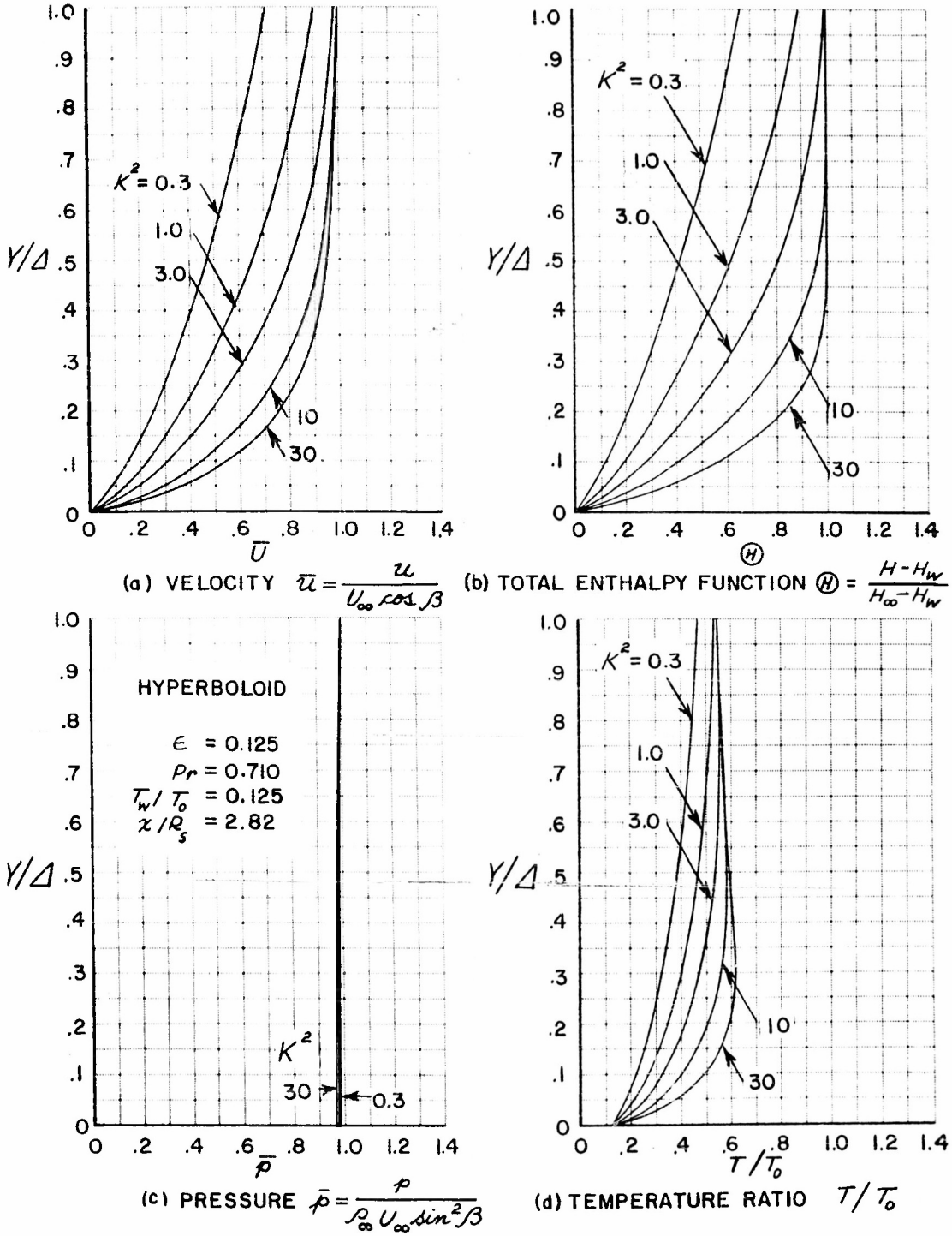

Figure 7.5 PROFILES OF VELOCITY, TOTAL-ENTHALPY FUNCTION, PRESSURE AND TEMPERATURE RATIO OVER THE BODY SUPPORTING A HYPERBOLOIDAL SHOCK AT $x/R_s = 2.82$

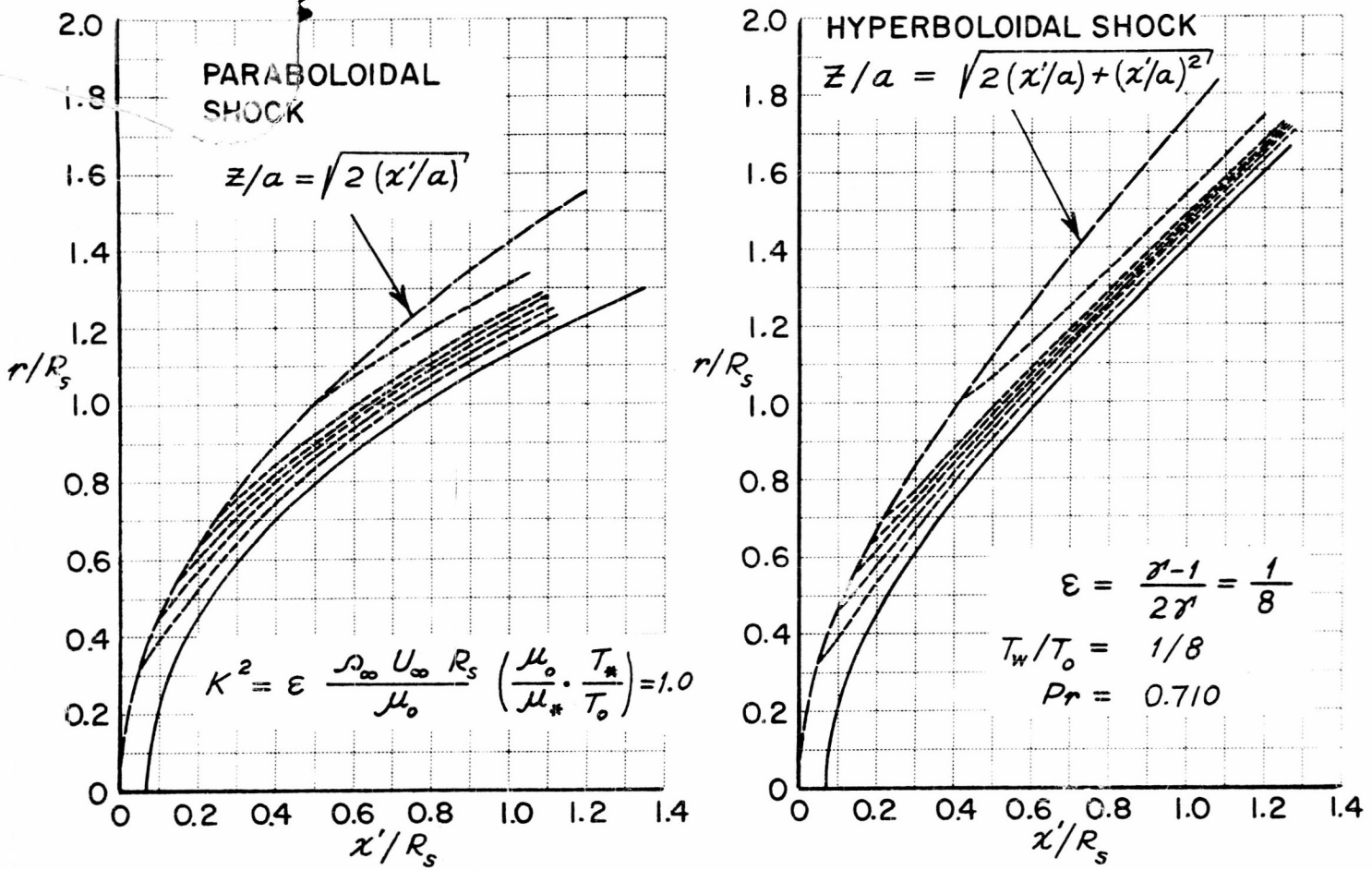

Figure 7.6 STREAMLINE PATTERN AND BODY SHAPES SUPPORTING THE PARABOLOID AND THE HYPERBOLOIDAL SHOCKS FOR $K^2 = 1$ (MERGED-LAYER REGIME)

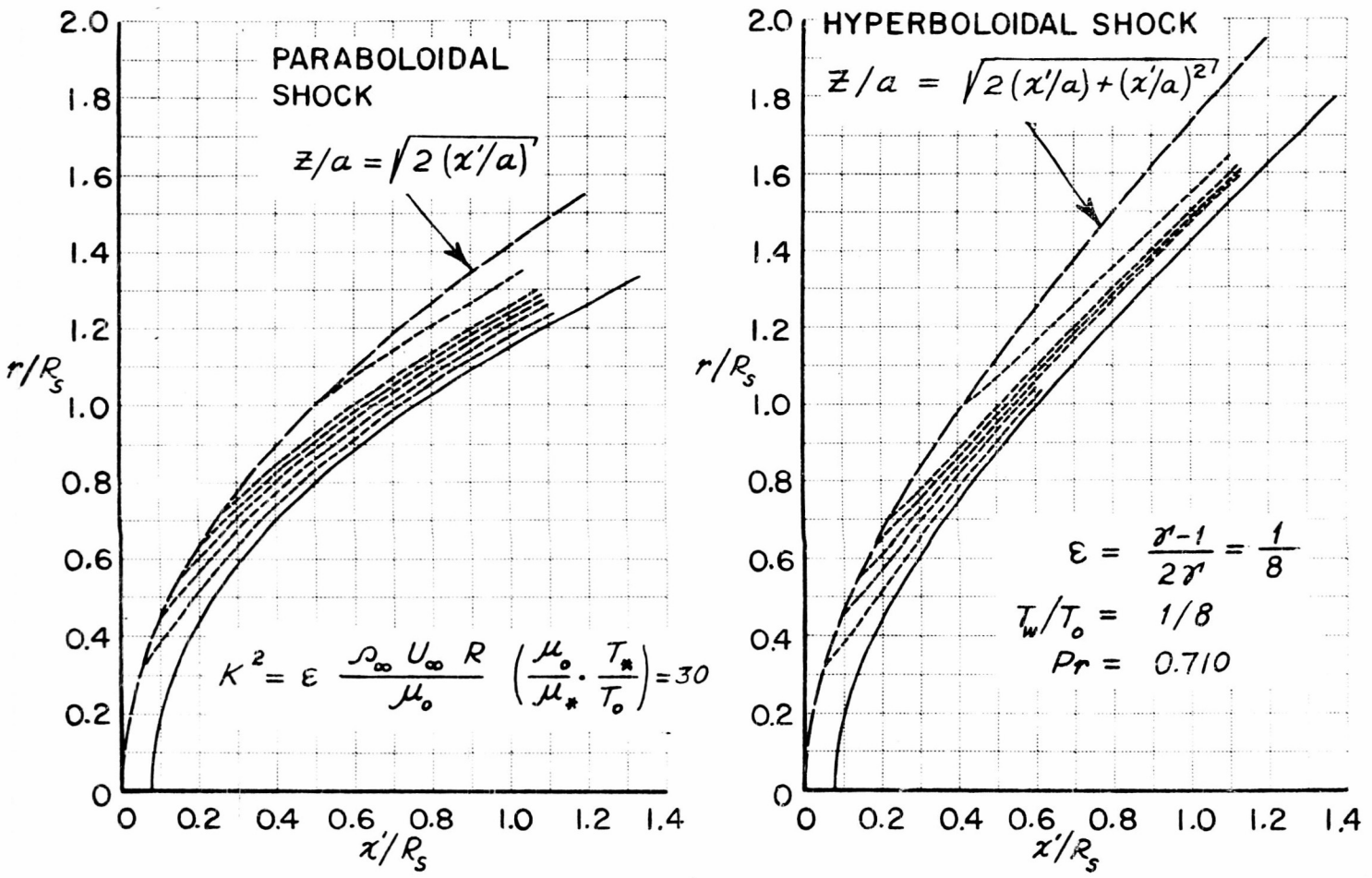

(a) PARABOLOID (b) HYPERBOLOID

Figure 7.7 STREAMLINE PATTERN AND BODY SHAPES SUPPORTING THE PARABOLOID AND THE HYPERBOLOIDAL SHOCKS FOR $K^2 = 30$ (VISCOUS-LAYER REGIME)

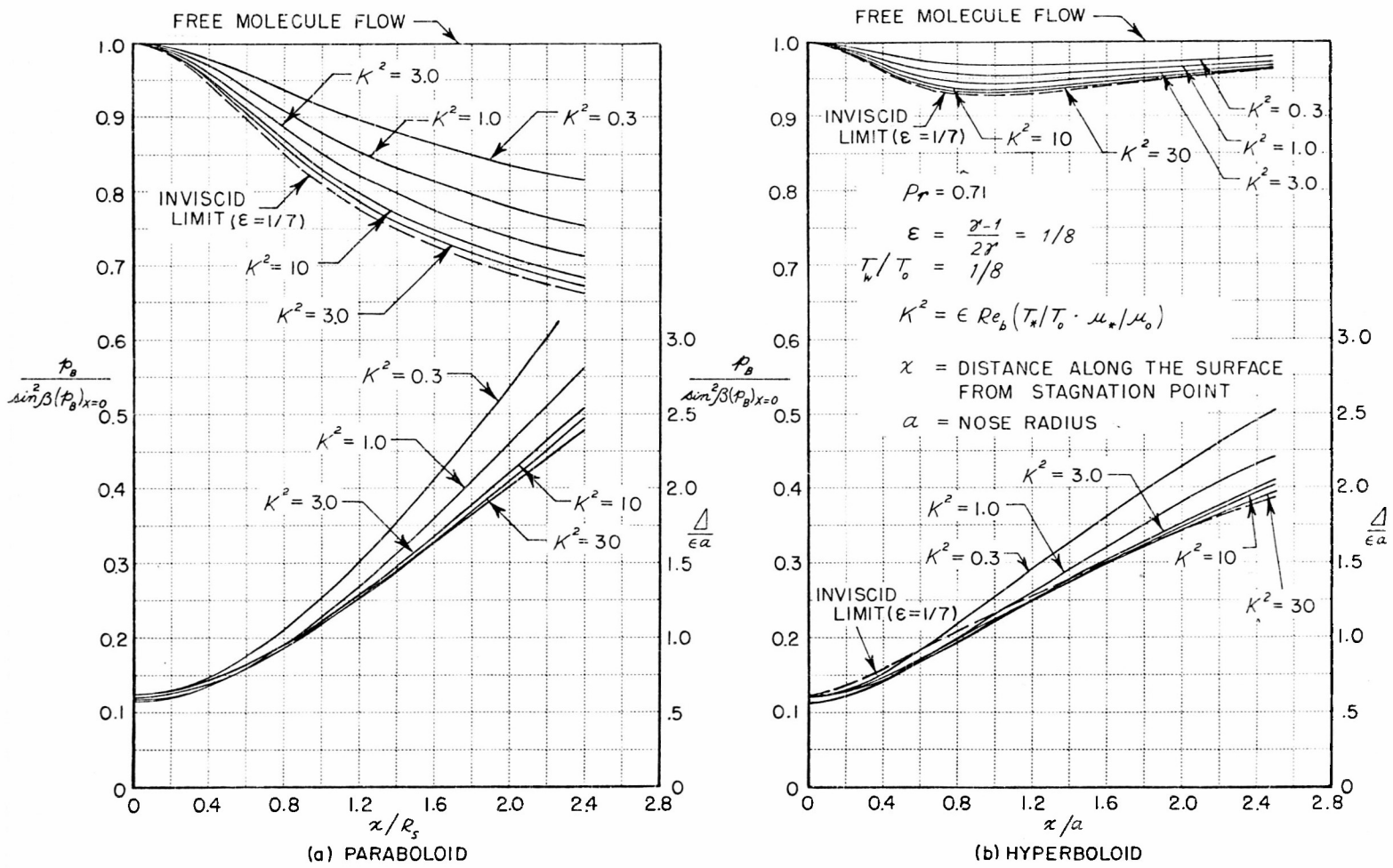

Figure 7.8 DISTRIBUTION OF SURFACE PRESSURE AND SHOCK-LAYER THICKNESS AROUND A PARABOLOID AND HYPERBOLOID

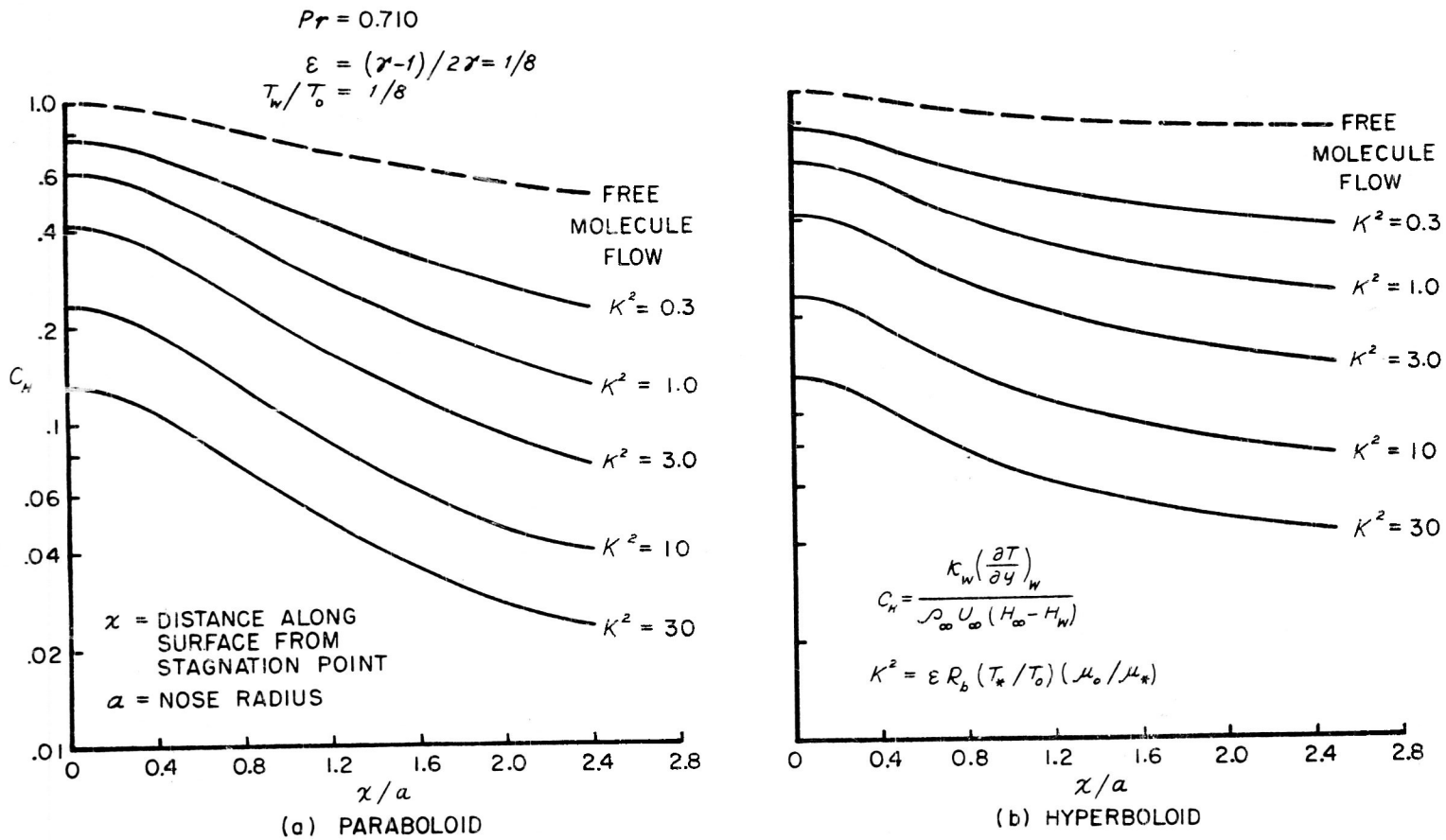

Figure 7.9 DISTRIBUTION OF SURFACE HEAT-TRANSFER RATE AROUND A PARABOLOID AND HYPERBOLOID

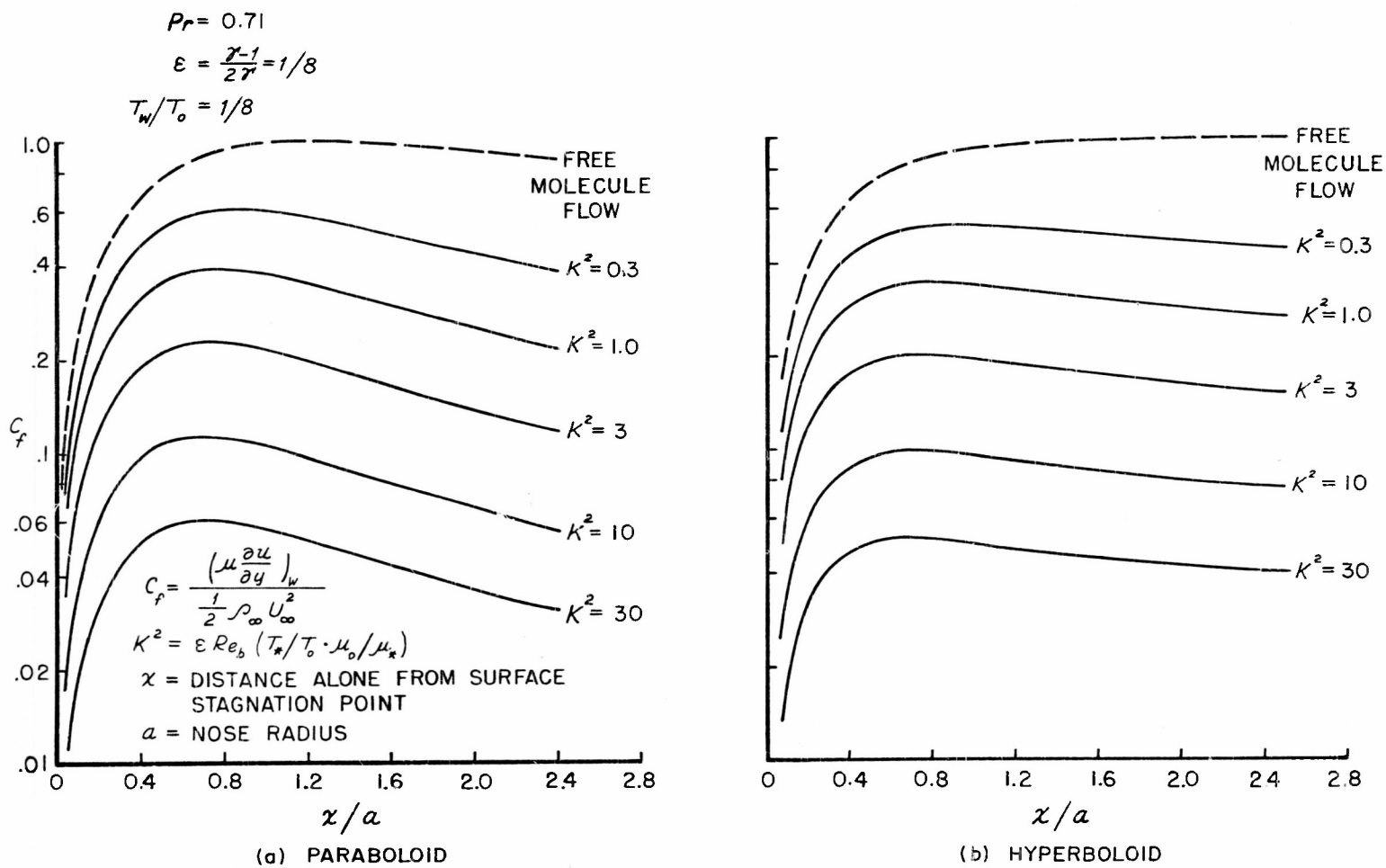

Figure 7.10 DISTRIBUTION OF SKIN FRICTION AROUND A PARABOLOID AND HYPERBOLOID

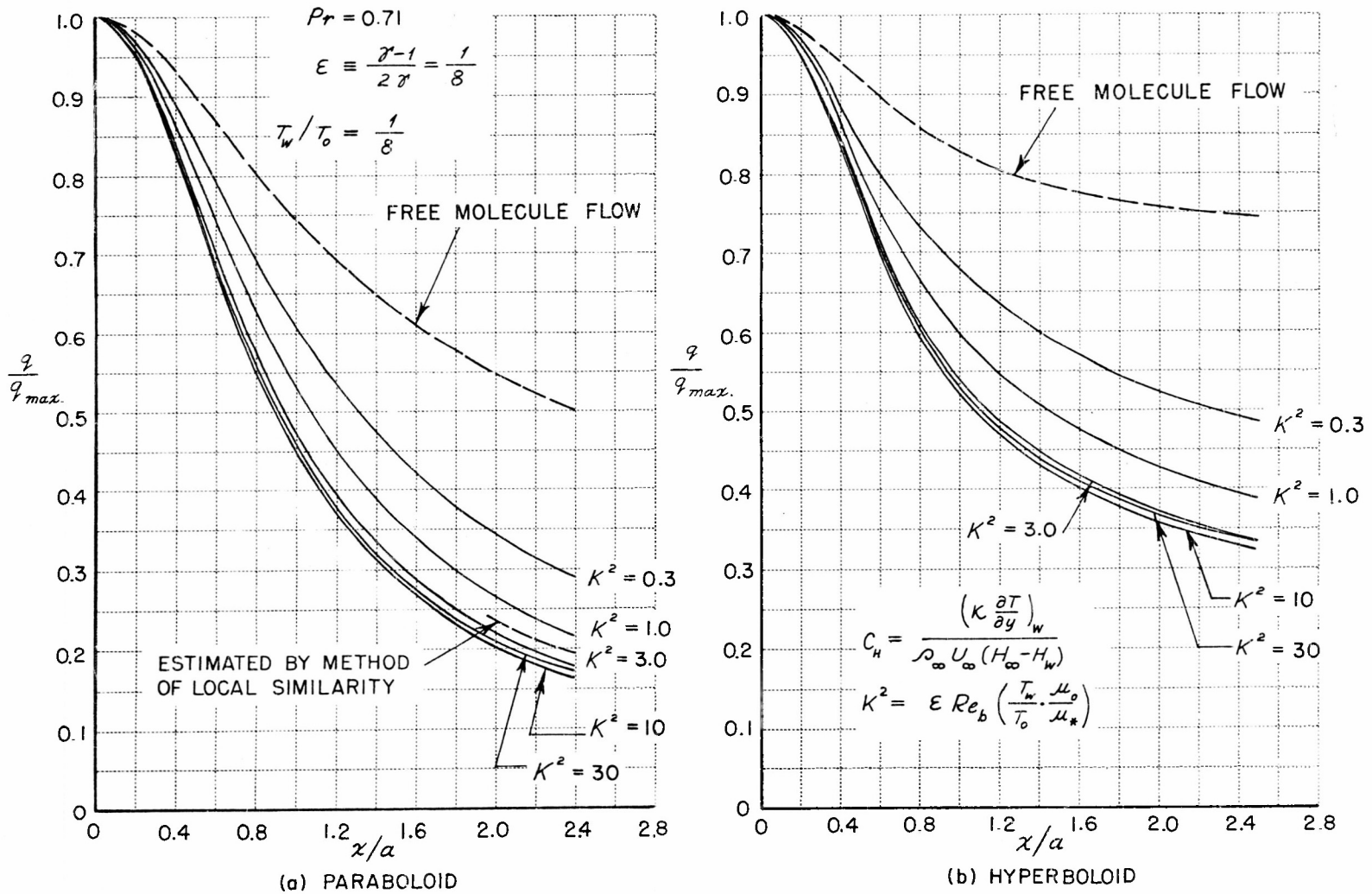

Figure 7.11 DISTRIBUTION OF RATIO OF LOCAL HEAT-TRANSFER RATES ON A PARABOLOID AND A HYPERBOLOID

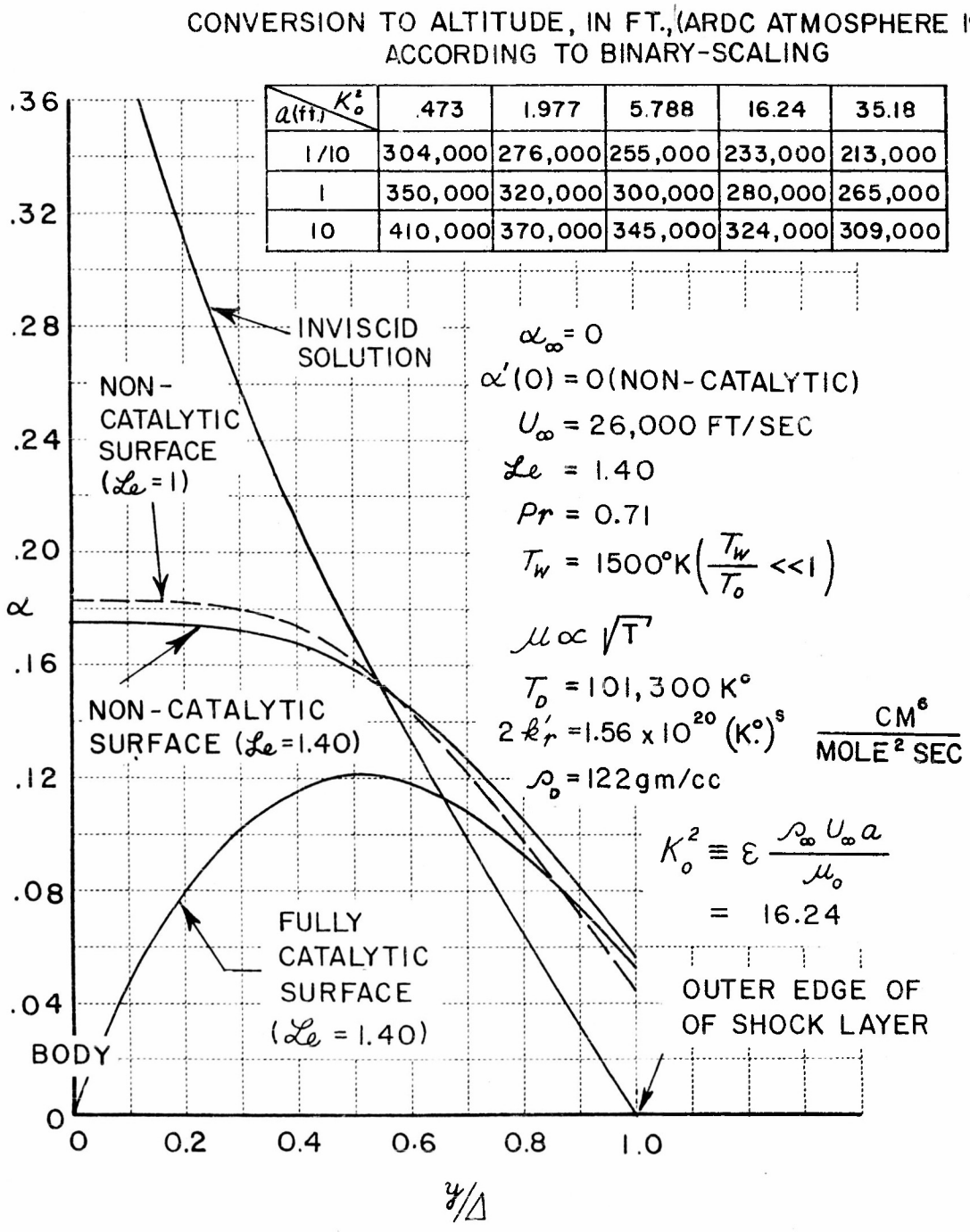

Figure 8.1 ATOM CONCENTRATION PROFILE IN THE STAGNATION REGION WITH NONEQUILIBRIUM DISSOCIATION UNDER STRONG SURFACE COOLING

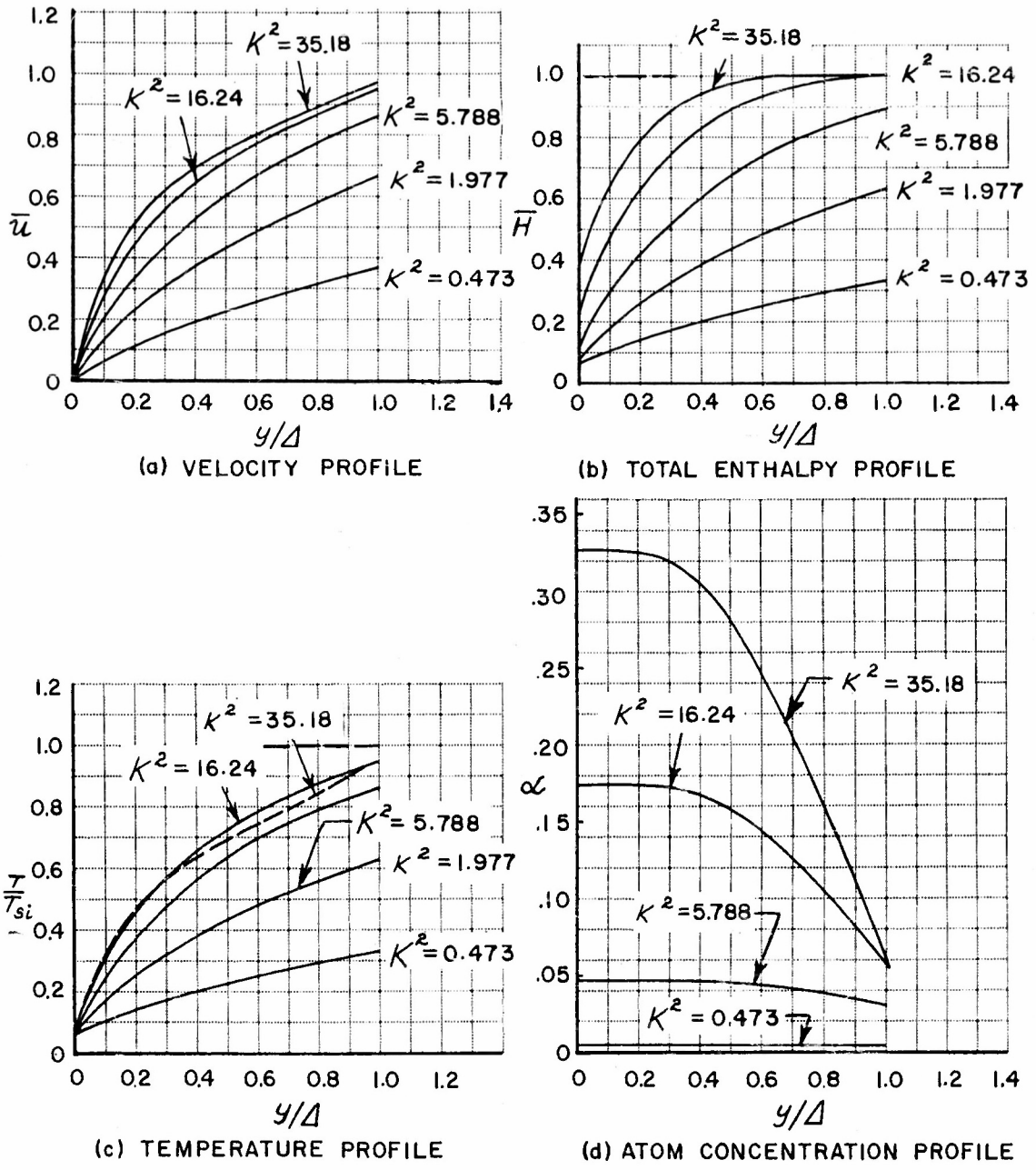

Figure 8.2 PROFILES OF VELOCITY, TOTAL ENTHALPY, TEMPERATURE AND ATOM CONCENTRATION IN THE STAGNATION REGION WITH NON-EQUILIBRIUM DISSOCIATION FOR A NONCATALYTIC SURFACE

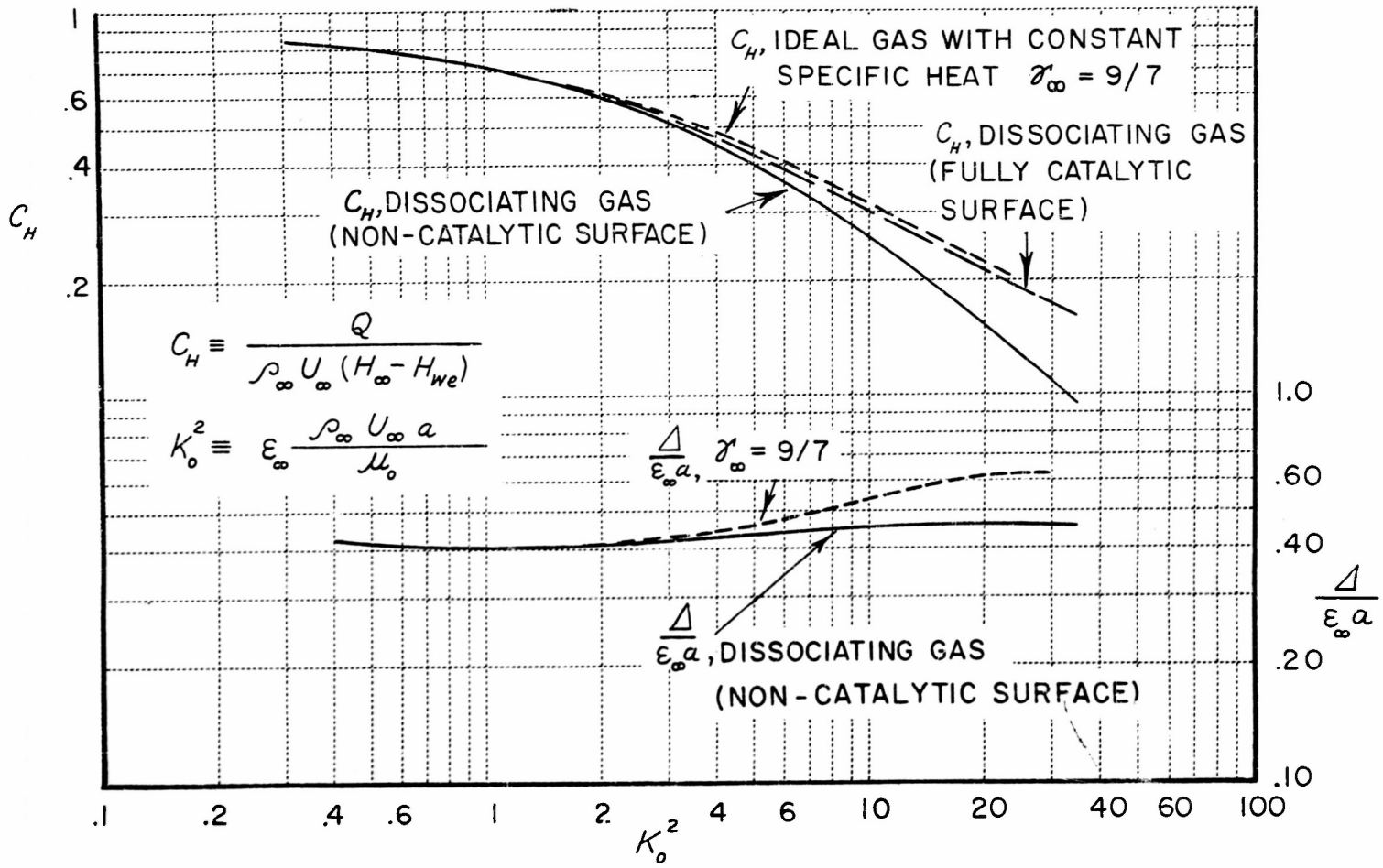

Figure 8.3 STAGNATION-POINT HEAT-TRANSFER RATE AND STAND-OFF DISTANCE AS AFFECTED BY GAS RAREFACTION AND NON-EQUILIBRIUM CHEMISTRY

FOR ERRATA

AD 411433

THE FOLLOWING PAGES ARE CHANGES

TO BASIC DOCUMENT

ERRATA - "The Blunt-Body Problem in Hypersonic Flow at Low Reynolds Number" by H. K. Cheng. CAL Report AF-1285-A-10, June 1963.

p. i — Third line from top, change "No. 2653(00)", to "Nonr 2653(00)".

p. ii — Third line from top, insert after "approximation" the following: "of the continuum (Navier-Stokes) theory".

p. iv — Eighth line from bottom, change "Eq. (5.1) and (5.2)" to "Section 5.3".

p. 8 — Third line from bottom, change "done by Van Dyke" to "accounted for by Lenard[25] and Maslen[26] with a dilated and shifted sphere. This treatment appears to be adequate in the stagnation region as has been shown in Van Dyke's study[12] on the basis of the constant-density model".

p. 21 — Eq. (4.2) should be written as $C_H = 1/\left[k^{2/3}\Gamma_{\frac{1}{3}}(k) + e^{-k}\right]$

p. 26 — Fifth line from bottom of the text, insert after "low" the word "constant".

p. 35 — Third line from bottom, add asterisk to the end of the sentence: add footnote as follows:
"* It is assumed that $\partial\bar{\tau}/\partial\bar{\eta} = O(\varepsilon)$ near the interface".

p. 43 — Fifth line from top, delete complete paragraph.

p. 47 — Third equation of Eq. (6.3), change the RHS of the equation to be $-\left(\frac{2}{1+\nu}\right)\frac{2\cos^3\beta}{\sigma\sin\beta}\frac{d\beta}{d\lambda}\,\bar{u}\cdot\zeta$

p. 62 — First line from top, change Ref. 43 to Ref. 71.

p. 70 — Delete sixth through tenth lines from top.

p. 74 — Ninth line from bottom, change Ref. 78 to Ref. 81. Fifth line from bottom, change "reading" to "reaching".

p. 87 — Seventh line from top, change "occurs however" to "appears to occur". Replace next sentence by "The existence of such a trend may however be established by numerical solutions based on boundary-layer theory and its higher approximations".

p. 95 — Reference 21, change "1960" to "1956".

DDC
RECEIVED
APR 6 1965
DDC-IRA A

p. 2. ERRATA for "The Blunt-Body Problem in Hypersonic Flow at Low Reynolds Number"

p. 103 Figure 5.1, the symbol "a" should be added to denote the nose radius of the body.

p. 104 The sonic line presented in Fig. 5.2 (a) is in error, the sonic line based on the present method, after correction, is in good agreement with the result of Van Dyke and Swigart.

p. 105 Exchange $\frac{u}{U_\infty \cos\beta}$ and $= \frac{v}{U_\infty \sin\beta}$ in Fig. 5.3.

p. 109 Figure 7.3 (a), extend the arrow from "3.0" down to the third curve counted from either left or right.

p. 119 Figure 8.2 (c), the arrow from "$K^2 = 5.788$" should be pointed to the third curve from the bottom.

AD 411433

END CHANGE PAGES